1973

Finite element analysis of plates and eccentrically stiffened plates, February 1973.

Anton W. Wegmüller

Celal N. Kostem

LEHIGH UNIVERSITY

OFFICE OF RESEARCH

FINITE ELEMENT ANALYSIS OF PLATES AND ECCENTRICALLY STIFFENED PLATES

BY
ANTON W. WEGMULLER
CELAL N. KOSTEM

FRITZ ENGINEERING LABORATORY REPORT NO. 378A.3

FINITE ELEMENT ANALYSIS OF PLATES AND ECCENTRICALLY STIFFENED PLATES

by

Anton W. Wegmuller

Celal N. Kostem

This work was conducted as a part of the project Overloading Behavior of Beam-Slab Highway Bridges, sponsored by the National Science Foundation.

Fritz Engineering Laboratory
Department of Civil Engineering
Lehigh University
Bethlehem, Pennsylvania

February, 1973

Fritz Engineering Laboratory Report No. 378A.3

TABLE OF CONTENTS

ABSTRACT

This report deals with the analysis of plates and stiffened plates in the elastic range using the finite element stiffness approach. The analysis is based on the classical theory of thin plates exhibiting small deformations.

A short description of the finite element techniques in use to date, and a review of some existing plate bending elements are presented. A refined rectangular plate bending element based on a higher order polynomial expression is then derived and a systematic procedure for the derivation of its stiffness matrix is outlined. The accuracy and convergence of solutions obtained with this new element are demonstrated on a few example structures showing that the new element compares favorably with presently known plate elements.

An analysis scheme for the stiffened plate structures in the linear elastic range is developed. The derivation of the component stiffness matrices is carried out first and the assemblage of the system stiffness matrix is described. The outlined general approach is then applied extensively to highway girder bridges and the versatility and accuracy of the method are demonstrated.

1. INTRODUCTION

1.1 Objective and Scope

Plates of various shapes are commonly used as structural systems or structural components. Most frequently, plates form part of floor systems in buildings or bridges, and are often used in connection with beams and columns. Generally, there is ample room for a variation in geometry, thickness and loading, as illustrated in Fig. 1 and hence, the analysis of such complex structures often presents considerable difficulties.

Stiffened plates of arbitrary shape are complex and highly redundant structures, the analysis of which is beyond the scope of currently used methods of analysis. Plates are often used in combination with beams and columns in floor systems of buildings and bridges, and in these cases, are predominantly loaded by forces acting perpendicular to the plate surface. In buildings, many different floor layouts are possible; consequently, there is virtually no restriction placed as far as geometry of the stiffened plate structure is concerned. The in-plane loading (if any) applied to such structures can often be neglected, thus simplifying the analysis considerably. This investigation is limited to the problem of analyzing transversely loaded stiffened plates; i.e. no in-plane loading is considered. However, due to the fact that the beams are eccentrically attached to the plate, in-plane deformation must be considered. To date, the analysis of beam-slab type

structures still constitutes a challenge to the structural engineer because no fully satisfactory method of analysis is available as yet.

It is widely accepted that a structure should be properly analyzed for working loads as well as at its failure stage. By means of an elastic analysis, one is able to determine the stresses and deformations, occurring under working loads, at selected points of a structure. If the determined stresses are kept below allowable stresses, then experience shows that a structure is not likely to fail. An accurate elastic analysis is also needed for considerations of fatigue and control of cracking in reinforced and prestressed concrete structures; i.e. stresses must be kept below certain levels in order to avoid fatigue or excessive cracking. Although the fatigue strength of reinforced or prestressed concrete structures is difficult to establish and reliable criteria for crack control are not final, an accurate elastic analysis is the prerequisite for establishing such guidelines.

1.2 Previous Work

For each of the problems considered in this report, a review of the previous work done in the area considered is given in the chapter devoted to each problem. Due to the practical importance of plate structures, engineers were early faced with the task of analyzing plates of various geometry and loading. Unfortunately, the governing differential equations are not solvable,

but for simple geometry and boundary conditions, and as a consequence many types of approximate analyses have been proposed to date. Extensive surveys of the state of the art of current plate analysis are given by Timoshenko (Ref. 46) and Girkman (Ref. 24).

Probably the most commonly used approximate method of analysis for solving plate problems of complex geometry is the method of finite differences. In this method, the governing differential equation of equilibrium is satisfied only at selected points of the plate structure. The satisfaction of boundary conditions at boundary points of the plate leads to additional equations which, together with the original set of equations, must be solved simultaneously. These additional equations, however, depend on the type of boundary and make it difficult to develop general purpose programs.

During the last two decades much progress has been made in the development of structural methods of analysis based on matrix algebra and a discretization of the structure into an assembly of discrete structural elements. In these methods, a displacement or a stress distribution is assumed within the element, and a complete solution is then obtained by combining these approximate displacement or stress distributions in a manner which satisfies the force-equilibrium and displacement-compatibility requirements at all the interfaces of the elements. Methods based on such approaches have been proven to be suitable for the analysis of complex structures. This led to the development of the finite element

methods (Ref. 56), which are essentially generalizations of standard structural procedures as described in Ref. 43, for example. To date, these methods have been successfully applied to many complex plate problems. Within the framework of the reported study a refined finite element for plate bending is developed. This new plate bending element is presented in Chapter 2 of this report.

To date, the elastic analysis of stiffened plate structures, as shown in Fig. 16, is performed in a more or less approximate manner. Though various types of methods are available, their application to complex shaped beam-plate type structures is doubtful for other than simple geometry of the structure to be analyzed. Particular attention has been given in the past to the analysis of floor systems of highway girder bridges due to their frequent occurrence. Consequently, most methods were originally developed for bridge structures.

In summary, it can be stated that as yet no fully adequate analysis exists capable of determining stresses and deformations in complex shaped beam-slab type structures. Current design methods are not completely rational because they are not based on a rigorous analysis, elastic or plastic (Refs. 3,4). Despite the fact that designs performed to date lead to successfully performing structures, it cannot be said with assurance that the designs resulting from such procedures are the best possible or that different parts of the same structure have consistent factors of safety against the failure load until better analytical methods

are available. A survey of available methods of analysis, some of which are described shortly, led to the conclusion that due to its great versatility, the finite element method is best suited for the analysis of arbitrarily shaped stiffened plates, as shown in Fig. 16. This analysis is presented in Chapter 3.

2. ANALYSIS OF PLATES

2.1 Introduction

The structural engineer is often faced with the analysis of complex shaped and loaded plates, as shown in Fig. 1. During the last decade, the versatility of the finite element approach has been well demonstrated and a number of plate bending elements have been developed. While most of these elements lead to accurate predictions for the displacement field, the internal moments computed are, in general, far less accurate (Ref. 53).

In this chapter, the development of a rectangular refined plate bending element is discussed. For the purpose of establishing the notation used in this text and the connection with conventional plate analyses, a review of the basic equations governing the behavior of plates is first presented. A short description of the finite element techniques in use to date is then given, followed by a review of some existing plate bending elements. The refined element, which is based on a higher order polynomial displacement field, is then described, and the derivation of the element stiffness matrices is outlined. Kinematically consistent load vectors are derived, and the enforcement of boundary conditions is described. A highly efficient technique for the solution of the often large system of stiffness equations is next described. Finally, the accuracy obtained with the new element is demonstrated on a few example solutions, and a comparison is made

with some presently known plate elements.

2.2 Small Deflection Theory of Thin Plates

2.2.1 Assumptions and Basic Equations

A transversely loaded plate structure should be treated as a three-dimensional problem of elasticity. Strain and stress components acting on an infinitesimal plate element of thickness h is shown in Fig. 2. The sign convention used in this study is shown in Fig. 3. By definition, stresses and forces are considered positive when acting in the directions shown. Introducing the assumptions of the classical theory of thin plates, a plate problem can be simplified into a two-dimensional elasticity problem. These assumptions can be stated as follows:

1. Plane sections normal to the middle surface before deformation remain plane and normal during deformation; also known as Kirchoff's assumption (Ref. 46).

2. The transverse displacement (w) is small in comparison to the thickness of the plate; i.e. $w \ll h$.

3. Stresses normal to the plane of the plate are negligible.

The first two assumptions imply that (1) shearing stresses in the transverse direction are neglected, and (2) the deflection (w) at any point of the plate is approximately equal to the deflection of the corresponding point located on the middle plane of the plate. The state of deformation can therefore be described in terms of

the transverse displacement (w) alone. Since the middle plane of the plate is assumed to be free of in-plane deformation, in-plane behavior is not considered in this chapter. Making use of the simplifying assumptions introduced above, the following relationships between in-plane displacements and the transverse displacement w exist:

$$U = u - z \frac{\partial w}{\partial x} \tag{2.1 a}$$

$$V = v - z \frac{\partial w}{\partial y} \tag{2.1 b}$$

where: u,v = Displacement in x-direction, or y-direction respectively, of a point lying in the middle plane of the plate.

U,V = Displacement in x-direction, or y-direction respectively, of a point lying at a distance z from the reference plane.

Both displacements u and v are assumed to be negligible in the classical theory of thin plates. The strain-displacement relations can be found by differentiating Eqs. 2.1:

$$\epsilon_x = \frac{\partial U}{\partial x} = \frac{\partial u}{\partial x} - z \frac{\partial^2 w}{\partial x^2} \tag{2.2 a}$$

$$\epsilon_y = \frac{\partial V}{\partial y} = \frac{\partial v}{\partial y} - z \frac{\partial^2 w}{\partial y^2} \tag{2.2 b}$$

$$\gamma_{xy} = \frac{\partial U}{\partial y} + \frac{\partial V}{\partial x} = \frac{\partial u}{\partial y} + \frac{\partial v}{\partial x} - 2 z \frac{\partial^2 w}{\partial x \partial y} \tag{2.2 c}$$

The stresses must satisfy the following two equations of equilibrium:

$$\frac{\partial \sigma_x}{\partial x} + \frac{\partial \tau_{yx}}{\partial y} = 0 \qquad (2.3\ a)$$

$$\frac{\partial \tau_{xy}}{\partial x} + \frac{\partial \sigma_y}{\partial y} = 0 \qquad (2.3\ b)$$

Using the strain-displacement relations (Eqs. 2.2), and assuming isotropic material, Hooke's Law can be written in terms of derivatives of displacement w:

$$\sigma_x = -\frac{E\,z}{1-\nu^2}\left[\frac{\partial^2 w}{\partial x^2} + \nu \frac{\partial^2 w}{\partial y^2}\right] \qquad (2.4\ a)$$

$$\sigma_y = -\frac{E\,z}{1-\nu^2}\left[\frac{\partial^2 w}{\partial y^2} + \nu \frac{\partial^2 w}{\partial x^2}\right] \qquad (2.4\ b)$$

$$\tau_{xy} = -2Gz\,\frac{\partial^2 w}{\partial x \partial y} \qquad (2.4\ c)$$

where: E = Modulus of Elasticity

G = Shear Modulus

ν = Poisson's Ratio

and G is related to E by

$$G = \frac{E}{2(1+\nu)} \qquad (2.5)$$

Stress resultants acting per unit width of the plate, as shown in Fig. 3, can be found by integrating appropriate stress components over the plate thickness:

$$M_x = \int_{-h/2}^{h/2} \sigma_x \, z \, dz \qquad (2.6\ a)$$

$$M_y = \int_{-h/2}^{h/2} \sigma_y \, z \, dz \qquad (2.6\ b)$$

$$M_{xy} = -\int_{-h/2}^{h/2} \tau_{xy} \, z \, dz \qquad (2.6\ c)$$

$$Q_x = \int_{-h/2}^{h/2} \tau_{xz} \, dz \qquad (2.6\ d)$$

$$Q_y = \int_{-h/2}^{h/2} \tau_{yz} \, dz \qquad (2.6\ e)$$

These equations can be easily integrated and lead to the well-known moment curvature relations:

$$\begin{bmatrix} M_x \\ M_y \\ M_{xy} \end{bmatrix} = \begin{bmatrix} D_{11} & D_{12} & 0 \\ D_{21} & D_{22} & 0 \\ 0 & 0 & D_{33} \end{bmatrix} \begin{bmatrix} \phi_x \\ \phi_y \\ \phi_{xy} \end{bmatrix} \qquad (2.7)$$

where: $D_{11} = D_{22} = Eh^3/12\ (1-\nu^2)$

$D_{12} = D_{21} = \nu\ D_{11}$

$D_{33} = (1 - \nu)\ D_{11}/2$

Defining the two vectors:

$$\{M\}^T = < M_x \quad M_y \quad M_{xy} > \tag{2.8 a}$$

$$\{\emptyset\}^T = < -\frac{\partial^2 w}{\partial x^2} \quad -\frac{\partial^2 w}{\partial y^2} \quad 2\frac{\partial^2 w}{\partial x \partial y} > \tag{2.8 b}$$

Eq. 2.7 can be written in compact form as

$$\{M\} = [D]\ \{\emptyset\} \tag{2.9}$$

2.2.2 The Differential Equation of Equilibrium

The fundamental equation of equilibrium is best derived by considering equilibrium of forces acting on an infinitesimal element of the continuum (Fig. 3). Summing up forces in z-direction yields:

$$\frac{\partial Q_x}{\partial x} + \frac{\partial Q_y}{\partial y} + q = 0 \tag{2.10}$$

Similarly, summation of forces about x-axis and y-axis, leads to

$$-\frac{\partial M_y}{\partial y} + \frac{\partial M_{xy}}{\partial x} + Q_y = 0 \tag{2.11}$$

$$\frac{\partial M_x}{\partial x} + \frac{\partial M_{yx}}{\partial y} - Q_x = 0 \tag{2.12}$$

Differentiating Eq. 2.11 and Eq. 2.12 and substituting the terms into Eq. 2.10 leads to the fundamental plate equilibrium equation in terms of moments:

$$\frac{\partial^2 M_x}{\partial x^2} + 2\frac{\partial^2 M_{xy}}{\partial x \partial y} + \frac{\partial^2 M_y}{\partial y^2} + q = 0 \qquad (2.13)$$

Finally, substitution of Eq. 2.9 into Eq. 2.13 yields

$$\frac{\partial^4 w}{\partial x^4} + 2\frac{\partial^4 w}{\partial x^2 \partial y^2} + \frac{\partial^4 w}{\partial y^4} - \frac{q}{D} = 0 \qquad (2.14\,a)$$

or

$$\nabla^4 w = \frac{q}{D} \qquad (2.14\,b)$$

2.3 Analysis of Plates Using the Finite Element Method

2.3.1 The Displacement Approach

The finite element technique is a relatively new, but very powerful, approach for the solution of engineering problems. The dominant reason for the extensive use of the finite element technique in solving structural problems is its great versatility and complete generality. In fact, the same basic procedure can be applied to structures of arbitrary shape, loading and boundary conditions. As a result, a single computer program can be used to solve a variety of problems.

The finite element concept, of which a comprehensive presentation is given in Ref. 56, was developed by extending known matrix structural theories to two and three-dimensional solids. Argyris (Ref. 5) introduced the two fundamental methods of matrix structural analysis, the force and the displacement method of

analyses, in which a systematic approach to automatic computation of displacements and forces was first attempted. The work by Turner et al. (Ref. 48), which may be interpreted as the first major step in the development of the finite element method, describes the direct stiffness approach. In this approach, insight into the behavior of elements in representation of structures is achieved, and consideration is given directly to the condition of equilibrium and compatibility. However, in the treatment of refined elements the physical behavior is obscured due to the more complex behavior of such elements.

The first step in the displacement approach is to discretize a structure into a suitable number of finite elements. The behavior of the actual structure is assumed to be approximated by the behavior of the discretized structure; i.e. by an assemblage of finite elements having simple elastic properties and being connected so as to represent the actual continuum. For practical reasons, the geometry of the elements must be simple, but generally could be of any shape. The elements are assumed to be interconnected at their nodal points, and the displacements of these nodal points constitute the basic unknown parameters of a problem.

Displacement functions, often called shape functions, are then chosen for each element to uniquely define the state of deformation in terms of nodal values, which are referred to a global coordinate system. Elemental displacement fields should be continuous (single-valued), and should satisfy deformation

continuity within the element and along element interfaces. Consequently, the entire displacement field of the discretized structure is continuous, piecewise differentiable, and in addition, is restrained to satisfy displacement boundary constraints. The displacement field assumed for an element is called compatible if full continuity of deformation is achieved within the element, as well as along its boundaries. In this case, the chosen displacement function uniquely defines the state of strain within an element in terms of its nodal displacements. Hence, together with possible initial strains, these strains will define the state of stress throughout the element, and on its boundaries.

The loading acting upon the system is approximated by a set of equivalent concentrated nodal forces, again referred to a global coordinate system. These external forces should equilibrate the internal boundary stresses, distributed loads and forces due to initial strains. This requirement leads to the relationship between generalized displacements and associated generalized forces. The matrix relating these two vectors is called the element stiffness matrix. Its elements are a function of the geometric and elastic properties of the element.

At this stage, a finite element solution follows standard structural procedures as described in detail in a number of references (e.g. Ref. 6). By appropriate superposition of the individual element stiffness relations, the corresponding relationship for the entire structure can be established. In this process, the

requirements of compatibility and equilibrium must be satisfied. Any system of displacements listed for the entire structure automatically satisfies all compatibility requirements. Establishing equilibrium conditions at all nodes leads to the force-displacement relationship of the entire structure. For this purpose, the element stiffness matrices, connecting nodal displacements to nodal forces must be transformed to a common coordinate system or reference frame. The formulation of the overall structural stiffness matrix proceeds then by adding appropriate element stiffness contributions framing into a common node. This procedure leads to a system of linear algebraic equations.

Finally, all kinematic restraints have to be imposed, and the resulting system of equations must be solved simultaneously for the unknown nodal displacements. Clearly, the satisfaction of a minimum number of prescribed displacements to prevent rigid body displacements is mandatory; otherwise the displacements could not be determined uniquely. The structure stiffness matrix is usually well-conditioned, sparsely populated, and narrowly banded if adequate nodal numbering of nodal points is provided. These properties permit an efficient, automatic assembly and solution of large systems of simultaneous equations. Once the solution of the unknown displacements has been obtained, the determination of internal stresses, or stress resultants, is straightforward. The selection of displacement functions and the evaluation of the element stiffness matrix are the most important steps in the finite

element displacement approach and will be discussed in subsequent sections.

Early derivations of finite element force-displacement relationships made no reference to variational considerations. Only recent developments have shown that these methods also have a solid theoretical foundation. The basic principles of linear structural mechanics are the principle of minimum total potential energy and the principle of minimum complementary energy. These variational methods form the basis for the derivation of element stiffness equations. The principle of minimum total potential energy is stated as (Ref. 51):

> Of all compatible displacement fields satisfying given boundary conditions, those which satisfy also the equilibrium conditions make the total potential energy π assume a stationary value.

$$\delta \pi = \delta (U + V) = 0 \qquad (2.15)$$

where: U = Strain energy of deformation.

V = Potential of external forces.

The stationary value of π is always a minimum, and therefore, a structure under a system of external loads represents a stable system. It can be shown (Ref. 8) that if the system of displacements is defined throughout the structure by the element displacement functions, with nodal parameters acting as undetermined parameters, then the procedure of minimizing the potential energy of

the system will result in precisely the same formulation as described above. This alternate approach of establishing stiffness equations shows that the finite element procedure is, in fact, identical with the Rayleigh-Ritz Approach.

In the finite element method the assumed displacement functions are associated with individual elements only. The displacements in the elements are uniquely defined in terms of the nodal point values, and the entire displacement field is assumed to consist of a number of piecewise continuous displacement fields each extending over the region of an element. Clearly, the finite element method, as well as the Ritz method, are approximate methods of analysis. However, if conforming elements are used, it can be shown that if the mesh size is gradually decreased, the solution tends toward the true solution; i.e. convergence is assured for a valid minimum potential energy approach. One can also show for this case that the strain energy is a lower bound, and the discretized structure is stiffer than the actual one if external loads are applied only.

2.3.2 Displacement Functions and Convergence Criteria

One of the most important steps in the finite element displacement approach is the selection of displacement functions which discretize the displacement field within an element. These assumed shape functions limit the infinite degrees of freedom of the system by expressing the deformation within a plate element in terms of displacement parameters at the nodal points. The accuracy obtained

depends on the extent to which the assumed deformation pattern can approximate the true displacement pattern. Generally, finer meshes lead to a closer approximation, although convergence is not necessarily assured if the displacement functions are not properly chosen.

So far, only limited attention has been given to the establishment of general rules for the selection of functional representations of element behavior. Recent research (Ref. 38) led to requirements for the assumed displacement functions in order to arrive at a convergent finite element solution.

As mentioned earlier, an approach based on a valid minimum potential energy solution assures monotonic convergence with decreasing mesh size. Melosh (Ref. 34) and Fraeijs de Veubeke (Ref. 20) set out specific conditions under which a valid minimum potential energy approach is preserved in a finite element formulation. One of the basic requirements for generating deformation consistent stiffness matrices is complete compatibility of displacement within the element and along its boundaries. Elements derived from such displacement fields are called compatible.

Melosh (Ref. 34) has shown that the selection of appropriate displacement fields can be accomplished by use of Langrangian or Hermitian interpolation techniques. The functions are chosen such that they become dependent only on the displacements of the end points, and additional points along a side of the element in consideration. Bogner et al. (Ref. 11) used this approach to derive the stiffness matrix for a compatible rectangular plate element.

Another general method for the selection of functions directly in terms of degrees of freedom is the spline interpolation concept. This approach was developed by Birkhoff (Ref. 10) as a general mathematical procedure and employed by Pian (Ref. 17).

A third approach used successfully in the functional representation of a displacement field is the concept of isoparametric element formulation. The shape functions chosen to describe the element boundaries are identical to those used to prescribe the variation of the displacement function. Ergatoudis (Ref. 18) has pioneered this approach, and Zienkiewicz (Ref. 28) has applied it to generate stiffness matrices for different two- and three-dimensional elements.

Often these interpolation concepts are difficult to apply; then a function is chosen, as outlined in Section 2.3.1, in terms of unknown nodal displacement parameters. These are normally chosen equal in number to the number of degrees of freedom for the element in consideration, and can be evaluated from the enforcement of compatibility conditions at the element nodes. The choice of this function proved to be a major source of difficulty since an arbitrary choice may result in an unsatisfactory element displacement behavior, and as a consequence, may not lead to convergence. Thus, the question arises as to which requirements the assumed displacement function should satisfy in order that the associated finite element solution will converge toward the true solution as the mesh size is reduced. At present, the

view is held that the sufficient conditions for the derivation of deformation consistent stiffness matrices are as follows:

1. Internal and interface compatibility must be satisfied.
2. Displacement function must depend linearly on nodal parameters.
3. Proper representation of all rigid body displacement states is required.
4. All uniform states of strain must be included.
5. The displacement field must be spatially isotropic.

Requirement (1), as already discussed, leads to a valid minimum potential energy approach, and this, in turn, bounds the strain energy of the discretized structure. As a result, monotonic behavior is obtained if the mesh is subdivided into elements of the same type so that all previous displacement states are contained in the new ones. This condition, as postulated by Melosh (Ref. 34), is in fact a sufficient criteria for monotonic convergence. On the other hand, if all of the above given conditions are met, with the exception of requirement (1), then numerical evidence has shown that satisfactory convergence can still be achieved; though it cannot be proved anymore via the principle of minimum total potential energy.

Requirement (2) leads to the desired linear system of equations since linearly elastic material is assumed.

Requirement (3) is needed to include the conditions of global equilibrium. Self-straining would occur when the nodal displacements were caused by rigid body displacements. Hence, the presence of all rigid body motion terms in the selected displacement function is essential.

Requirement (4) is necessary for the convergence to the actual strain field. In fact, the exclusion of constant strain states could result in convergence toward an incorrect result. As the mesh size is decreased, nearly constant strain conditions will prevail in the element. If the condition is not met, such strain states could not be attained as the mesh size is reduced. Hence, it must be possible to represent constant curvatures in the case of pure plate bending. Conditions (3) and (4) are often referred to as completeness criterion. Furthermore, rigid body displacements are actually a particular case of the constant strain conditions, having zero values for strain.

Requirement (5) insures that the resulting generalized force-displacement relations are independent of the position of the global coordinate system. Hence, the chosen displacement functions must be independent of the particular shape of the element and the orientation of the element with respect to the coordinate system to which the functions are referred. Thus, attention should be given to requirement (5) when truncated polynomials are used as displacement functions.

Polynomial expressions have been used nearly exclusively

for the generation of different element stiffness matrices. First, this choice simplifies algebraic as well as automatic manipulations. Furthermore, polynomials satisfy the constant strain criteria and simplify the investigation of compatibility requirements. Complete polynomials also satisfy the invariance criterion.

A lower bound to the strain energy and monotonic convergence to the correct solution is obtained if conforming shape functions are used and the completeness criterion is satisfied. Oliveira (Ref. 38) proved that completeness and conformity are necessary but not sufficient criteria for convergence. According to Oliveira, completeness is the only requirement which the displacement function must meet to arrive at a convergent finite element solution. However, completeness does not necessarily lead to monotonic convergence.

Considerable difficulty is experienced, in some cases, to find fully compatible displacement functions. Non-conforming displacement functions will cause, in general, infinite strains at the element interfaces. Hence, only an approximation to the true strain energy is found since,in calculating the energy as in the usual finite element approach, no consideration is given to the contributions to energy at the lines of discontinuity. However, if for finer mesh sizes the extent of the discontinuity tends to vanish, then an incompatible formulation will lead to the correct result. Indeed, some finite element stiffness matrices derived from discontinuous displacement functions yield excellent results.

2.3.3 Alternate Approaches

Most of the finite element approaches developed to date are based on the principle of minimum total potential energy, as described in Section 2.3.1. However, an alternate procedure is possible if the functional to be minimized is the complementary energy of a system. The basis for such an approach is the principle of minimum complementary energy, which can be stated as follows (Ref. 51):

> Of all statically admissible stress states, i.e. satisfying equations of equilibrium and all boundary conditions on stresses, those which also satisfy the compatibility equations make the total complementary energy π^* assume a stationary value. It can be shown again that this value is a minimum.

$$\delta \pi^* = \delta (U^* + V) = 0 \qquad (2.16)$$

where: U^* = Complementary strain energy.

V = Potential of applied loads.

Therefore, it is possible to arrive at an alternate finite element formulation if, in place of a compatible displacement field, an admissible stress field is taken to define strains, and hence the complementary energy. In this context, a stress field is called conforming if it is in equilibrium within the element and balances all prescribed surface stresses. The stresses within the element are assumed in terms of stress functions which in turn are

expressed in terms of nodal parameters. The principle of minimum complementary energy is then applied to derive flexibility equations. Hence, the emphasis in this approach lies in the search for conforming stress fields.

Pioneered by DeVeubeke (Ref. 19), this approach is in general much more difficult since the search for equilibrium stress fields is more demanding than that of compatible displacement fields. It can be shown that this approach will give an upper bound of the strain energy and thus overestimates the displacements. If both the compatible displacement approach and the approach based on the principle of minimum complementary energy are taken, valuable bounds to the true displacements are obtained. The principle of minimum complementary energy has so far been applied to derive element stiffness matrices for simple elements in the elastic range. An extension of this formulation to arrive at flexibility equations for more complex elements is difficult since conforming stress fields are difficult to establish. An extension of this approach to elastic-plastic problems is not feasible since for a non-linear material behavior, the complementary energy does not provide for a reliable basis for the derivation of flexibility equations.

Besides these two basic formulations, a number of alternate avenues can be taken to establish stiffness or flexibility equations. A comprehensive study of such approaches is given in the survey by Pian and Tong (Ref. 41). For example, other functionals

could be selected, permitting the simultaneous variation of stresses and displacements together with assumptions made on both these quantities. Such approaches are called mixed formulations. In these methods, generally neither equilibrium nor compatibility is fully satisfied, and for this reason, convergence must be proven for each particular case.

2.3.4 Existing Rectangular Plate Bending Elements

During the last decade, much research effort has been devoted to determine reliable element stiffness matrices for various shapes of plate bending finite elements. Attention has been given to triangular, rectangular, and quadrilateral elements. Recent surveys of presently available triangular elements are given by Bell (Ref. 9) and Gallagher (Ref. 23). These surveys show that a variety of fine performing triangular elements are available.

Comparative studies have shown that rectangular elements show greater accuracy than triangular elements for the same number of degrees of freedom. In view of the refined rectangular plate element developed in this report, a short review of some published rectangular and quadrilateral plate elements is given in this section. It should be stated that in the case of plate bending, continuity of displacement throughout the plate element implies continuity of deflection and slopes, i.e. first derivatives of the lateral displacement w. Thus, both the deflection and the

slopes must be continuous within the element and across its boundaries in order to fully satisfy the conditions of displacement compatibility.

A survey of rectangular finite elements for plate bending is given by Clough and Tocher (Ref. 15). Various displacement functions have been used to develop the stiffness matrix for a rectangular plate element. Within the framework of Kirchhoff's plate bending theory, the deformations in a plate element are completely defined by the lateral deflection w. With this deflection and two rotations unknown at each nodal point, a rectangular element, as shown in Fig. 4, possesses twelve degrees of freedom.

One of the earliest functional representations for the deflection was suggested by Pappenfuss (Ref. 39):

$$w = (a_1 + a_2x + a_3x^2 + a_4x^3)\ (b_1 + b_2y + b_3y^2 + b_4y^3) \quad (2.17)$$

It can be verified that this function satisfies interelement continuity of w, and the rigid body displacement modes are included. However, due to the absence of the term representing constant twist, the constant strain condition is not satisfied, and hence, convergence does not occur towards the correct solution.

In another early paper, Melosh (Ref. 33) derived a different plate bending stiffness matrix, on the basis of physical reasoning.

The simplest expression which has been used in deriving

the element stiffness matrix for a rectangular plate element, known as ACM element (Ref. 34), is the twelve term polynomial

$$w = a_1 + a_2x + a_3y + a_4xy + a_5x^2 + a_6y^2 + a_7xy^2 + a_8x^2y + a_9x^3 + a_{10}y^3 + a_{11}x^3y + a_{12}xy^3 \qquad (2.18)$$

It is noted first that the chosen function does not represent a complete polynomial. Geometric isotropy is maintained, due to the choice of the two fourth order terms. It is observed that the rigid body mode is included and constant strain states are allowed for in this expression. A test reveals that transverse displacements are interelement compatible, but the element lacks compatibility of normal slope. However, lack of satisfaction of interelement compatibility does not necessarily result in lack of convergence, due to this reason this functional representation yields relatively good accuracy in displacement but at the same time less accuracy in internal moments is obtained.

As an example of achieving interelement compatibility by means of the Hermitian interpolation concept, Bogner et al. (Ref. 11) developed a compatible rectangular plate element having four degrees of freedom at each nodal point. In addition to the usual displacement components w, $\partial w/\partial x$ and $\partial w/\partial y$, the twist $\partial^2 w/\partial x\partial y$ was introduced as an unknown displacement component. Numerical results indicate that in addition to exhibiting monotonic convergence, a good approximation of the displacement behavior was achieved; however, no results for internal moments are reported.

DeVeubeke (Ref. 21) derived a compatible finite element by subdividing an arbitrary quadrilateral into four triangles and assuming a complete cubic polynomial displacement field within each triangle. Besides the four corner nodes, four midside nodes, with one degree of freedom at each of those nodes, were defined.

Clough and Felippa (Ref. 16) derived a compatible quadrilateral element having four corner nodes, only with three degrees of freedom each. It was built up from four triangles, and each of these triangles in turn consists of three subtriangles represented by a complete third order polynomial in w, the transverse displacement.

Of all the elements discussed so far, the last three approaches show the best results. In most of the available literature, the convergence of an element is judged by plotting the accuracy of the solution against the number of subdivisions for a problem in consideration. A more appropriate comparison would be to plot the accuracy versus the total number of degrees of freedom involved.

Little work has been done to date in the derivation of stiffness matrices based on the alternate approach of minimizing the total complementary energy. Efforts to accomplish formulations based on this functional or on Reissner's energy principle have been mainly concerned with the triangle. A number of mixed approaches however, have been advanced during recent times. In a paper by Pian (Ref. 40), a hybrid approach was developed in

which stresses were selected within the element, and a displacement function was prescribed on the boundaries. A similar approach was undertaken by Severn and Taylor (Ref. 44) and generalized to the arbitrary quadrilateral by Allwood and Cornes (Ref. 2).

In summary, a number of rectangular or quadrilateral finite elements for plate bending analysis are presently in use. Most elements show good convergence for displacements towards the true solution. However, the rate of convergence does differ substantially for different elements. Moreover, despite acceptable accuracy for displacements, some elements show poor accuracy for internal moments.

2.4 A Refined Rectangular Plate Bending Element

2.4.1 Choice of Displacement Field

Investigations on triangular elements, using higher order polynomial approximations for the assumed shape functions, showed that the use of such expressions leads to improved accuracy on displacement and stresses. Similar investigations have not yet been made for rectangular elements. Hence, in this chapter the stiffness matrix for a refined rectangular plate bending element is derived and comparisons are made with some presently available rectangular and quadrilateral elements.

Refinements in a finite element approach can be achieved, for example, by a better approximation of the displacement field. In order to arrive at a valid variational formulation based on

minimum potential energy, certain continuities of the unknown function must be maintained. This allows the determination of the functional to be minimized, which will be unique. Thus, as was noted earlier, the deflection w and two slopes must be continuous for a plate bending problem. One can prove that, in this case, the solution will converge monotonically towards the correct solution. On the other hand, formulations based on deflection functions not satisfying compatibility of normal slopes along interelement boundaries will not necessarily show monotonic convergence as the mesh size is decreased. It is the basic thought of the present investigation that a refinement in element behavior can be achieved through the use of a higher order polynomial approximation of the displacement field (Ref. 53).

Consider the rectangular finite element, shown in Fig. 4, along with the introduced local coordinate system with its origin located at the centroid of the element. The displacement components are assumed positive as shown. The basic unknowns in a plate bending problem are the lateral deflection w, the two slopes θ_x and θ_y, and the internal moments per unit length, defined in Eq. 2.6. For the present approach, at each node (i) of a finite element, the following generalized displacement components are introduced.

$$\{\delta_i\}^T = < w \quad \theta_x \quad \theta_y \quad \emptyset_x \quad \emptyset_y \quad \emptyset_{xy} > \tag{2.19}$$

where: w = $w(x,y)$ = lateral deflection in z-direction

θ_x = slope about x-axis

θ_y = slope about y-axis

ϕ_x = curvature of plate surface in x-direction

ϕ_y = curvature of plate surface in y-direction

ϕ_{xy} = twist of plate surface

Under the assumptions of the theory of thin plates, the slopes and curvatures can be expressed in terms of derivatives of the lateral deflection w, as follows:

$$\theta_x = \partial w/\partial y \tag{2.20 a}$$

$$\theta_y = -\partial w/\partial x \tag{2.20 b}$$

$$\phi_x = -\partial^2 w/\partial x^2 \tag{2.20 c}$$

$$\phi_y = -\partial^2 w/\partial y^2 \tag{2.20 d}$$

$$\phi_{xy} = \partial^2 w/\partial x \partial y \tag{2.20 e}$$

Element displacements can now be given as the listing of nodal displacements:

$$\{\delta^e\}^T = < \delta_i^T \quad \delta_j^T \quad \delta_k^T \quad \delta_l^T > \tag{2.21}$$

Similarly, the element force vector is defined as:

$$\{F^e\}^T = < F_i^T \quad F_j^T \quad F_k^T \quad F_l^T > \tag{2.22}$$

The six degrees of freedom introduced at each nodal point lead to a 24-degree-of-freedom element, and permit the choice of a higher order polynomial for the approximation of the displacement field. Using this improved field, it should be possible to approximate the actual displacement field more closely, resulting in an improvement in the accuracy and convergence. The presence of curvature terms in the vector of unknown nodal parameters should also allow certain types of boundary conditions to be satisfied more properly than can be done in the usual displacement approach, having w and its slopes as unknowns. The continuity requirements imposed on the curvature terms should especially improve the moment field since moments at all mesh points can be made continuous in this approach. Finally, since the internal moments are obtained directly by summing the appropriate curvature terms, they need not be computed separately. The chosen polynomial can be conveniently represented by Pascal's triangle, as shown in Fig. 5. Twenty-eight free constants are associated with this polynomial, i.e. one constant for each term. A completely conforming solution could be constructed by introducing additional nodes at each of the midsides of the rectangle and requiring that the normal slope be continuous at these points. Possessing the same number of known conditions as there are unknowns in this case, the interpolation problem could be solved uniquely. However, this approach is not taken here, since it would result in different degrees of freedom for different nodal points, and hence, complicate the assembly of the system stiffness

matrix. In addition, it would increase the band width of the resulting system of linear equations. It would however, result in a valid potential energy approach.

For the present approach, only twenty-four terms of the complete sixth-order polynomial are retained (the terms underlined in Pascal's triangle are omitted), since the deflection function for w can be defined in terms of these twenty-four parameters only. With geometric symmetry of the element, no preferential direction should exist. The terms with the highest even powers in x and y must be omitted in order to satisfy compatibility of w. Despite omitting these terms, geometric isotropy is retained. It will be seen later that the retention of inappropriate terms would result in a singular transformation matrix. Inspecting the chosen function, it is recognized that along any line of constant x or y coordinate, the displacement w varies as a fifth-order function. The element boundaries, for example, are composed of such lines. A fifth-order polynomial is uniquely defined by six constants. The two end values of deflection, slopes, and curvatures at the end points will therefore uniquely define the displacement along these boundaries. As such values are common to adjacent elements, continuity of w will result along all interfaces.

Furthermore, it can be seen that the gradient of w normal to any boundary varies as a fourth-order function. With only one slope and curvature term imposed at each of the two end points of a boundary line, this function is not uniquely specified, and hence,

discontinuity of the normal slope generally occurs. Clearly, the chosen displacement function is of the non-conforming type. However, it is evident that the completeness criterion is satisfied, since all rigid body displacement modes, as well as all constant curvatures, are included in the chosen functional representation.

For the sake of a simpler derivation, it is best to introduce at this point non-dimensionalized coordinates defined as:

$$\xi = \frac{x}{a} \quad \text{and} \quad \eta = \frac{y}{b} \tag{2.23}$$

The displacement field can then be written as:

$$\begin{aligned} w = w\ (x,y) = {} & \alpha_1 + \alpha_2\xi + \alpha_3\eta + \alpha_4\xi^2 + \alpha_5\xi\eta + \alpha_6\eta^2 + \alpha_7\xi^3 \\ & + \alpha_8\xi^2\eta + \alpha_9\xi\eta^2 + \alpha_{10}\eta^3 + \alpha_{11}\xi^4 + \alpha_{12}\xi^3\eta \\ & + \alpha_{13}\xi^2\eta^2 + \alpha_{14}\xi\eta^3 + \alpha_{15}\eta^4 + \alpha_{16}\xi^5 + \alpha_{17}\xi^4\eta \\ & + \alpha_{18}\xi^3\eta^2 + \alpha_{19}\xi^2\eta^3 + \alpha_{20}\xi\eta^4 + \alpha_{21}\eta^5 \\ & + \alpha_{22}\xi^5\eta + \alpha_{23}\xi^3\eta^3 + \alpha_{24}\xi\eta^5 \end{aligned} \tag{2.24}$$

Listing all polynomial terms in the row-vector

$$< P > = < 1 \quad \xi \quad \eta \quad \xi^2 \quad \xi\eta \quad \eta^2 \quad \cdots\cdots \quad \xi\eta^5 > \tag{2.25}$$

Eq. 2.24 can be written as

$$w = w\ (x,y) = < 1 \quad \xi \quad \eta \quad .... \quad \xi\eta^5 > \begin{Bmatrix} \alpha_1 \\ \alpha_2 \\ \vdots \\ \alpha_{24} \end{Bmatrix} \tag{2.26 a}$$

or simply as

$$w = w\ (x,y) = < P > \quad \{\alpha\} \tag{2.26 b}$$

The constants α_i, with $i = 1, 2, ... 24$ can be evaluated by establishing compatibility of deformation in displacement w, its slopes and curvatures at each of the four nodal points. The determination of these twenty-four generalized coordinates solves this interpolation problem in two dimensions.

First define a modified nodal displacement vector as:

$$\{\bar{\delta}_i\}^T = < w \quad b\theta_x \quad a\theta_y \quad a^2\phi_x \quad b^2\phi_y \quad ab\phi_{xy} > \tag{2.27 a}$$

or

$$\{\bar{\delta}_i\}^T = < w \quad b\frac{\partial w}{\partial y} \quad -a\frac{\partial w}{\partial x} \quad -a^2\frac{\partial^2 w}{\partial x^2} \quad -b^2\frac{\partial^2 w}{\partial y^2} \quad ab\frac{\partial^2 w}{\partial x \partial y} > \tag{2.27 b}$$

and similarly the corresponding modified element displacement vector

$$\{\bar{\delta}^e\}^T = < \bar{\delta}_i^T \quad \bar{\delta}_j^T \quad \bar{\delta}_k^T \quad \bar{\delta}_l^T > \tag{2.28}$$

After the enforcement of compatibility of deformation, the twenty-four equations in matrix form will be listed as:

$$\{\bar{\delta}^e\} = [\bar{C}]\ \{\alpha\} \tag{2.29}$$

where $[\bar{C}]$ is a square matrix of size 24 x 24, consisting of numbers only. This non-symmetric and fully populated transformation matrix can conveniently be inverted in a digital computer, and the unknown vector of generalized coordinates can be found from

$$\{\alpha\} = [\bar{C}]^{-1}\ \{\bar{\delta}^e\} \tag{2.30}$$

The inverse of matrix $[\bar{C}]$ remains the same for all elements involved in the analysis and must be evaluated only once. The value of the determinant of this matrix is a measure of how well this matrix is conditioned. No complications in the inversion process occur if the absolute value of the determinant is large. In fact, this was found to be so, underlining the importance of the choice of appropriate terms in a truncated polynomial expression. A bad choice could, in fact, lead to a singular matrix $[\bar{C}]$ and would thus complicate the inversion.

The unknowns in the final solution are listed in the originally defined nodal displacement vector; this vector being related to the modified nodal displacement vector by

$$\{\bar{\delta}^e\} = [T_1]\ \{\delta^e\}$$

where the transformation matrix $[T_1]$ is a diagonal matrix composed of four diagonal submatrices of the form

$$[T_1] = \begin{bmatrix} 1 & 0 & 0 & 0 & 0 & 0 \\ 0 & b & 0 & 0 & 0 & 0 \\ 0 & 0 & a & 0 & 0 & 0 \\ 0 & 0 & 0 & -a^2 & 0 & 0 \\ 0 & 0 & 0 & 0 & -b^2 & 0 \\ 0 & 0 & 0 & 0 & 0 & ab \end{bmatrix} \qquad (2.32)$$

The vector of generalized coordinates can therefore be found by the relationship

$$\{\alpha\} = [\bar{C}]^{-1} \; [T_1] \; \{\delta^e\} \qquad (2.33\,a)$$

or

$$\{\alpha\} = [C]^{-1} \; \{\delta^e\} \qquad (2.33\,b)$$

The transformation matrix $[T_1]$ being sparsely populated, the matrix product in Eq. 2.33 a can be evaluated in an efficient way. It is now possible to write the function describing the displacement within an element in terms of the nodal displacement components

$$w = w\,(x,y) = <P> \; \{\alpha\} = <P> \; [C]^{-1} \; \{\delta^e\} \qquad (2.34)$$

2.4.2 Derivation of Element Stiffness Matrices

In this section, the element stiffness matrix for the proposed refined element is generated. The derivation is valid for small strains and rotations; i.e. the linearized form of the strain-displacement equations is assumed to be valid.

For the purpose of a plate analysis, it is simplest to define the curvatures as generalized strains. In order to

properly evaluate the internal work in the determination of the strain energy, a factor of two must be added to the twisting curvature. This in turn allows the retention of the twisting moment M_{xy} only in the analysis, since M_{yx} is numerically identical. The curvatures are related to the lateral displacement by Eq. 2.20. As introduced in Section 2.2.1, and defined in Eq. 2.8 b, the vector of generalized strains can be written as:

$$\{\emptyset\}^T = < -\frac{\partial^2 w}{\partial x^2} \quad -\frac{\partial^2 w}{\partial y^2} \quad 2\frac{\partial^2 w}{\partial x \partial y} >$$

and the corresponding vector of generalized stresses (Eq. 2.8 a) as

$$\{M\}^T = < M_x \quad M_y \quad M_{xy} >$$

The vector of generalized strains must be related to the joint displacements. This vector can be written in terms of generalized coordinates by simply evaluating all needed derivatives:

$$\{\emptyset\} = [Q] \quad \{\alpha\} \tag{2.35}$$

Using Eq. 2.34, it follows immediately that

$$\{\emptyset\} = [Q] \quad [C]^{-1} \quad \{\delta^e\} = [B] \quad \{\delta^e\} \tag{2.36}$$

One of the essential features in a finite element displacement approach is the definition of the displacement field for the purpose of establishing this fundamental relationship.

Examining matrix [Q], it is of interest to note that the chosen displacement function permits a state of constant curvatures to exist, and hence, satisfies the criterion of constant strain, stated in Section 2.3.2.

The constitutive law for a linearly elastic material, already introduced in Section 2.2.1, is generally written in the form

$$\{M\} = [D] \quad \{\emptyset\} \tag{2.37}$$

where [D] is a symmetric elasticity matrix, relating generalized stresses (in this case, internal moments) to generalized strains (in this case, curvatures). For a general anisotropic material, matrix [D] is fully populated, and of the form

$$[D] = \begin{bmatrix} D_{11} & D_{12} & D_{13} \\ D_{21} & D_{22} & D_{23} \\ D_{31} & D_{32} & D_{33} \end{bmatrix} \tag{2.38 a}$$

Six constants at most are needed, since matrix [D] is always symmetric, i.e.

$$D_{ij} = D_{ji} \quad \text{for } i \neq j$$

Isotropic materials are characterized by only two constants, E and ν,

where E = Modulus of elasticity of plate material

ν = Poisson's ratio

Thus, for an isotropic material, matrix [D] will reduce to

$$[D] = \frac{Eh^3}{12(1-\nu^2)} \begin{bmatrix} 1 & \nu & 0 \\ \nu & 1 & 0 \\ 0 & 0 & \frac{1-\nu}{2} \end{bmatrix} \qquad (2.38\,b)$$

In this expression, h denotes the plate thickness. For an orthotropic plate material, with principal axis of orthotropy coinciding with the x and y axis of the local coordinate system, four constants are needed to define the behavior of the plate, i.e.

$$[D] = \begin{bmatrix} D_x & D_1 & 0 \\ D_1 & D_y & 0 \\ 0 & 0 & D_{xy} \end{bmatrix} \qquad (2.38\,c)$$

As shown in greater detail in Appendix I, the application of the principle of minimum total potential energy leads to the derivation of the element stiffness matrix:

$$[K^e] = \iint_A [B]^T [D] [B] \, dxdy \qquad (2.39)$$

Substituting Eq. 2.36 into the above equation yields

$$[K^e] = [C^{-1}]^T \left(\iint_A [Q]^T [D] [Q] \, dxdy \right) [C^{-1}] \qquad (2.40)$$

In the above formula, the integration is to be carried out over area A of the finite element. The introduction of non-dimensionalized

coordinates leads to a particularly simple integration. This integration could in fact be carried out automatically due to the simplicity of the terms to be integrated. The integration was performed algebraically, considering one term of the elasticity matrix [D] at a time. The matrices within the integration can easily be multiplied out and integrated without difficulty. This operation leads to the final expression for the stiffness matrix of the refined rectangular plate element. Assuming orthotropic material it can be written as:

$$[K^e] = [C^{-1}]^T \left(D_x [K_1] + D_1 [K_2] + D_y [K_3] + D_{xy} [K_4] \right) [C^{-1}] \quad (2.41)$$

This derivation is described in more detail in Appendix I, where the component matrices $[K_i]$, $i = 1, 2, 3, 4$, are listed.

The final evaluation of the element stiffness matrix, which is of size 24 x 24, is performed in the digital computer. It should be noted that the component matrices $[K_i]$, $i = 1, 2, 3, 4$, are sparsely populated, and if made use of in the actual computations, this property would reduce the time required for the generation of the element stiffness matrix. Furthermore, use can be made of the fact that all component matrices are symmetric.

The resulting element stiffness matrix generated is a symmetric, square and singular matrix. Its singularity stems from the fact that rigid body displacements are included in the assumed displacement function, as given by Eq. 2.24. Enforcing known

boundary conditions, these rigid body modes will be eliminated after the formulation of the overall stiffness matrix.

The system stiffness matrix can be assembled as described in Section 2.3.1. The element stiffness matrix, as derived above, is referred to the local coordinate system. The first step in the assembly procedure would be to transfer this relation to a global or reference coordinate system. However, in the present investigation the local coordinate system is always parallel to the global coordinate system, therefore the stiffness relations established need not be transformed. The formation of the complete stiffness matrix for the discretized plate structure is finally accomplished by the direct addition of appropriate element stiffnesses at nodal points.

2.4.3 Kinematically Consistent Force Vectors

Applied loads are usually distributed on structural elements. Equivalent concentrated forces, at the location and in the direction of the global or reference coordinate system, are required for the analysis. In addition, concentrated forces may be applied at points other than nodal points of an element, and forces caused by initial strain conditions need to be considered. The latter may be caused by temperature, shrinkage, or lack of fit. Considering all of these contributions, the basic stiffness equation for an element can be cast into the form

$$\{R\}^e = [K^e]\ \{\delta^e\} + \{F\}^e_p + \{F\}^e_c + \{F\}^e_i \qquad (2.42)$$

where: $\{R\}^e$ = Vector of external forces applied at the nodes

$\{F\}^e_p$ = Nodal forces required to balance distributed loads

$\{F\}^e_c$ = Nodal forces required to balance concentrated forces acting within an element

$\{F\}^e_i$ = Nodal forces required to balance initial strains caused by temperature, lack of fit, etc.

The final system of simultaneous equations is obtained by establishing equilibrium at all nodal points. Each external force component must be equated to the sum of the component forces contributed by the elements meeting at the node in consideration. All forces can be collected and the final equilibrium equation can be written in the form:

$$\{F\} = [K] \quad \{\delta\} \tag{2.43}$$

where: $\{\delta\}$ = Overall systems displacement vector

$\{F\}$ = Resultant systems force vector consistent with the overall displacement vector

$[K]$ = Overall structural stiffness matrix

For all common loading conditions, the equivalent concentrated nodal forces can be determined from an energy approach which is consistent with the evaluation of the element stiffness matrix. For example, for distributed loads $p(x,y)$, defined as acting on

a unit area of the element, this derivation leads to the following equivalent nodal force vector

$$\{F\}_p^e = -[C^{-1}]^T \iint_A \langle P \rangle^T \, p(x,y) \, dxdy \qquad (2.44)$$

This vector is listed in Appendix II along with a more detailed description of the derivation.

2.4.4 Enforcement of Boundary Conditions

The system of linear simultaneous equations represented by Eq. 2.43 can only be solved after sufficient boundary conditions are prescribed. The equation includes the rigid body displacements of the structure. Therefore, a minimum number of prescribed displacements must be substituted in the equation. The number of kinematic restraints prescribed is usually far greater than the number required to prevent rigid body motions. These constraints can be imposed by deleting appropriate rows and columns of the system stiffness matrix. This constitutes a relatively cumbersome and time consuming procedure for an automatic computation, though it results in a reduction of the total number of equations.

This investigation uses a more convenient approach, proceeding with a direct solution of the original number of equations to avoid rearranging of rows and columns. In this approach, the diagonal element of the system stiffness matrix, at the point concerned, is multiplied by a very large number. At the same time the term on the left-hand side of the equation, i.e. the element

of the global force vector at the point concerned, is replaced by the same large number multiplied by the prescribed displacement value. The effect of these manipulations is to replace the original equation by one which states that the displacement in question is equal to the specified displacement. This procedure of enforcing boundary conditions is easily implemented in a general computer program, and all programs described in this report operate successfully, using this approach.

The deformed shape of a plate structure must be found in such a way that all boundary conditions adhering to a problem under consideration are satisfied. In a finite element displacement approach, such restraints can be at the selected nodal points only, since only the deformation components at the nodes are entered as field quantities. Boundary conditions in plate bending problems usually include both the force (or static) and displacement (or kinematic) types. Only displacement type boundary conditions, i.e. restraints which can be expressed in terms of displacement components, can usually be satisfied in a pure finite element displacement approach. However due to the fact that in the present approach the three curvature terms are included in the final displacement vector, certain types of plate boundary conditions can be approximated more closely if the plate is made of isotropic or orthotropic material.

Some common boundary conditions to be satisfied in a plate problem, along with the associated constraint equations, are listed in Fig. 6. The top half of the figure lists the boundary

conditions as introduced in conventional plate theory. As derived in Section 2.2.1, the internal moments are linear combinations of the curvatures of w. The introduction of the curvatures as nodal parameters also makes it possible to exactly satisfy some static boundary conditions. If the boundary conditions of a simply supported plate are considered (Fig. 6) the classical theory of thin plates requires the following boundary conditions to be satisfied, at x = a

$$w = 0 \tag{2.44 a}$$

$$\theta_x = \frac{\partial w}{\partial y} = 0 \tag{2.44 b}$$

$$M_x = -D \left(\frac{\partial^2 w}{\partial x^2} + \nu \frac{\partial^2 w}{\partial y^2}\right) = 0 \tag{2.44 c}$$

A conventionally formulated displacement approach will not satisfy Eq. 2.44 c, called the static boundary condition. However, from the geometry of the deformed plate surface, it is known that

$$\frac{\partial^2 w}{\partial y^2} = 0 \tag{2.45 a}$$

along the straight and simply supported edge at x = a. From a consideration of the static boundary condition (Eq. 2.44 c) it can be concluded that the following equation will also hold

$$\frac{\partial^2 w}{\partial x^2} = 0 \tag{2.45 b}$$

Therefore, the proposed approach allows all boundary conditions

associated with a simply supported edge to be satisfied exactly. This conclusion is only valid if no externally applied moments are acting along the boundary under consideration.

Similarly, the boundary conditions associated with a clamped edge can also be satisfied exactly, as this can be done in the conventional displacement approach where only displacement-type boundary conditions are to be met.

The boundary conditions for a free edge are due to Kirchhoff (Ref. 46), and are listed in the classical theory as follows:

$$V_x = Q_x - \frac{\partial M_{xy}}{\partial y} = 0 \qquad (2.46\ a)$$

$$\frac{\partial^3 w}{\partial x^3} + (2 - \nu) \frac{\partial^3 w}{\partial y^2} = 0 \qquad (2.46\ b)$$

and

$$M_x = 0 \qquad (2.47\ a)$$

or

$$\frac{\partial^2 w}{\partial x^2} + \nu \frac{\partial^2 w}{\partial y^2} = 0 \qquad (2.47\ b)$$

The condition for zero vertical reaction at the free edge cannot be satisfied since in the present approach it is not possible to express this quantity in terms of nodal parameters. This is due to the fact that no third order derivatives are listed in the vector of unknown nodal displacement components. The requirement of zero normal moment could be satisfied exactly if, instead of the curvature

terms, their linear combinations, i.e. internal moments, would be introduced in the displacement vector. However, since the case of a free edge is relatively rare, no effort was made in this investigation to arrive at a more refined approach for satisfying this particular boundary condition.

2.4.5 Solution of the Stiffness Equations

The displacement approach as described in Section 2.3.1, and in more detail in Ref. 14, leads very often to a large system of linear simultaneous equations. In this set, the structure stiffness matrix connects the known vector of generalized forces to the unknown vector of generalized displacements. This matrix is always positive definite and symmetric for a linear elastic analysis. In addition, the stiffness matrix is usually well-conditioned and sparsely populated, and with adequate arrangement of the equations narrowly banded. These properties permit a very efficient, automatic assembly and solution of large systems.

The time required for the solution of the set of simultaneous equations is the single most important expense in solving large scale problems. Hence, the availability of an efficient solution technique is of upmost importance in solving elastic, and especially elastic-plastic, problems.

There are two fundamental groups of methods for solving linear algebraic equations, the methods of iteration or relaxation, and methods based on elimination. The main advantages of iterative

solution techniques are the relatively easy coding of such methods and the small amount of computer storage required. Solutions can be obtained with reasonable computer time if the governing system of equations is well-conditioned. The latter requirement is not always met and considerable difficulties may be experienced in solving large ill-conditioned systems. Though these methods can be efficiently applied in the solution of linear elastic problems, their application in solving elastic-plastic problems is doubtful due to the fact that the initially elastic and diagonally dominant system can become ill-conditioned at latter stages following extensive plastic flow. At such a stage, the diagonal elements of the stiffness matrix become small compared to the off-diagonal elements. For this reason, iterative or relaxation methods can become inefficient in solving elastic-plastic problems. In addition, elastic-plastic procedures require the solution of the stiffness equations in incremental form if the complete load-deflection behavior of a structure is sought. Each step, in turn, requires an iterative solution technique itself, and hence, the entire analysis would become too time-consuming. Furthermore, iterative methods do not allow multiple load vectors to be processed simultaneously. This is a serious drawback in the elastic analysis of structures subjected to many different loading conditions.

On the other hand, elimination methods do not require a well-conditioned system; only the number of equations to be solved and the bandwidth of the system are important. These methods do,

however, require larger amounts of computer storage. The Choleski decomposition method is among the most efficient and accurate elimination methods. This method was chosen as basis for the solution of the resulting set of stiffness equations, for all the analyses presented in this report. The key to this method is the fact that any symmetric square matrix can be expressed as the product of an upper and a lower triangular square matrix. Hence, it is possible to decompose the symmetric and banded structure stiffness matrix [K] into the product of a triangular matrix [L] and its transpose $[L]^T$, as shown in Fig. 7. This can be written as:

$$[K] = [L] \quad [L]^T \tag{2.48}$$

in which the terms $L_{ij} = 0$ for $i < j$, and $L_{ij}^T = 0$ for $i > j$. Hence, the first step in this approach is to decompose matrix [K] into these two component matrices. It is observed that both of these matrices are also of banded nature with a bandwidth which is equal to half the bandwidth of the system stiffness matrix. Considering the special coordinate system introduced, the elements of [L] can be obtained by simple recursive relations. It is further noted that in order to calculate column j of [L], only the elements in the shaded triangular area, as shown in Fig. 7, and the elements of column number j of the original matrix [K] are required. The fundamental stiffness equation, Eq. 2.43, can now be written in the form:

$$[L] \quad [L]^T \quad \{\delta\} = \{F\} \tag{2.49}$$

Introducing an auxiliary vector, defined as:

$$\{Y\} = [L]^T \{\delta\} \tag{2.50}$$

the stiffness equation can be written as

$$[L] \{Y\} = \{F\} \tag{2.51}$$

The solution of the original stiffness equation is accomplished in two steps: first vector $\{Y\}$ is found by a forward sweep, and the unknown vector $\{\delta\}$ is finally determined by backward substitution of $\{Y\}$ into Eq. 2.50.

The fact that only a small part of the overall matrix is used at any time during processing is of considerable importance in the development of finite element programs capable of handling structures involving many thousands of degrees of freedom. In order to save on core storage, the stiffness matrix is generated in blocks in the present approach, and the information is transferred to magnetic disc storage. The efficient use of the OVERLAY feature and of magnetic discs allows large scale problems to be treated using relatively little computer storage. A subroutine, capable of handling large banded systems of simultaneous equations was developed, based on the above described decomposition technique. The amount of information needed for processing at any time can be adjusted, and is called from discs accordingly.

The analyzed examples show that the described direct elimination technique is very efficient and accurate. The fact

that multiple load vectors can be processed at the same time, allows complex structures to be analyzed for different loading conditions in a very efficient way. Provided the bandwidth is not excessive, this method also proved to be very powerful for the elastic-plastic analysis of plates, as described in a subsequent section.

It should be noted in this context that for a large bandwidth, the described method, which operates on all elements within the band, may require considerable computer time. Improved solution routines, processing non-zero elements or submatrices only, have been developed in recent years. Whetstone (Ref. 55) presented recently a method which virtually eliminates both trivial arithmetic and wasted data storage space. Melosh (Ref. 35) describes a solution algorithm based on the wavefront concept and a modified Gauss algorithm.

According to these authors, such approaches can treat larger problems than bandwidth programs, involve negligible penalities, and at the same time, yield more accurate solutions than approaches using the Choleski algorithm. However, such approaches clearly involve years of intensive research, and hence, were not possible to accomplish within the framework of this investigation.

2.5 Examples of Solution

2.5.1 Selected Examples

The following examples have been selected to illustrate

the application of the derived refined finite element, and to discuss its rate of convergence and accuracy. To simplify the comparison with analytic solutions, isotropic material is assumed and only simple examples are chosen. It should be noted here that the general computer program developed is capable of handling plates of arbitrary geometry, as defined in Section 2.1, and orthotropic material can be treated.

Four example problems, schematically represented in Fig. 8, have been selected in this investigation. For all problems, four different meshes, as shown in Fig. 9, were processed with the mentioned digital computer program, using the derived refined element as the basic element. Making use of symmetry, only one quadrant of each problem was analyzed. All structures were subjected either to a uniformly distributed load, or a single concentrated load acting at the center of the plate. The equilibrium equations were solved using the very efficient solution technique described in Section 2.4.5. All runs were processed in the CDC 6400 computer of the Lehigh University Computing Center.

In a first example (Problem P1), a square isotropic plate with four fully fixed boundaries was discretized using the four meshes shown in Fig. 9. The boundary conditions, as described in Section 2.4.4, can be satisfied exactly for this example. Poisson's ratio was assumed to be $\nu = 0.30$.

Problem P2 represents the analysis of a simply supported square isotropic plate. Again all boundary conditions can be

satisfied exactly, and the same value for ν was assumed as in Problem P1.

In a third example (Problem P3), a panel of a plate supported by rows of equidistant columns (flat plate) was analyzed. In order to be able to compare with available solutions, a value of $\nu = 0.20$ was chosen for this example. All boundary conditions can be deduced from the geometry of the deflected surface and can be satisfied exactly. To simplify this problem, it was assumed that the cross-sectional dimensions of the columns were small in comparison to the span of the plate panel, and could be neglected in so far as deflection and moments at the center of the plate are concerned. Timoshenko (Ref. 46) has discussed in length the implication of this assumption. However, the dimensions of the columns could be easily included in the analysis.

The fourth example (Problem P4) is a square isotropic plate supported by columns at the corners only. As discussed in Section 2.4.4, the boundary conditions for free edges cannot be satisfied exactly by the presented finite element approach. This example was chosen to study the effect of this deficiency. No exact solution to this problem is available, though various experimental and approximate solutions are known.

2.5.2 Accuracy and Convergence of Solutions

The plate geometry and the finite element idealization of the selected examples are shown in Fig. 8 and Fig. 9,

respectively. For the four problems, Tables 1, 2, and 3 list in sequence, the computed center deflection for both loading cases, along with some results found from existing plate elements and the exact values, where available (Ref. 46). Excellent accuracy and convergence is observed for both loading cases. The complete deflection profiles along a center-line of the plate together with exact values, are given in Table 4 for uniformly distributed loading and in Table 5 for the case of a single concentrated load. Exact values were found by evaluating the series solutions derived in Ref. 1 at all points of interest. Good agreement of displacements is apparent, as the convergence is fast and monotonic.

Tables 6 through 9 list the computed internal moments M_x and M_y along a center-line of the plate, together with exact values, where available. It can be seen that even for relatively rough meshes, the computed values for internal moments show good accuracy. Finally, Table 10 shows the internal twisting moment along a diagonal of the plate for the case of uniformly distributed load. From the results found, it is evident that excellent accuracy for displacements and internal moments is obtained with the refined plate element.

In order to study the effect of the enforcement of boundary conditions, as discussed in Section 2.4.4, a number of comparisons have been made. For the purpose of these comparisons the following types of boundary conditions can be defined:

Type I: Only displacement type boundary conditions associated with w, $\partial w/\partial x$ and $\partial w/\partial y$ are enforced.

Type II: In addition to the constraints of Type I, curvature terms derived from a knowledge of the geometry of the deflected surface are enforced.

Type III: In addition to the constraints of Type II, curvature terms derived from static considerations are enforced.

Tables 11 and 12 list, in part, the results of this investigation. In the conventional finite element displacement formulation, which is based on three degrees of freedom per node, i.e. on deflection w and its first derivatives, only boundary conditions of Type I can be satisfied. The present formulation also allows the enforcement of boundary conditions of the Types II and III. Comparing the computed values for the center deflection of problems P1 and P2 for the different types of boundary conditions enforced, it can be stated that if boundary conditions of Types II and III are enforced, then the structures tend to become stiffer. However, for finer meshes no difference can be recognized, thus leading to the conclusion that the imposition of additional curvature constraints does not improve the computed center deflection. As can be seen from Tables 13 and 14, in which results from this investigation for internal moments are compiled, the imposition of additional curvature terms does, however, improve the moment field, especially in the vicinity of the boundaries.

2.5.3 Comparison with Existing Plate Elements

Results found in the literature for the different elements discussed in Section 2.3.4, are compiled in Tables 1, 2, and 3. Internal moments are mostly reported in the form of graphs, thus lacking the numerical accuracy needed for an exact comparison. Hence, in order to be able to compare the results obtained with the refined plate element, missing internal moments were found for the ACM (Ref. 1) element in particular, using an auxiliary finite element plate program.

A direct comparison of the different finite elements used in the examples, in terms of mesh size, is not appropriate, since the computational effort is different for different elements and meshes. Most results available in the literature are listed separately for each mesh, and hence Tables 1, 2, and 3 were set up for reference only.

In a finite element approach involving fine meshes, the major part of the computer time required is used for the solution of the typically large system of simultaneous equations. Hence, a more reasonable way of comparing the results is to plot the percentage error in deflection or internal moment against the number of degrees of freedom; the solution time being directly proportional to this number in the proposed decomposition technique. The total number of degrees of freedom is defined here as the number of nodal points involved in the analysis, times the number of degrees of freedom per nodal point.

In Figs. 10, 11, 12, and 13 the percentage error in central deflection is plotted against the number of degrees of freedom of a problem for different finite elements for plate bending. Clearly, the new element shows improved results over most other elements at a given number of degrees of freedom. Similarly, in Figs. 14 and 15, the percentage error in internal moments is plotted against the total number of degrees of freedom.

As already pointed out in Section 2.3.4, existing plate elements are deficient because they are not capable of predicting internal moments with sufficient accuracy, unless very fine mesh idealizations are used. It may be added that the evaluation of internal moments using some of these elements represents a significant computational effort. As shown in the above-cited figures, the refined element is capable of determining reliable internal moment values even for relatively rough meshes, thus confirming one of the basic ideas for the derivation of this element.

An even better index for comparison would be the time of the computational effort needed for the entire solution of larger sized problems. In fact, the computer time needed to generate the element stiffness matrices, to assemble the system stiffness matrix, to generate force vectors, to solve the resulting large system of simultaneous equations, and finally, to find all internal moments would be a better measure for the discussion of the relative merits of different proposed elements.

2.6 Summary

A refined rectangular plate element for use in a finite element analysis of arbitrarily shaped plates is presented. Along with the three usual nodal displacements, three curvature terms are entered as unknowns in the vector of generalized displacements. Results found for four example solutions indicate that the refined element gives very good accuracy for displacements as well as for internal moments. The new approach, though of a non-conforming type, leads to a better accuracy at any given number of degrees of freedom than obtained with most presently known rectangular or quadrilateral finite elements.

3. ANALYSIS OF STIFFENED PLATES

3.1 Introduction

In this chapter, an analysis of complex shaped stiffened plates, as shown in Fig. 16, using the finite element stiffness approach is presented. Some of the currently used approximate analysis techniques applicable to beam-slab type structures are discussed. This survey of available methods of analysis shows that there is as yet no fully adequate method of analysis capable of determining stresses and deformations in complex shaped beam-slab type structures.

It is shown that a stiffened plate structure can adequately be discretized using plate and stiffener elements. Stiffness matrices for bending and in-plane behavior are derived for the beam and plate elements. A new approach for the evaluation of the St. Venant torsional constant is presented, and the stiffness relations associated with torsion in the stiffener elements are derived. Also discussed are the assembly of the stiffness matrix and the solution of the final set of equilibrium equations.

The outlined approach is applied to the analysis of a beam-slab highway bridge which was field tested. An extensive study of the effects of the variables governing the lateral load distribution is made, demonstrating the applicability and versatility of the proposed approach. The inclusion of curb and parapet sections, as well as diaphragms, in the analysis is discussed. Finally,

convergence and accuracy of the method are studied (Refs. 53 and 54).

3.2 Methods of Analysis for Stiffened Plate Structures

A structural analysis is performed in order to determine stresses and deformations at selected points of a structure which is subjected to external forces, or constraint to deform, in a prescribed pattern. In this section, a short survey of some available methods of analysis of plate-beam type structures is given. A complete survey of the state of the art of current grillage design was made by Kerfoot and Ostapenko (Ref. 29).

For a beam-slab type structure, an elastic analysis can be formulated by combining the classical beam and plate theories. As is usually done in continuum mechanics, the equations of equilibrium and compatibility, together with the stress-strain relations, could be used to develop a set of partial differential equations for deformations or stresses at every point of the structure. However, the exact solution of these equations is virtually impossible for complex shaped structures, because of the task of determining suitable solution functions which satisfy both the governing differential equations and the specified boundary conditions. The assumptions introduced in the theory of plates and the conventional beam theory allow for a reduction in the number of independent variables and make certain boundary conditions more tractable. These assumptions of the conventional plate theory which are applicable to thin plates are listed in Section 2.2.

In classical beam theory it is assumed that all deformations can be described in terms of the displacements of the longitudinal axis and the rotation of the beam cross-section. The latter assumption precludes a deformation of the cross-section, and hence, strains normal to the longitudinal axis are neglected. Formulating equilibrium of a beam element leads to a set of three differential equations.

Conceptually at least, plate and beam theories can be directly applied to the analysis of stiffened plate type structures. For this purpose, different physical models are used to represent the beam-slab type structure. These models are highly redundant. The compatibility and the load-deformation behavior of the elements of the models must be taken into account to develop the additional requirements beyond those obtained from static equilibrium in order to determine the response of the assumed model. A force or deformation method of analysis is usually applied to solve for the unknown quantities. However, by inspecting the resulting partial differential equations it can be recognized that these equations are not readily solvable for other than simple structures.

Often the effective width concept is utilized to reduce the analysis of stiffened plates to the analysis of the stiffeners. This approach assumes that the stiffeners behave as beams, the flanges of which are made up of some portion of the slab. The portion of the plate assumed to act effectively as a flange of the

consisting of a concrete slab acting compositely with steel beams. Bares and Massonnet (Ref. 7) have published a book devoted to the analysis and design of grillages under transverse loads by means of the orthotropic plate theory. This approach cannot be used to adequately predict the state of stress in the plate and the governing differential equations are again difficult to solve for other than simply bounded structures.

Another group of approaches are the discrete element methods. These methods replace the actual structure by a system of discrete elements which leads to a set of simultaneous algebraic equations. These equations are developed directly by replacing the differential equation by the corresponding finite difference equations. Hrennikoff (Ref. 27) presented a number of gridwork models for the solution of plate bending and elasticity problems, along with guidelines for establishing the equivalence between the model and the continuum. Newmark (Ref. 37) has proposed a model made up of rigid bars and springs for plate bending. Recently, Lopez and Ang (Ref. 32) developed a lumped parameter model by means of which the effects of large deformation and inelastic behavior can be included in the analysis of plates. In order to simplify the problem, the analysis herein has been restricted to sandwich plates. Although the formulation would become more difficult, this method could probably be used to analyze stiffened plates.

To analyze complex shaped stiffened plate structures, the finite element method is found to be best suited. For reasons

explained in Chapter 1, the finite element displacement approach is preferable. Gustafson (Ref. 25) has employed the finite element approach in the analysis of skewed grillage structures subjected to transverse loads. The results of this analysis were found to compare well with the results of tests performed on such structures. Little work has been done to take into account second order effects and inelastic action of the material in the analysis of plates and virtually no work has been done as far as stiffened plate structures are concerned.

3.3 A Finite Element Analysis of Stiffened Plates

3.3.1 Application of the Method to the Plate and Stiffener System

In this section, the application of the finite element displacement approach in the analysis of beam-slab type structures is described. The beam-slab type structure, shown in Fig. 16, can be bounded by arbitrarily shaped boundaries as long as they fit into a rectilinear mesh. The plate is stiffened by a set of beams running in longitudinal direction, which is assumed to be parallel to the global x-axis for all further discussions. In addition, a set of transverse stiffeners (called diaphragms) can be present although their inclusion in the analysis will be discussed in a later section. Neither the plate nor the stiffeners need to be of uniform thickness.

The first step is to discretize the structure into a

suitable number of finite plate and stiffener elements. In order to arrive at a simple formulation for this analysis, it is necessary that the stiffeners are attached along the mesh lines of the plate elements. However, they need not be continuously attached along the entire plate. Two types of finite elements, plate and stiffener elements, are needed to discretize the structure. In order to be able to study the convergence behavior of the method with respect to the criterion postulated by Melosh (Ref. 34) the broader mesh must always be contained in the next finer mesh. As shown in Fig. 16, a rectangular element involves the four nodal points I, J, K and L, and the beam element, being a straight line element, involves the two nodal points I and K. The mesh lines, or surfaces of separation, are again to be considered imaginary. The structure can be arbitrarily loaded by concentrated loads or uniformly distributed loads.

Due to the fact that the stiffeners are eccentrically attached to the plate, coupling between bending and stretching exists in the middle plane of the plate, and hence, in-plane deformations must be considered. The approach is described assuming small deformation theory and linearly elastic material. It should be noted that elements of different shapes can easily be used in combination in a finite element displacement approach, if they possess the same number of degrees of freedom at all common nodes. Here, all nodal points are best defined in a common plane. This plane will be called plane of reference for all further discussions, and

is assumed to coincide with the middle plane of the plate. The response of the beams must first be found with respect to this plane, and one of the objectives of this report is to illustrate how the eccentricity of the stiffeners can be taken into account.

Five displacement components are introduced as unknowns at each nodal point in the present approach. These are the displacement u in x-direction and the displacement v in y-direction. In addition, the deflection w and the two slopes θ_x and θ_y are considered. These five deformation components enable the description of the state of deformation in a plate and stiffener element. An analysis based on small deformation theory is greatly simplified since the in-plane and the out-of-plane stiffness matrices of the involved finite elements can be derived separately. However, deformation compatibility between beam and plate elements must be enforced and overall equilibrium must be established at each nodal point.

3.3.2 Derivation of Bending and In-Plane Plate Stiffness Matrices

The classical theory of plates assumes that the state of deformation in the plate can be described entirely in terms of the deformations of the middle plane of the plate. Basically, the refined plate element, as described in Chapter 2, could be used in representing the plate behavior of the stiffened plate structure. However, due to the presence of the torsional resistance of

the beam elements, discontinuities in some curvature terms occur along the lines of intersection of the stiffeners with the plate. Since these terms were entered as unknowns in the nodal displacement vector and made continuous at the nodal points, the refined element is best not used in the present approach. Basically, any known finite element could be used to represent the out-of-plane plate behavior.

For the present analysis, the ACM element, as originally proposed by Adini, Clough and Melosh (Ref. 1) and described in detail by Zienkiewicz (Ref. 56), is taken to represent the out-of-plane plate behavior. An incomplete third-order polynomial, as indicated in Fig. 5, is assumed for the representation of the displacement behavior within the element:

$$w = w\ (x,y) = \alpha_1 + \alpha_2 x + \alpha_3 y + \alpha_4 xy + \ldots + \alpha_{12} xy^3 \qquad (3.1)$$

Although this element is of the non-conforming type, it yields reasonably accurate results. The vertical displacement w and the two slopes θ_x and θ_y are entered as unknowns in the nodal displacement vector. Since this element will also be used for the elastic-plastic analysis of plates and stiffened plates, which will be presented in later chapters, the stiffness matrix is presented in Appendix III.

In order to determine the stiffness characteristics of the entire structure, which are required in the analysis, the stiffness properties of the plate elements for in-plane behavior

must also be established. As shown in Fig. 4, the displacement components governing the in-plane behavior are denoted by u and v, respectively. The selection of appropriate displacement functions is again subject to the requirements listed in Section 2.3.2. If the stiffness for a rectangle in plane stress is sought, eight force-displacement equations are to be formulated. Clough (Ref. 14) suggested the following functions:

$$u = \alpha_1' + \alpha_2' x + \alpha_3' y + \alpha_4' xy \tag{3.2}$$

$$v = \alpha_5' + \alpha_6' x + \alpha_7' y + \alpha_8' xy \tag{3.3}$$

A prime is attached to the unknown generalized coordinates to underline that they are not the same set as originally used. From Pascal's triangle, as shown in Fig. 5, it is noted that all of the constant and linear terms are chosen, along with one of the quadratic terms. The chosen functions are not complete polynomials. But, with the choice of the symmetric terms $\alpha_4' xy$ and $\alpha_8' xy$, and because of the geometric symmetry of the element itself, no preferential direction exists. Inclusion of all pertinent constant strains is assured, as well as proper representation of the rigid body motion states. From the equations it can be concluded that all edges displace as straight lines. Hence, the chosen displacement functions automatically guarantee continuity of displacement with adjacent elements. The assumed shape functions are of the conforming type

and since all the criteria listed in Section 2.3.2 are met, convergence to the true solution should occur. Enforcing compatibility of deformation at all nodal points, the unknown vector of generalized coordinates can be determined. The evaluation of the stiffness matrix governing the in-plane behavior of the plate element follows standard procedures. This derivation is performed in more detail in Appendix IV.

3.3.3 Derivation of Bending and In-Plane Beam Stiffness Matrix

The final stiffness relations for the stiffened plate structure express equilibrium at nodal points lying in the plane of reference. The response of the beams with respect to this plane of reference is needed. It is first assumed that a stiffener, as shown in Fig. 17, is attached to the plate along a boundary of the rectangular plate element. Next, it is assumed that external loads are applied only at plate elements or directly at the nodal points. Furthermore, it is assumed that the stiffener is symmetric with respect to its local z-axis, and weak in bending about this axis. In addition, shearing deformations are neglected. It should be noted that some of these restrictions could be lifted in a more refined analysis.

Owing to the above assumptions, only four of the five displacement components introduced at each nodal point of the reference surface are used to describe the behavior of the stiffener

element. The assumed displacement function for the in-plane behavior of the plate element predicts straight lines for the edges of the deformed plate elements. Consequently, no bending moments about the local z-axis are taken by the stiffener elements. Hence, the displacement component v in the direction of the y-axis does not need to be considered in describing the behavior of the beam elements. Since the stiffener element is assumed to be integrally attached to the plate, compatibility of deformation must be enforced along the juncture line between beam and plate. The same displacement functions chosen for the in-plane and the out-of-plane behavior of the plate element must be taken for the stiffener element in order to be able to satisfy this requirement:

$$u = \alpha''_1 + \alpha''_2 x \tag{3.4 a}$$

$$w = \alpha''_3 + \alpha''_4 x + \alpha''_5 x^2 + \alpha''_6 x^3 \tag{3.4 b}$$

Introducing the nodal displacement vector for node I of the beam element associated with its bending and in-plane behavior:

$$\{\delta^s_i\}^T_B = < u \quad w \quad \theta_y > \tag{3.5}$$

the element displacement vector needed for the generation of the stiffness matrix governing bending and in-plane behavior can be written as:

$$\{\delta^s\}^T_B = < u_i \; w_i \; \theta_{yi} \quad u_k \; w_k \; \theta_{yk} > \tag{3.6}$$

Enforcing compatibility at the two nodal points I and K leads to six algebraic equations which can be written as:

$$\{\delta^s\}_B = [C_s''] \quad \{\alpha''\} \tag{3.7}$$

where the vector of generalized coordinates is defined as:

$$\{\alpha''\}^T = < \alpha_1'' \quad \alpha_2'' \quad \alpha_3'' \quad \alpha_4'' \quad \alpha_5'' \quad \alpha_6'' > \tag{3.8}$$

These six generalized coordinates are uniquely defined by the nodal displacements introduced at the ends of the stiffener element. Inversion of Eq. 3.7 leads to

$$\{\alpha''\} = [C_s'']^{-1} \quad \{\delta^s\}_B \tag{3.9 a}$$

which can be written explicitely as:

$$\begin{bmatrix} \alpha_1'' \\ \alpha_2'' \\ \alpha_3'' \\ \alpha_4'' \\ \alpha_5'' \\ \alpha_6'' \end{bmatrix} = \begin{bmatrix} 1 & 0 & 0 & 0 & 0 & 0 \\ -1/L & 0 & 0 & 1/L & 0 & 0 \\ 0 & 1 & 0 & 0 & 0 & 0 \\ 0 & 0 & -1 & 0 & 0 & 0 \\ 0 & -3/L^2 & 2/L & 0 & 3/L^2 & 1/L \\ 0 & 2/L^3 & -1/L^2 & 0 & -2/L^3 & -1/L^2 \end{bmatrix} \begin{bmatrix} u_i \\ w_i \\ \theta_{yi} \\ u_k \\ w_k \\ \theta_{yk} \end{bmatrix} \tag{3.9 b}$$

Using the displacement relations, which, for the case of a uniaxially stressed stiffener, reduce to

$$U(z) = u - z \frac{\partial w}{\partial x} \tag{3.10}$$

in which u is the displacement in x-direction of a point lying in the reference surface, and U is the displacement in x-direction of a point lying outside this plane, the strain-displacement relation can be written as:

$$\epsilon_x = \frac{\partial U}{\partial x} = \frac{\partial u}{\partial x} - z \frac{\partial^2 w}{\partial x^2} \tag{3.11}$$

Introducing Hooke's law, which for the present case reduces to its simplest form, leads to the stress-displacement relation:

$$\sigma_s = E_s \left[\frac{\partial u}{\partial x} - z \frac{\partial^2 w}{\partial x^2} \right] \tag{3.12}$$

The joint forces shown in Fig. 17 associated with the joint displacements must be defined at the location and in the direction of these deformation components. Forces defined at the centroid of the beam element could be found using an appropriate transformation matrix which would have to be derived from a consideration of equilibrium of forces applied to the stiffener element. Integrating the stresses with respect to the plane of reference, and using Eq. 3.12 leads to

$$N_s = \iint_{A_s} \sigma_s \, dA_s = E_s \left[\frac{\partial u}{\partial x} A_s - \frac{\partial^2 w}{\partial x^2} S_s \right] \qquad (3.13\,a)$$

$$M_s = \iint_{A_s} \sigma_s \, z \, dA_s = E_s \left[\frac{\partial u}{\partial x} S_s - \frac{\partial^2 w}{\partial x^2} I_s \right] \qquad (3.13\,b)$$

where: E_s = Modulus of elasticity of stiffener

A_s = Cross-sectional area of stiffener

S_s = First moment of the stiffener area with respect to the plane of reference

I_s = Moment of inertia of the stiffener area with respect to the plane of reference

Eqs. 3.13 a and 3.13 b, constituting the force-displacement relations for the eccentrically stiffened beam element, can be written in the form:

$$\begin{bmatrix} N_s \\ M_s \end{bmatrix} = E_s \begin{bmatrix} A_s & S_s \\ S_s & I_s \end{bmatrix} \begin{bmatrix} \frac{\partial u}{\partial x} \\ -\frac{\partial^2 w}{\partial x^2} \end{bmatrix} \qquad (3.14\,a)$$

or simply as:

$$\{M_s\} = [D_s] \{\epsilon_s\} \qquad (3.14\,b)$$

This equation relates the internal stress resultants acting on a stiffener element, and defined at nodal points lying in the plane of reference, to the vector of generalized strains. The vector of

generalized strains can be found in terms of the vector of generalized coordinates making use of the assumed displacement fields:

$$\begin{bmatrix} \frac{\partial u}{\partial x} \\ -\frac{\partial^2 w}{\partial x^2} \end{bmatrix} = \begin{bmatrix} 0 & 1 & 0 & 0 & 0 & 0 \\ 0 & 0 & 0 & 0 & -2 & -6x \end{bmatrix} \begin{bmatrix} \alpha_1'' \\ \alpha_2'' \\ \alpha_3'' \\ \alpha_4'' \\ \alpha_5'' \\ \alpha_6'' \end{bmatrix} \qquad (3.15\text{ a})$$

which can be simply written as:

$$\{\epsilon_s\} = [Q_s] \quad \{\alpha''\} \qquad (3.15\text{ b})$$

in which the matrix $[Q_s]$ is found by differentiating Eqs. 3.4. Making use of Eq. 3.9 a, the above expression can be written as:

$$\{\epsilon_s\} = [Q_s] \quad [C_s'']^{-1} \quad \{\delta^s\}_B = [B_s] \quad \{\delta^s\}_B \qquad (3.15\text{ c})$$

Hence, Eq. 3.14 b can be written as

$$\{M_s\} = [D_s] \quad [B_s] \quad \{\delta^s\}_B \qquad (3.16)$$

Having established all basic relationships, the stiffness matrix relating beam bending moment, shear, and axial force to corresponding displacement components can be derived using the virtual work

principle. In this approach a set of virtual nodal displacements is imposed on the beam element, and the external and internal works done by the various forces are equated. Application of this procedure leads to:

$$\{\tilde{\delta}^s\}_B^T \{F_s\}_B = \int_0^L \{\epsilon_s\}^T \{M_s\} \, dx \tag{3.17}$$

Using Eqs. 3.15 c and 3.16 gives:

$$\{\tilde{\delta}^s\}_B^T \{F_s\}_B = \{\tilde{\delta}^s\}_B^T \left\{ \int_0^L [B_s]^T [D_s] [B_s] \, dx \right\} \{\delta^s\}_B$$

Since this relationship must hold for any arbitrary set of virtual displacements, one can conclude that the stiffness relation is given by:

$$\{F_s\}_B = \left\{ \int_0^L [B_s]^T [D_s] [B_s] \, dx \right\} \{\delta^s\}_B \tag{3.18}$$

The stiffness matrix is found to be:

$$[K_s]_B = \int_0^L [B_s]^T [D_s] [B_s] \, dx \tag{3.19}$$

where the integration is to be taken over the length of the prismatic stiffener element. Performing this integration leads to:

$$\begin{bmatrix} N_i \\ Z_i \\ M_i \\ N_k \\ Z_k \\ M_k \end{bmatrix} = \begin{bmatrix} A_s/L & 0 & S_s/L & -A_s/L & 0 & -S_s/L \\ & 12I_s/L^3 & -6I_s/L^2 & 0 & -12I_s/L^3 & -6I_s/L^2 \\ & & 4I_s/L & -S_s/L & 6I_s/L^2 & 2I_s/L \\ & & & A_s/L & 0 & S_s/L \\ & \text{Symmetric} & & & 12I_s/L^3 & 6I_s/L^2 \\ & & & & & 4I_s/L \end{bmatrix} \begin{bmatrix} u_i \\ w_i \\ \theta_{yi} \\ u_k \\ w_k \\ \theta_{yk} \end{bmatrix} \tag{3.20}$$

3.3.4 Inclusion of Torsional Stiffness of Beam Elements

The torsional resistance of the beams is often of importance in the behavior of stiffened plates. In beam theory (Ref. 47), it is shown that the total twisting moment applied to a beam is resisted by two different kinds of torsion, St. Venant or pure torsion, and warping torsion:

$$T = T_{St.V.} + T_w \tag{3.21}$$

The St. Venant torsional moment is resisted by shearing stresses, whereas the warping torsional moment is carried by axial stresses introduced due to flange bending. For rectangular or stocky solid beam cross sections, most of the applied twisting moment is carried by St. Venant torsion, whereas thin-walled I-sections carry most of the applied torsional moment by warping action. Both twisting moments are related to the angle of twist $\emptyset$ as follows:

$$T_{St.V.} = GK_T \, \phi' \tag{3.22}$$

$$T_w = -EI_w \, \phi''' \tag{3.23}$$

where: $\phi' = \frac{\partial}{\partial x} \left(\frac{\partial w}{\partial y}\right)$ = Rate of change of angle of twist

G = Shear modulus

K_T = St. Venant torsional constant

I_w = Warping constant

Warping is not considered in the presently proposed finite element approach for the analysis of stiffened plates. To account for warping, the higher order derivatives of the angle of twist should be included in the choice of the unknown displacement components introduced at the nodal points. It can be seen that owing to the assumed displacement pattern for the vertical displacement w, the rate of twist ϕ', i.e. the change of θ_x along a line of constant y-coordinate, varies as a cubic function. Since only two boundary conditions are available at the ends of the stiffener elements, the last two terms in the cubic function are disregarded. A linear variation of the angle of twist is assumed:

$$\theta_x = \frac{\partial w}{\partial y} = \alpha_1''' + \alpha_2''' \, x \tag{3.24}$$

Introducing the displacement vector associated with the torsional modes of the beam element:

$$\{\delta^s\}_T^T = < \theta_{xi} \quad \theta_{xk} > \tag{3.25}$$

one can write:

$$\{\delta^s\}_T = [C_s^{III}] \quad \{\alpha^{III}\} \tag{3.26}$$

where the vector of generalized coordinates is defined as:

$$\{\alpha\}^T = < \alpha_1^{III} \quad \alpha_2^{III} > \tag{3.27}$$

Enforcing compatibility of deformation for the angle of twist at the ends of the stiffener element, the two generalized coordinates are uniquely determined. Solution of Eq. 3.26 leads to

$$\{\alpha^{III}\} = [C_s^{III}]^{-1} \quad \{\delta^s\}_T \tag{3.28 a}$$

or written explicitly:

$$\begin{bmatrix} \alpha_1^{III} \\ \alpha_2^{III} \end{bmatrix} = \begin{bmatrix} 1 & 0 \\ -1/L & 1/L \end{bmatrix} \quad \begin{bmatrix} \theta_{xi} \\ \theta_{xk} \end{bmatrix} \tag{3.28 b}$$

Using the differential equation for St. Venant torsion, Eq. 3.22, which is derived, for example, in Ref. 22, the force-displacement relationship becomes:

$$\{T_s\} = [D_s] \quad \{\emptyset'\} \tag{3.29}$$

where

$$[D_s] = GK_T \tag{3.30}$$

The vector of generalized strains $\{\emptyset'\}$ can be found in terms of the vector of generalized coordinates by making use of the assumed displacement function Eq. 3.24:

$$\{\emptyset'\} = \begin{bmatrix} 0 & 1 \end{bmatrix} \begin{bmatrix} \alpha_1''' \\ \alpha_2''' \end{bmatrix} = [Q_s] \{\alpha'''\} \tag{3.31}$$

Using Eq. 3.28 a, this relationship in turn can be written as:

$$\{\emptyset'\} = [Q_s] [C_s'''^{-1}] \{\delta^s\}_T = [B_s] \{\delta^s\}_T \tag{3.32}$$

Again applying the principle of virtual work, the stiffness matrix for a beam element subjected to torsion is found to be:

$$[K_s]_T = \int_0^L [B_s]^T [D_s] [B_s] \, dx \tag{3.33}$$

The integration can be carried out in a straight forward manner leading to:

$$\begin{bmatrix} T_i \\ T_k \end{bmatrix} = \frac{GK_T}{L} \begin{bmatrix} 1 & -1 \\ -1 & 1 \end{bmatrix} \begin{bmatrix} \theta_{xi} \\ \theta_{xk} \end{bmatrix} \tag{3.34}$$

This stiffness relation, together with the previously derived Eq. 3.20, describes the behavior of an eccentrically stiffened beam element with respect to the plane of reference. These

relationships, together with the previously derived stiffness relations for the in-plane and out-of-plane behavior of the plate elements, are the basic components of the presented analysis of stiffened plate structures.

3.3.5 Evaluation of the St. Venant Torsional Constant K_T

The torsional stiffness matrix derived in the previous section can be evaluated once the St. Venant torsional constant K_T of the stiffener section is known. The estimation of K_T may present difficulties depending on the cross section of the stiffener. As shown in Ref. 45, for example, St. Venant torsion is governed by the partial differential equation:

$$\nabla^2 \psi = \frac{\partial^2 \psi}{\partial y^2} + \frac{\partial^2 \psi}{\partial z^2} = -2G\,\phi' \qquad (3.35)$$

where: $\psi = \psi\,(y,z)$ = Stress function

ϕ' = Rate of twist

This is Poisson's equation, which is encountered frequently in mathematical physics. Its solution can be obtained by different techniques,and for simple shapes no problems arise. A solution to the elastic torsion problem can also be obtained experimentally by means of the membrane analogy suggested by Prandtl, which is described in Ref. 42 As given in Ref. 30, a number of approximate formulae have been proposed for irregular shapes. Using membrane

analogy, the St. Venant torsional constant K_T for a thin-walled open section, which is composed of n rectangularly shaped elements, can be evaluated as:

$$K_T = \sum_{i=1}^{n} b_i t_i^3 \tag{3.36}$$

where: b_i = Length of element i

t_i = Width of element i

However, this formula is accurate only if the elements are small. Solid cross-sections with reentrant corners are best broken down into parts, and the St. Venant torsional constant K_T for such a section can be approximately evaluated as follows:

$$K_T = \sum_{i=1}^{n} \frac{A_i^4}{40 I_{pi}} \tag{3.37}$$

where: A_i = Area of element i

I_{pi} = Polar moment of inertia of element i

These formulae can be used to obtain an estimate on the torsional constant K_T; however, in some cases, significant errors might be introduced when using these approximations, thus necessitating a more accurate analysis. A means of solving the governing partial differential equation is to use the finite-difference method since its application is relatively simple.

An alternate way of solving this differential equation was found in the process of this investigation. The method is based

on the fact that the differential equation of torsion and that of the corresponding transversely loaded plate problem are formally identical, and thus, a solution can be accomplished by solving the corresponding plate problem using the finite element method. This technique is described in detail in Appendix V. Due to the versatility of the finite element approach, the St. Venant torsional constant K_T for complex shaped solid cross sections can be computed easily using the general plate program described in Chapter 2.

3.3.6 Assembly of the System Stiffness Matrix and Solution of the Field Equations

The assembly of the component stiffness matrices, as derived in the previous sections, to the system stiffness matrix is described in this section. The stiffness matrices of the individual elements can be assembled to form a single stiffness matrix, called system stiffness matrix of the entire structure. This procedure is explained in detail in Section 2.3.1.

For the present analysis, the in-plane displacements u in x-direction and v in y-direction, the deflection w, and the two slopes of the deflected surface are entered as unknowns at each nodal point. The vector of nodal displacements at node i is introduced as follows:

$$\{\delta_i\}^T = < u \quad v \quad w \quad \theta_x \quad \theta_y > \tag{3.38}$$

In a first step, the torsional stiffness matrix of the stiffener element, as given by Eq. 3.34, is combined with the stiffness for

bending, shear and axial force, given by Eq. 3.20, to form one single stiffness relation for the stiffener element:

$$\{F_s\} = [K_s]\ \{\delta^s\} \tag{3.39 a}$$

Explicitely, Eq. 3.39 a can be written as:

$$\begin{Bmatrix} N_i \\ V_i \\ Z_i \\ T_i \\ M_i \\ N_k \\ V_k \\ Z_k \\ T_k \\ M_k \end{Bmatrix} = \frac{E_s}{L^3} \begin{bmatrix} A_s L^2 & 0 & 0 & 0 & S_s L^2 & -A_s L^2 & 0 & 0 & 0 & -S_s L^2 \\ & 0 & 0 & 0 & 0 & 0 & 0 & 0 & 0 & 0 \\ & & 12I_s & 0 & -6I_s L & 0 & 0 & -12I_s & 0 & -6I_s L \\ & & & \gamma L^2 & 0 & 0 & 0 & 0 & -\gamma L^2 & 0 \\ & & & & 4I_s L^2 & -S_s L^2 & 0 & 6I_s L & 0 & 2I_s L^2 \\ & & & & & A_s L^2 & 0 & 0 & 0 & S_s L^2 \\ & & & & & & 0 & 0 & 0 & 0 \\ & & & & & & & 12I_s & 0 & 6I_s L \\ & & & & \text{Symmetric} & & & & \gamma L^2 & 0 \\ & & & & & & & & & 4I_s L^2 \end{bmatrix} \begin{Bmatrix} u_i \\ v_i \\ w_i \\ \theta_{xi} \\ \theta_{yi} \\ u_k \\ v_k \\ w_k \\ \theta_{xk} \\ \theta_{yk} \end{Bmatrix} \tag{3.39 b}$$

where, in order to have a compatible listing of deformation components for the entire structure, the nodal force and nodal displacement vectors are defined as:

$$\{\delta^s\}^T = < u_i \quad v_i \quad w_i \quad \theta_{xi} \quad \theta_{yi} \quad u_k \quad v_k \quad w_k \quad \theta_{xk} \quad \theta_{yk} > \tag{3.40}$$

$$\{F_s\}^T = < N_i \quad V_i \quad Z_i \quad T_i \quad M_i \quad N_k \quad V_k \quad Z_k \quad T_k \quad M_k > \tag{3.41}$$

where γ is defined as:

$$\gamma = \frac{GK_T}{E_s} \tag{3.42}$$

In a similar way, the stiffness relations governing the in-plane and out-of-plane behavior of the plate elements, as derived in the Appendices III and IV, can be cast into one single relationship:

$$\{F_p\} = [K_p] \quad \{\delta^p\} \tag{3.43}$$

where the element displacement vector is defined as:

$$\{\delta^p\}^T = < \{\delta_i\}^T \quad \{\delta_j\}^T \quad \{\delta_k\}^T \quad \{\delta_l\}^T > \tag{3.44}$$

and $\{F_p\}$, the element force vector, is defined consistent with the element displacement vector. The stiffness matrix $[K_p]$ governing the in-plane and out-of-plane behavior of a plate element is of size 20 x 20, and is best assembled in a digital computer.

The stiffness coefficients for each adjoining element can simply be added for the different elements framing into a common node. In fact, this operation establishes equilibrium of forces at a node in the direction of each of the five introduced nodal displacement components. Each row of the assembled stiffness matrix represents an equilibrium equation found by enforcing equilibrium of nodal forces and the generalized loads at a given node, for one of the five degrees of freedom. Once this system stiffness matrix is assembled, the final stiffness relations for

the entire stiffened plate structure can again be cast into one single matrix equation of the form:

$$\{F\} = [K] \quad \{\delta\} \tag{3.45}$$

where: $\{F\}$ = Systems vector of generalized loads

$[K]$ = Overall or systems stiffness matrix

$\{\delta\}$ = Systems displacement vector

From this point on, one can proceed as in the usual finite element displacement approach, described in Section 2.3.1. It should be noted that only displacement type boundary conditions can be satisfied exactly because only displacement components are entered as unknowns in the nodal displacement vector. Upon enforcement of the known displacements as described in Section 2.4.3, the system of simultaneous equations, represented by Eq. 3.45, can be solved. Large systems of simultaneous equations require special solution techniques in order to minimize computer costs. The Choleski decomposition technique, as described in Section 2.4.5, was used, and proved to be very efficient.

Once the unknown systems displacement vector is determined, all unknown field quantities can be found by substituting appropriate displacement components back into the relations derived either in the appendices or the main text. In addition, at each nodal point, the forces acting on beam elements and the stress resultants associated with the in-plane and out-of-plane behavior of

the plate elements are determined. The fact that the forces acting on beam and plate elements can be separated in the proposed method of analysis is of significant importance in the design of a stiffened plate structure.

In order to implement the above described approach, a general computer program was developed for the analysis of arbitrarily shaped stiffened plates. Any shape, as long as it fits into a rectilinear mesh, can be treated and transverse stiffeners can be included. Orthotropy of the plate can be considered and multiple load vectors can be processed simultaneously.

3.4 Application of the Method to the Analysis of Highway Bridges

3.4.1 Description of the Test Structure

The need for a more rational analysis of beam-slap type bridges is great, especially in regard to a more reliable analysis of the stresses occurring in the bridge deck, the effect of diaphragms on lateral distribution of load and on slab stresses, and the effect of the orthotropic behavior of the bridge deck.

It was decided to verify the proposed finite element approach with the aid of field test results of an I-beam girder bridge field tested in 1969 by a research team at Fritz Engineering Laboratory, Lehigh University. Chen and VanHorn (Ref. 12) describe in detail the field testing of this existing beam-slab type highway bridge, which is constructed with five prestressed concrete I-beams supporting a cast-in-place concrete slab. A

description of the behavior of the slab of the same bridge structure is given in Ref. 52. The testing of this bridge was part of an overall investigation, initiated in 1968, to develop information on several aspects of the structural behavior of I-beam bridges. Prior to this investigation, the problem of load distribution in spread box beam bridges was studied extensively by the field testing of several bridges of the box-beam type (Ref. 49) and by means of a theoretical analysis (Ref. 36). From all of these investigations it was concluded that the present AASHO Standard Specifications for Highway Bridges (Ref. 4) do not give an accurate prediction for the lateral distribution of load in box-beam and I-beam bridges. Furthermore, the specifications do not account for many variables which have significant effects on load distribution.

The structure analyzed in this investigation is a simply supported, right I-beam bridge with a span length of 68 feet 6 inches center-to-center of bearings. The cross section of the test bridge, as shown in Fig. 18, consists of five identical prestressed I-beams, of AASHO Type III cross section, covered with a cast-in-place reinforced concrete deck. The deck provides a roadway width of 32 feet and the specified minimum thickness of the slab is 7-1/2 inches. However, measurements indicated that the actual slab thickness ranges from 6.1 to 7.3 inches at the section of maximum moment, which is located 3.55 feet off midspan. Diaphragms between the beams are located at the ends of the span above the end supports

and at midspan. The dimensions of the midspan diaphragm, as well as those of the beam cross section, are shown in Fig. 19. The test vehicle used for testing was a tractor and semi-trailer unit, approximating the AASHO HS 20-44 design loading (Ref. 4). A photo of the test vehicle, along with the wheel spacings and the actual axle loading, is shown in Fig. 20. Four loading lanes were located on the roadway, as shown in Fig. 21, such that the center-line of the truck would coincide with the center-line of the girders or with a line located midway between girders.

3.4.2 Study of Variables Governing Load Distribution

Although the actual cross section of the bridge could be approximated more closely in the present analysis, it was, for the sake of a simpler input, approximated as shown in Fig. 21. The slab thickness was assumed to be 7.5 inches throughout the width of the deck. First, the curb and parapet sections, as well as the midspan diaphragm, were neglected. Their inclusion will be discussed in subsequent sections. The entire bridge was considered to be made of an isotropic material. Poisson's ratio was taken as 0.15, and a modulus of elasticity of $E = 5000$ ksi was assumed. A ratio of torsional-to-bending stiffness of the beam elements $\gamma^* = GK_T/E_sI_s = 0.035$ was taken, as found from an analysis as discussed in Section 3.3.5. The actual truck loading was simulated by appropriate concentrated forces instead of the distributed wheel loads. The structure was analyzed for a truck centered, in turn, in each of the lanes as shown in Fig. 21.

The general finite element program yields the entire displacement field at all specified nodal points, as well as all internal stress resultants acting on the beam and plate elements. The forces associated with in-plane and out-of-plane behavior are printed separately for all plate elements. Due to space limitations, only the results associated with the lateral distribution of load will be presented. All following results are for a discretization of the structure shown in Fig. 22. A mesh with N subdivisions in the transverse direction and M subdivisions in the longitudinal direction is referred to as Mesh N * M in the remainder. During the actual testing of this structure, a section near midspan, shown as Section M in Fig. 22, was gaged. This section corresponds to the section of maximum moment for the structure idealized as a simple beam, and subjected to the given group of loads.

The results obtained from tests, as reported in detail in Ref. 12, were derived based upon an experimentally measured strain distribution in the beams. This distribution of strain is due to the combined action of all stress resultants acting on a beam element. It is not possible to separate these forces in an experimental investigation. For the sake of simplicity, it was assumed that only beam bending occurs. The proposed finite element analysis determines all stress resultants acting on the beam and plate elements separately. In order to compare the results obtained from the analysis with the test results, equivalent beam bending moments causing the same distribution of strain as would

result under the combined action of axial force and beam bending moment must be obtained from the analysis. This procedure is based on the concept of equating the first moments of area of the compressive and tensile areas of each composite beam (Ref. 12). Finally, distribution coefficients (or moment percentages) were computed. These are defined as the moment carried by a particular beam divided by the sum of moments carried by all beams.

Fig. 23 shows distribution coefficients obtained from the analysis and the field test results for a truck moving in lane 1. Similarly, Figs. 24 and 25 show distribution coefficients for a truck moving in lanes 3 and 4, respectively. Influence lines for beam bending moments could be constructed as shown in Figs. 26 and 27. Such plots could be used to advantage by the designer to determine the maximum bending moment occurring at the section of maximum moment under the action of multiple trucks crossing the bridge simultaneously. It should be noted that theoretical values are obtained for a bridge without diaphragms at midspan, whereas the actual field test results include their effect. The inclusion of the diaphragms brings theoretical results closer to field results. In addition, analytical results are obtained for a bridge with a theoretical slab thickness of 7.5 inches, and subject to the assumptions listed at the beginning of this section.

3.4.2.1 Effect of Span Length

Fig. 28 shows the effect of the span length on the lateral

distribution of load for the I-beam bridge investigated. Figs. 29 and 30 show influence lines for the outermost and center beam bending moment, respectively, pointing out the influence of the span length on the beam bending moment. A study of these figures reveals a significant influence of the span length on the lateral distribution of load. Plotting the distribution coefficient for the center beam bending moment against the span length, as done in Fig. 31, reveals clearly this dependency. An almost linear relationship is obtained if the moment percentages of the center beam are plotted against the reciprocal of the span length, as done in Fig. 32. Hence, it can be concluded that the load distribution is likely to be inversely proportional to the span length, a factor not accounted for in the present AASHO Standard Specifications for highway bridges. A similar conclusion was reached in the investigation on bridges of the box-beam type (Ref. 36).

3.4.2.2 Effect of Deck Thickness

The effect of the thickness of the slab is shown in Fig. 33. It is seen from this graph that the thickness of the deck significantly affects the lateral load distribution for an I-beam bridge. This is in contrast to results found from the analysis of a box-beam bridge (Ref. 36), where it was concluded that the load distribution is not very sensitive to a variation in slab thickness. The present investigation shows that a thicker slab distributes the load more uniformly to the girders. Again, this effect is not accounted for in the present specifications.

3.4.2.3 Effect of Beam Spacing

Another important factor influencing the lateral distribution of load is the spacing of the girders, as shown in Fig. 34. As can be seen from this figure, a closer spacing distributes the load more evenly. This effect is partly accounted for in the present AASHO Standard Specifications for Highway Bridges (Ref. 4) in which the load distribution factors are given in the form of spacing divided by a constant number. Actually, the optimum spacing should be determined for a given roadway width of the bridge. Such an investigation could be easily made using the present finite element program.

3.4.2.4 Effect of Beam Size

The effect of the size of the beam cross section on lateral distribution of load is illustrated in Fig. 35. Four standard precast beams of a size suggested by AASHO (Ref. 4) have been included in this investigation. This effect is significant and smaller beams are seen to distribute the load more evenly to the girders.

3.4.2.5 Effect of Torsional Stiffness of Beams

The effect of the torsional resistance of the beams on the lateral distribution of load is shown in Fig. 36. The moment percentages are plotted in this figure for torsionally weak beams with $GK_T/E_sI_s = 0$ as well as for a ratio of 0.120. As expected, it is recognized that this ratio has some effect on the

lateral distribution of loads, and it underlines the need for an accurate analysis of K_T, as shown in Section 3.3.5 as well as for a consideration of the torsional resistance of the beams in future specifications.

3.4.2.6 Effect of Eccentricity of Beams

This eccentricity is defined here as distance from the centroid of the beam element to the plane of reference, as indicated in Fig 37. For a theoretical slab thickness of 7.5 inches, this distance becomes 27.98 inches using AASHO Type III beams. The figure depicts the structural behavior of an I-beam bridge for a variation of this distance of $\pm$ 0.5 inches, caused, for example, by a misfit during the construction of the bridge. It is seen that the load distribution is not significantly affected by such a deviation.

3.4.2.7 Effect of Poisson's Ratio

Poisson's ratio varies widely, depending upon the age of concrete, type of aggregate, and other factors. To observe the effect of this ratio, a high and low limiting values of $\nu = 0.25$ and $\nu = 0.05$ were chosen for this comparison, and the effect of these two values of ν on the lateral distribution of load is shown in Fig. 38. It can be concluded that the distribution of load is nearly unaffected by this ratio. However, the slab bending moments and the in-plane forces are considerably dependent on ν.

3.4.2.8 Effect of Moduli of Elasticity of Beams and Slab

An accurate determination of the moduli of elasticity of the beam and slab material used in an actual bridge is not possible. Hence, some degree of engineering judgment must be used in the assumption of appropriate values for these material properties. For the lateral distribution of load, only the ratio of the moduli of elasticity of the beam and slab materials is of importance, and hence, the effect of this ratio was studied in this investigation. Usually, the modulus of elasticity of the precast prestressed concrete beams is higher than that of the cast-in-place reinforced concrete slab. The response of the structure was analyzed for different ratios of moduli of elasticity and the result of this investigation is plotted in Fig. 39. It is seen from this figure that the effect of this paratmeter on the lateral distribution of load is not very significant. However, the shifting of load to the center beam for larger values of the modulus of elasticity of the beam should be noted.

3.4.2.9 Effect of Orthotropy of Bridge Deck

Orthotropy is caused by unequal amounts of reinforcing steel for the transverse and longitudinal reinforcement of the bridge slab, or by cracking of the slab, for example. The effect that such cracking might have on the lateral distribution of load is of interest. For the sake of simplicity, it was assumed in this investigation that the entire slab width was cracked uniformly, parallel to the girders, along the total length of the

bridge. The associated decrease in stiffness is accounted for in the ratio D_y/D_x, of transverse to longitudinal stiffness of the slab. Figure 40 illustrates that a cracked slab causing a loss in transverse stiffness shifts slightly more load to the center girder, and at the same time, decreases the load in both exterior girders. Further results of this investigation are compiled in Table 15. It should be noted that the crack pattern described above leads to an orthotropic behavior of the slab as described by Timoshenko (Ref. 46). The stress matrix for this particular case becomes:

$$[D] = \begin{bmatrix} D_{11} & D_{12} & 0 \\ D_{21} & D_{22} & 0 \\ 0 & 0 & D_{33} \end{bmatrix}$$

where the terms in the matrix should be evaluated according to Huber (Ref. 46) as follows:

$$D_{11} = \frac{E_c I_{cx}}{1-\nu^2}$$

$$D_{22} = \frac{E_c I_{cy}}{1-\nu^2}$$

$$D_{12} = D_{21} = \nu\sqrt{D_{11} D_{22}}$$

$$D_{33} = \frac{1-\nu}{2} \sqrt{D_{11} D_{22}}$$

in which: E_c = Modulus of elasticity of concrete deck

I_c = Transformed moment of inertia, taking reinforcement into account

ν = Poisson's ratio

A generally anisotropic material behavior would result if the cracks were not to open parallel to the global x-axis. However, such cracking could also be investigated by first finding the stiffness of a cracked panel with respect to a local coordinate system with x-axis in the direction of the cracks, and then transforming this stiffness to the global coordinate system.

3.4.2.10 Effect of Type of Loading

The effect of different types of loading encountered in bridge design on the lateral distribution of load is shown in Fig. 41. Two loading cases must be considered according to the AASHO specifications: (1) uniformly distributed lane load, and (2) the truck load. The analysis of the structure yields almost identical distribution percentages for these two loading cases. However, a significantly different distribution of load is obtained for a single concentrated load.

3.4.2.11 Two-Span Continuous Bridge

This example is chosen to demonstrate the versatility of the proposed finite element approach and the effect of different boundary conditions on the lateral distribution of loads. In

Fig. 42, a comparison of load distribution for a single span and a two-span continuous bridge is made. Two trucks are located in such a way on the bridge as to obtain symmetry of loading with respect to the center support. It is interesting to observe that the load distribution at the center support and at Section M, the section of maximum moment for the corresponding single span bridge, is not very different. However, the pronounced difference in load distribution between a single span and a two-span continuous bridge should be observed in the design of such bridges.

3.4.3 Inclusion of Diaphragms

One of the features of the method is the inclusion of stiffeners running in transverse direction, often called diaphragms. The general computer program developed for this investigation is capable of including any pattern of transverse stiffeners, as long as they are attached along plate element interfaces. As mentioned above, the test structure investigated so far has one midspan diaphragm only, the cross section of which is shown in Fig. 19. The results of the analysis performed for a structure including this diaphragm are shown in Figs. 23, 24 and 25. It is seen that for I-beam bridges the effect of such a midspan diaphragm on the lateral distribution of load is significant, and hence, due consideration should be given in the design.

3.4.4 Inclusion of Curb and Parapet

The results presented so far are for an idealized bridge

cross section, as shown in Fig. 21, neglecting curb and parapet. Basically, curbs and parapets are not intended as load-carrying members in a bridge. However, field tests (Ref. 49) showed a partial effectiveness of the curb and parapet section acting compositely with the exterior beam. In a field test, the effect of the diaphragm can not be separated from the behavior of the exterior beam. The results of the analysis on the effectiveness of curb and parapet are shown in Figs. 23, 24, and 25. For this analysis, curb and parapet were approximately accounted for by considering the curb and parapet together with the exterior beam as one unit and treating this unit as a modified exterior beam. A more refined analysis could be performed by taking the curb and parapet as separate beam elements and proceeding as discussed in Section 3.3.6. From Figs. 23 through 27 it can be concluded that the effect of curbs and parapets on the lateral distribution of load in the I-beam type superstructure may not be very significant, thus the designer is on the conservative side, at least for the interior beams, if he chooses to disregard their effects.

3.5 Convergence and Accuracy of Solutions

The above study of variables governing the lateral distribution of load in I-beam bridges makes it clear that the developed finite element analysis is well suited for the analysis of beam-slab type bridge structures. For this analysis, a minimum of simplifying assumptions in the idealization of the structure are required. A comparison of the values for displacements and stress

resultants predicted by the finite element method with those of the field tests proves the validity of the developed approach. Although only results associated with the lateral distribution of load are shown in this report, it should be pointed out that the method allows for the determination of the entire stress and displacement field at all predefined nodal points. A study of the behavior of the slab of the Bartonsville Bridge (Ref. 52), revealed that there is no satisfactory method of slab analysis presently available. In fact, currently used methods of slab analysis do not account for many variables involved in the structural behavior of the slab, and none is thoroughly verified by test results. On the other hand, since the present analysis allows for a separation of forces acting on beam and plate elements, it would be ideally suited for a more extensive study of the behavior of the slab. The response of a slab panel acted upon by a distributed wheel load could be determined accurately by reanalyzing this panel as a plate, enforcing the boundary conditions as found form an analysis of the entire structure

The accuracy to be expected from the developed finite element approach depends on the discretization of the structure. In a finite element displacement approach making use of fully compatible elements, the displacement field converges toward the true displacement field if the mesh size is reduced. However, no bounds can be given for the associated stress field. For the present formulation, a non-conforming displacement function was chosen

for the representation of the out-of-plane behavior of the plate. A compatible formulation was chosen for the representation of the in-plane behavior of the plate and the behavior of the beam elements. The convergence of the combined model cannot be proven via the principle of minimum total potential energy. A numerical evaluation of the structural response of the I-beam bridge was investigated for different mesh sizes in order to study the convergence behavior of the proposed approach. All dimensions and material properties were chosen as listed in Section 3.4.1, and the effects of diaphragm, curb and parapet were not considered. The structure was again loaded by a truck load, and three different mesh sizes were processed. Some results of these investigations are shown in Tables 16 through 19 for the section of maximum moment and the truck occupying lanes 1 through 4. The tables also contain the deflection values measured during the actual field testing of this bridge. In comparing the theoretical results with the experimental values, it should be kept in mind that the theoretical and the actual bridge have different dimensions. A comparison of different mesh sizes indicates convergence for a decreasing mesh size. Furthermore, the validity of the solutions is supported by the actual field test results listed in the same tables.

3.6 Summary

A method of analysis based on the finite element displacement approach capable of analyzing complex shaped stiffened

plates has been presented. Stiffeners in longitudinal as well as in transverse direction can be taken into account, and the stiffness of the slab can be arbitrarily varied to account for thickness changes in the slab. The orthotropic nature of the plate can be accounted for, as well as a varying cross section of the beams. A minimum of simplifying assumptions associated with the discretization of a structure is required in the analysis.

On the basis of the application of this method to the analysis of an I-beam bridge, described in detail, a few conclusions can be drawn: (1) The model approximates the true physical behavior of a structure more closely than methods which use either the effective width concept to find an equivalent grid structure, or orthotropic plate theory, which is not able to predict the slab stresses accurately. (2) The presented approach allows a separation of forces acting on beam and plate elements, thus giving the designer more detailed information about the behavior of a structure. (3) The study of variables governing the lateral distribution of load demonstrates the versatility of the proposed approach.

4. SUMMARY AND CONCLUSIONS

4.1 Summary

This report presents two different types of finite element analyses of transversely loaded plates and eccentrically stiffened plates: (1) a finite element analysis of elastic plates based on a new, refined plate bending element, and (2) a finite element analysis of elastic, eccentrically stiffened plates subjected to transverse loading. The formulations of these methods, which are all based on linear geometry, are described in detail in Chapters 2 and 3. For each type of analysis, a general computer program has been developed and was applied in the analysis of several sample structures.

In Chapter 2, a refined plate bending element for use in a finite element displacement analysis of arbitrarily shaped elastic plates is described. Along with the three basic nodal displacement parameters: w, θ_x and θ_y, three curvature terms are entered as unknowns in the vector of generalized displacements at each nodal point. A higher-order polynomial expression is assumed for the displacement field within an element and based on this expression, the stiffness matrix of the refined element is derived in a systematic way. The method adopted in solving the system of simultaneous equations makes efficient use of the bandedness of the overall stiffness matrix. The accuracy and convergence of

solutions obtained with this new element is demonstrated on a few example problems analyzed in this chapter.

In Chapter 3, a method of analysis based on the finite element displacement approach, and capable of analyzing complex shaped eccentrically stiffened plates is presented. The discretization of such a structure into an assemblage of plate and beam elements is first discussed. The stiffness matrices associated with the in-plane and out-of-plane behavior of a plate element and with the behavior of a beam element are derived and the assembly of the overall stiffness matrix is described. Longitudinal as well as transverse stiffeners can be taken into account in this analysis. A variation of the thickness of the slab and its orthotropic nature can be accounted for as well as variable beam cross section. The power of the proposed method lies in its versatility and in the fact that forces occurring in beam and plate elements can be separated. The approach is applied to the analysis of I-beam bridges in this dissertation and is verified with the aid of field test results. An extensive study of most of the parameters governing the behavior of I-beam bridges is included in this chapter. In addition, a new approach capable of determing the St. Venant torsion constant K_T of arbitrarily shaped solid cross sections is presented in this chapter. This method is based on the fact that the differential equations governing the torsional behavior of a solid cross section and that of the corresponding transversely loaded plate problem of the same shape are formally

identical. A solution can therefore be accomplished by solving the analogous plate problem using the finite element method.

4.2 Conclusions

The methods of analysis presented in this report are of a general nature and can be applied to a variety of plate structures. Each of the methods discussed has been implemented with the aid of a general finite element program.

a. The following conclusions can be drawn based on the finite element analysis of elastic plates using the refined plate element:

   1. The refined plate bending element yields better accuracy for displacements and internal moments than most of the presently known rectangular plate bending elements for any given number of degrees of freedom. The actual displacement field is approximated more closely by the chosen higher-order polynomial.

   2. Internal moments need not be computed separately since the associate curvature terms are introduced as unknown parameters in the displacement vector.

   3. For the examples studied, it was found that the enforcement of known curvature terms at boundary points does not, in general, improve the displacement field; it does, however, improve internal

moments in the vicinity of the boundary points where the curvature terms were enforced.

b. Based on the elastic analysis of eccentrically stiffened plates, presented in Chapter 3 and applied in this investigation to I-beam bridges, the following conclusions can be drawn:

   1. The developed approach provides a powerful tool for the analysis of complex shaped longitudinally and transversely stiffened plate structures.

   2. The introduced model consisting of beam and plate elements approximates the actual behavior of the structure more closely than the methods used today for the analysis of I-beam bridges. It allows the separation of the forces acting in the beam and plate elements and the computation of more reliable plate stresses.

   3. Due to the versatility of the method a number of important variables governing the lateral distribution of load can be studied. Diaphragms and the orthotropic nature of the bridge deck can be included in the analysis.

   4. The most significant variables governing the lateral distribution of load in an I-beam bridge are seen to

be the span length of the bridge, the deck thickness, the spacing of the beams and the type of beam used. The type of loading applied to the bridge is also important as well as the support conditions of the bridge.

5. The following variables found to have less effect on the lateral distribution of load are: Curb and parapet of the cross section, torsional stiffness of beams, Poisson's ratio and the modular ratio between beam and slab material.

5. APPENDICES

APPENDIX I

5.1 Derivation of Stiffness Matrix of the Refined Plate Bending Element

This appendix presents the stiffness matrix for the refined plate bending element, discussed in Chapter 2, under the assumption of homogeneous orthotropic material behavior. The assumed displacement field represented by Eq. 2.24 was discussed in Section 2.4.1. The unknown displacement components at node i are listed in the nodal displacement vector as:

$$\{\delta_i\}^T = < w \quad \theta_x \quad \theta_y \quad \phi_x \quad \phi_y \quad \phi_{xy} > \tag{A1.1}$$

Element displacements are given as the listing of nodal displacements:

$$\{\delta^e\}^T = < \delta_i^T \quad \delta_j^T \quad \delta_k^T \quad \delta_\ell^T > \tag{A1.2}$$

The consistent element force vector is given by:

$$\{F^e\}^T = < F_i^T \quad F_j^T \quad F_k^T \quad F_\ell^T > \tag{A1.3}$$

The vector of generalized coordinates was derived as:

$$\{\alpha\} = [\bar{C}]^{-1} [T_1] \{\delta^e\} = [C]^{-1} \{\delta^e\} \tag{A1.4}$$

The connection matrix $[\bar{C}]$ consists of numbers only and is listed

in this appendix, whereas the matrix $[T_1]$ is given in Section 2.4.2. The stress matrix relates generalized stresses to generalized strains:

$$\{M\} = [D]\ \{\emptyset\} \tag{A1.5}$$

in which:

$$[D] = \begin{bmatrix} D_x & D_1 & 0 \\ D_1 & D_y & 0 \\ 0 & 0 & D_{xy} \end{bmatrix} \tag{A1.6}$$

$$\{M\}^T = < M_x \quad M_y \quad M_{xy} > \tag{A1.7}$$

and

$$\{\emptyset\}^T = < -\frac{\partial^2 w}{\partial x^2} \quad -\frac{\partial^2 w}{\partial y^2} \quad 2\frac{\partial^2 w}{\partial x \partial y} > \tag{A1.8}$$

Generalized strains can be expressed in terms of nodal displacements as shown in Section 2.4.1

$$\{\emptyset\} = [Q]\ [C]^{-1}\ \{\delta^e\} = [B]\ \{\delta^e\} \tag{A1.9}$$

The magnitude of nodal forces, given by Eq. A1.3, can be found by applying the principle of virtual work, which leads to:

$$\{\delta^e\}^T\ \{F^e\} = \iint_A \{\emptyset\}^T\ \{M\}\ dA \tag{A1.10}$$

where the integration is to be taken over the area A of the rectangular plate element. When Eq. A1.5 and Eq. A1.9 are substituted

into Eq. A1.10, and account is taken of the fact that the last equation must be valid for any arbitrary virtual displacement vector; i.e. also for the actual displacement pattern, the following equation results:

$$\{F^e\} = \left[\iint_A [B]^T [D] [B] \, dxdy \right] \{\delta^e\} \qquad (A1.11)$$

This is the element force-deformation relationship, and hence, the stiffness matrix is given by:

$$[K^e]_{24x24} = \iint_A [B]^T [D] [B] \, dxdy \qquad (A1.12)$$

The introduction of non-dimensionalized coordinates, as explained in Section 2.4.2, leads to a particularly simple integration and is best done by considering one term of the stress matrix [D] at a time. The result can be given in the form:

$$[K^e]_{24x24} = [C^{-1}]^T \left[D_x[K_1] + D_1[K_2] + D_y[K_3] + D_{xy}[K_4] \right] [C^{-1}] \qquad (A1.13)$$

Carrying out the necessary operations yields the component matrices as listed below. The final stiffness matrix is assembled in the digital computer.

Matrix $[\bar{C}]$

1	-1	1	1	-1	1	-1	1	-1	1	1	-1	1	-1	1	-1	1	-1	1	-1	1	-1	-1	-1
0	0	1	0	-1	2	0	1	-2	3	0	-1	2	-3	4	0	1	-2	3	-4	5	-1	-3	-5
0	-1	0	2	-1	0	-3	2	-1	0	4	-3	2	-1	0	-5	4	-3	2	-1	0	-5	-3	-1
0	0	0	-2	0	0	6	-2	0	0	-12	6	-2	0	0	20	-12	6	-2	0	0	20	6	0
0	0	0	0	0	-2	0	0	2	-6	0	0	-2	6	-12	0	0	2	-6	12	-20	0	6	20
0	0	0	0	1	0	0	-2	2	0	0	3	-4	3	0	0	-4	6	-6	4	0	5	9	5
1	-1	-1	1	1	1	-1	-1	-1	-1	1	1	1	1	1	-1	-1	-1	-1	-1	-1	1	1	1
0	0	1	0	-1	-2	0	1	2	3	0	-1	-2	-3	-4	0	1	2	3	4	5	-1	-3	-5
0	-1	0	2	1	0	-3	-2	-1	0	4	3	2	1	0	-5	-4	-3	-2	-1	0	5	3	1
0	0	0	-2	0	0	6	2	0	0	-12	-6	-2	0	0	20	12	6	2	0	0	-20	-6	0
0	0	0	0	0	-2	0	0	2	6	0	0	-2	-6	-12	0	0	2	6	12	20	0	-6	-20
0	0	0	0	1	0	0	-2	-2	0	0	3	4	3	0	0	-4	-6	-6	-4	0	5	9	5
1	1	1	1	1	1	1	1	1	1	1	1	1	1	1	1	1	1	1	1	1	1	1	1
0	0	1	0	1	2	0	1	2	3	0	1	2	3	4	0	1	2	3	4	5	1	3	5
0	-1	0	-2	-1	0	-3	-2	-1	0	-4	-3	-2	-1	0	-5	-4	-3	-2	-1	0	-5	-3	-1
0	0	0	-2	0	0	-6	-2	0	0	-12	-6	-2	0	0	-20	-12	-6	-2	0	0	-20	-6	0
0	0	0	0	0	-2	0	0	-2	-6	0	0	-2	-6	-12	0	0	-2	-6	-12	-20	0	-6	-20
0	0	0	0	1	0	0	2	2	0	0	3	4	3	0	0	4	6	6	4	0	5	9	5
1	1	-1	1	-1	1	1	-1	1	-1	1	-1	1	-1	1	1	-1	1	-1	1	-1	-1	-1	-1
0	0	1	0	1	-2	0	1	-2	3	0	1	-2	3	-4	0	1	-2	3	-4	5	1	3	5
0	-1	0	-2	1	0	-3	2	-1	0	-4	3	-2	1	0	-5	4	-3	2	-1	0	5	3	1
0	0	0	-2	0	0	-6	2	0	0	-12	6	-2	0	0	-20	12	-6	2	0	0	20	6	0
0	0	0	0	0	-2	0	0	-2	6	0	0	-2	6	-12	0	0	-2	6	-12	20	0	6	20
0	0	0	0	1	0	0	2	-2	0	0	3	-4	3	0	0	4	-6	6	-4	0	5	9	5

Matrix $[K_1]$

Multiplier $\frac{16b}{105a^3}$

0																								
0	0																							
0	0	0																						
0	0	0	105																					
0	0	0	0	0																				
0	0	0	0	0	0																			
0	0	0	0	0	0	315																		
0	0	0	0	0	0	0	35																	
0	0	0	0	0	0	0	0	0																
0	0	0	0	0	0	0	0	0	0															
0	0	0	210	0	0	0	0	0	0	756														
0	0	0	0	0	0	0	0	0	0	0	105													
0	0	0	35	0	0	0	0	0	0	70	0	21												
0	0	0	0	0	0	0	0	0	0	0	0	0	0											
0	0	0	0	0	0	0	0	0	0	0	0	0	0	0										
0	0	0	0	0	0	630	0	0	0	0	0	0	0	0	1500									
0	0	0	0	0	0	0	70	0	0	0	0	0	0	0	0	252								
0	0	0	0	0	0	105	0	0	0	0	0	0	0	0	210	0	63							
0	0	0	0	0	0	0	21	0	0	0	0	0	0	0	0	42	0	15						
0	0	0	0	0	0	0	0	0	0	0	0	0	0	0	0	0	0	0	0					
0	0	0	0	0	0	0	0	0	0	0	0	0	0	0	0	0	0	0	0	0				
0	0	0	0	0	0	0	0	0	0	0	210	0	0	0	0	0	0	0	0	0	500			
0	0	0	0	0	0	0	0	0	0	0	63	0	0	0	0	0	0	0	0	0	126	45		
0	0	0	0	0	0	0	0	0	0	0	0	0	0	0	0	0	0	0	0	0	0	0	0	0

Symmetric

Matrix $[K_2]$

Multiplier $\frac{16}{1575ab}$

0																							
0	0																						
0	0	0																					
0	0	0	0																				
0	0	0	0	0																			
0	0	0	1575	0	0																		
0	0	0	0	0	0	0																	
0	0	0	0	0	0	0	0																
0	0	0	0	0	0	1575	0	0															
0	0	0	0	0	0	0	1575	0	0														
0	0	0	0	0	3150	0	0	0	0	0													
0	0	0	0	0	0	0	0	0	0	0	0												
0	0	0	525	0	525	0	0	0	0	1890	0	350											
0	0	0	0	0	0	0	0	0	0	0	1575	0	0										
0	0	0	3150	0	0	0	0	0	0	6300	0	1890	0	0									
0	0	0	0	0	0	0	0	3150	0	0	0	0	0	0	0								
0	0	0	0	0	0	0	0	0	3150	0	0	0	0	0	0	0							
0	0	0	0	0	0	945	0	525	0	0	0	0	0	0	2250	0	630						
0	0	0	0	0	0	0	525	0	945	0	0	0	0	0	0	1890	0	630					
0	0	0	0	0	0	3150	0	0	0	0	0	0	0	0	6300	0	1890	0	0				
0	0	0	0	0	0	0	3150	0	0	0	0	0	0	0	0	6300	0	2250	0	0			
0	0	0	0	0	0	0	0	0	0	0	0	0	3150	0	0	0	0	0	0	0	0		
0	0	0	0	0	0	0	0	0	0	0	945	0	945	0	0	0	0	0	0	0	2250	1134	
0	0	0	0	0	0	0	0	0	0	0	3150	0	0	0	0	0	0	0	0	0	6300	2250	0

Symmetric

Matrix $[K_3]$

Multiplier $\frac{16a}{105b^3}$

0																								
0	0																							
0	0	0																						
0	0	0	0																					
0	0	0	0	0																				
0	0	0	0	0	105																			
0	0	0	0	0	0	0																		
0	0	0	0	0	0	0	0																	
0	0	0	0	0	0	0	0	35																
0	0	0	0	0	0	0	0	0	315															
0	0	0	0	0	0	0	0	0	0	0														
0	0	0	0	0	0	0	0	0	0	0	0													
0	0	0	0	0	35	0	0	0	0	0	0	21												
0	0	0	0	0	0	0	0	0	0	0	0	0	105											
0	0	0	0	0	210	0	0	0	0	0	0	70	0	756										
0	0	0	0	0	0	0	0	0	0	0	0	0	0	0	0									
0	0	0	0	0	0	0	0	0	0	0	0	0	0	0	0	0								
0	0	0	0	0	0	0	0	21	0	0	0	0	0	0	0	0	15							
0	0	0	0	0	0	0	0	0	105	0	0	0	0	0	0	0	0	63						
0	0	0	0	0	0	0	0	70	0	0	0	0	0	0	0	0	42	0	252					
0	0	0	0	0	0	0	0	0	630	0	0	0	0	0	0	0	0	210	0	1500				
0	0	0	0	0	0	0	0	0	0	0	0	0	0	0	0	0	0	0	0	0	0			
0	0	0	0	0	0	0	0	0	0	0	0	0	63	0	0	0	0	0	0	0	0	45		
0	0	0	0	0	0	0	0	0	0	0	0	0	210	0	0	0	0	0	0	0	0	126	500	

Symmetric

Matrix $[K_4]$

Multiplier $\frac{16}{1575ab}$

0																															
0	0																														
0	0	0																													
0	0	0	0																												
0	0	0	0	1575																											
0	0	0	0		0	0																									
0	0	0	0		0	0	0																								
0	0	0	0		0	0	0	2100																							
0	0	0	0		0	0	0		0	2100																					
0	0	0	0		0	0	0		0		0	0																			
0	0	0	0		0	0	0		0		0	0	0																		
0	0	0	0	1575	0	0		0		0	0	0	2835																		
0	0	0	0		0	0	0		0		0	0	0		0	2800															
0	0	0	0	1575	0	0		0		0	0	0	1575		0	2835															
0	0	0	0		0	0	0		0		0	0	0		0		0	0													
0	0	0	0		0	0	0		0		0	0	0		0		0	0	0												
0	0	0	0		0	0	0	2520		0	0	0		0		0		0	0	0	3600										
0	0	0	0		0	0	0		0	2100	0	0		0		0		0	0	0		0	3780								
0	0	0	0		0	0	0	2100		0	0	0		0		0		0	0	0	2520		0	3780						
0	0	0	0		0	0	0		0	2520	0	0		0		0		0	0	0		0	2520		0	3600					
0	0	0	0		0	0	0		0		0	0	0		0		0	0	0		0		0		0		0	0			
0	0	0	0	1575	0	0		0		0	0	0	3375		0	1575	0	0		0		0		0		0	0	4375			
0	0	0	0	1575	0	0		0		0	0	0	2835		0	2835	0	0		0		0		0		0	0	3375	5103		
0	0	0	0	1575	0	0		0		0	0	0	1575		0	3375	0	0		0		0		0		0	0	1575	3375	4375	

Symmetric

APPENDIX II

5.2 Consistent Force Vector for Uniformly Distributed Load On a Refined Plate Element

In this section, the kinematically consistent force vector for uniformly distributed loads $p(x,y)$, defined as acting on a unit area of the refined plate element, is derived. The equivalent concentrated forces in the directions of the element displacements, as defined in Section 2.4.3, are represented by the vector $\{F\}_p^e$. These concentrated nodal forces must be made statically equivalent to the distributed loads $p(x,y)$ acting on an element.

The simplest procedure to achieve this equivalence is to impose an arbitrary virtual nodal displacement and to equate the external and internal work done by the distributed loads and the equivalent concentrated nodal forces. Let such a displacement be $\{\delta^e\}$ at the nodes. Using Eq. 2.26 b, and denoting virtual by a tilde, the displacement within an element is given by:

$$\tilde{w} = <P> \{\tilde{\alpha}\} \qquad \text{(A2.1)}$$

or making use of Eq. 2.33 b, by:

$$\tilde{w} = <P> [C^{-1}] \{\tilde{\delta}^e\} \qquad \text{(A2.2)}$$

Equating the internal work to the external one leads to

$$\{\tilde{\delta}^e\}^T \{F\}_p^e = -\iint_A p(x,y)\ \tilde{w}(x,y)\ dxdy \qquad (A2.3)$$

or:

$$\{\tilde{\delta}^e\}^T \{F\}_p^e = \{\tilde{\delta}^e\}^T \left[-[C^{-1}]^T \iint_A <P>^T p(x,y)\ dxdy \right]$$

From this equation it follows that:

$$\{F\}_p^e = -[C^{-1}]^T \iint_A <P>^T p(x,y)\ dxdy \qquad (A2.4)$$

It should be noted that any distribution of load $p(x,y)$ can be treated using this approach. The integration is performed explicitely for a uniformly distributed load

$$q = p(x,y) = \text{constant} \qquad (A2.5)$$

The result is listed below. The final load vector is generated in the digital computer. In a similar way, the force vector for any other distribution of load or for a concentrated load acting within the element could be derived. In the same way, force vectors corresponding to distributed edge loads can be derived.

Force vector for uniformly distributed load:

$$\{F\}_p^e = -[C^{-1}]^T \, q\,a\,b \int_{-1}^{+1}\int_{-1}^{+1} \begin{bmatrix} 1 \\ \xi \\ \eta \\ \xi^2 \\ \xi\eta \\ \eta^2 \\ \xi^3 \\ \xi^2\eta \\ \xi\eta^2 \\ \eta^3 \\ \xi^4 \\ \xi^3\eta \\ \xi^2\eta^2 \\ \xi\eta^3 \\ \eta^4 \\ \xi^5 \\ \xi^4\eta \\ \xi^3\eta^2 \\ \xi^2\eta^3 \\ \xi\eta^4 \\ \eta^5 \\ \xi^5\eta \\ \xi^3\eta^3 \\ \xi\eta^5 \end{bmatrix} d\eta d\xi = -[C^{-1}]^T \frac{4qab}{45} \begin{bmatrix} 45 \\ 0 \\ 0 \\ 15 \\ 0 \\ 15 \\ 0 \\ 0 \\ 0 \\ 0 \\ 9 \\ 0 \\ 5 \\ 0 \\ 9 \\ 0 \\ 0 \\ 0 \\ 0 \\ 0 \\ 0 \\ 0 \\ 0 \\ 0 \end{bmatrix}$$

APPENDIX III

5.3 Derivation of Stiffness Matrix of the ACM Plate Bending Element

As discussed in Section 3.3.2, the polynomial expression representing the displacement field within an element is given by Eq. 3.1. The displacement components introduced at node i of the finite plate element are:

$$\{\delta_i\}^T = < w \quad \theta_x \quad \theta_y > \tag{A3.1}$$

Element displacements are given as the listing of the following nodal displacements:

$$\{\delta^e\}^T = < \delta_i^T \quad \delta_j^T \quad \delta_k^T \quad \delta_\ell^T > \tag{A3.2}$$

Similarly, element forces are given by:

$$\{F^e\}^T = < F_i^T \quad F_j^T \quad F_k^T \quad F_\ell^T > \tag{A3.3}$$

The derivation of the stiffness matrix proceeds exactly as described for the refined plate element, shown in Appendix I. First, the vector of generalized coordinates is expressed as:

$$\{\alpha\} = [\bar{C}]^{-1} [T_1] \{\delta^e\} = [C]^{-1} \{\delta^e\} \tag{A3.4}$$

in which $[T_1]$ is a (12 x 12) transformation matrix relating the modified element displacement vector to the actual displacement vector, defined by Eq. A3.2. Matrix $[\bar{C}]$ is a connection matrix consisting of numbers only; both matrices are listed in this appendix. The relationship between generalized stresses and generalized strains is given by:

$$\{M\} = [D]\ \{\emptyset\} \tag{A3.5}$$

where

$$[D] = \begin{bmatrix} D_{11} & D_{12} & D_{13} \\ D_{21} & D_{22} & D_{23} \\ D_{31} & D_{32} & D_{33} \end{bmatrix} \tag{A3.6}$$

$$\text{with } D_{ij} = D_{ji} \text{ for } i \neq j$$

$$\{M\}^T = < M_x \quad M_y \quad M_{xy} > \tag{A3.8}$$

and

$$\{\emptyset\}^T = < -\frac{\partial^2 w}{\partial x^2} \quad -\frac{\partial^2 w}{\partial y^2} \quad 2\frac{\partial^2 w}{\partial x \partial y} > \tag{A3.9}$$

All terms of the stress matrix [D] must be considered in this derivation, since for the elastic-plastic analysis, the stiffness matrix will be used in its complete form. Generalized strains can be expressed in terms of element displacements by:

$$\{\emptyset\} = [Q]\ [C]^{-1}\ \{\delta^e\} = [B]\ \{\delta^e\} \tag{A3.10}$$

Minimization of the total potential energy leads to the stiffness relation governing the out-of-plane behavior of the plate element:

$$\{F^e\} = \left[\iint_A [B]^T [D] [B] \, dxdy \right] \{\delta^e\} \tag{A3.11}$$

Hence, the stiffness matrix is given by:

$$[K^e]_{12x12} = \iint_A [B]^T [D] [B] \, dxdy \tag{A3.12}$$

where the integration is to be taken over the area of the plate element. Carrying out the necessary operations, the result can again be given in a form suitable for the elastic-plastic analysis:

$$[K^e]_{12x12} = [C^{-1}]^T \Big[D_{11}[K_1] + D_{12}[K_2] + D_{13}[K_3] + D_{22}[K_4] + D_{23}[K_5] + D_{33}[K_6] \Big] [C^{-1}] \tag{A3.13}$$

The component matrices are listed subsequently and the final assembly of the stiffness matrix is again performed with the aid of the digital computer.

$$[T_1] = \begin{bmatrix} 1 & 0 & 0 & & & & & & & & & \\ 0 & b & 0 & & & & & & & & & \\ 0 & 0 & a & & & & & & & & & \\ & & & 1 & 0 & 0 & & & & & & \\ & & & 0 & b & 0 & & & & & & \\ & & & 0 & 0 & a & & & & & & \\ & & & & & & 1 & 0 & 0 & & & \\ & & & & & & 0 & b & 0 & & & \\ & & & & & & 0 & 0 & a & & & \\ & & & & & & & & & 1 & 0 & 0 \\ & & & & & & & & & 0 & b & 0 \\ & & & & & & & & & 0 & 0 & a \end{bmatrix}$$

$$[\bar{C}] = \begin{bmatrix} 1 & -1 & 1 & 1 & -1 & 1 & -1 & 1 & -1 & 1 & -1 & -1 \\ 0 & 0 & 1 & 0 & -1 & 2 & 0 & 1 & -2 & 3 & -1 & -3 \\ 0 & -1 & 0 & 2 & -1 & 0 & -3 & 2 & -1 & 0 & -3 & -1 \\ 1 & -1 & -1 & 1 & 1 & 1 & -1 & -1 & -1 & -1 & 1 & 1 \\ 0 & 0 & 1 & 0 & -1 & -2 & 0 & 1 & 2 & 3 & -1 & -3 \\ 0 & -1 & 0 & 2 & 1 & 0 & -3 & -2 & -1 & 0 & 3 & 1 \\ 1 & 1 & 1 & 1 & 1 & 1 & 1 & 1 & 1 & 1 & 1 & 1 \\ 0 & 0 & 1 & 0 & 1 & 2 & 0 & 1 & 2 & 3 & 1 & 3 \\ 0 & -1 & 0 & -2 & -1 & 0 & -3 & -2 & -1 & 0 & -3 & -1 \\ 1 & 1 & -1 & 1 & -1 & 1 & 1 & -1 & 1 & -1 & -1 & -1 \\ 0 & 0 & 1 & 0 & 1 & -2 & 0 & 1 & -2 & 3 & 1 & 3 \\ 0 & -1 & 0 & -2 & 1 & 0 & -3 & 2 & -1 & 0 & 3 & 1 \end{bmatrix}$$

$$[K_1] = \frac{16b}{15a^3}\begin{bmatrix}
0 & & & & & & & & & & & \\
0 & 0 & & & & & & & & & & \\
0 & 0 & 0 & & & & & & & & & \\
0 & 0 & 0 & 15 & & & & & & & & \\
0 & 0 & 0 & 0 & 0 & & & & & & & \\
0 & 0 & 0 & 0 & 0 & 0 & & & & & & \\
0 & 0 & 0 & 0 & 0 & 0 & 45 & & & & & \\
0 & 0 & 0 & 0 & 0 & 0 & 0 & 5 & & & & \\
0 & 0 & 0 & 0 & 0 & 0 & 0 & 0 & 0 & & & \\
0 & 0 & 0 & 0 & 0 & 0 & 0 & 0 & 0 & 0 & & \\
0 & 0 & 0 & 0 & 0 & 0 & 0 & 0 & 0 & 0 & 15 & \\
0 & 0 & 0 & 0 & 0 & 0 & 0 & 0 & 0 & 0 & 0 & 0
\end{bmatrix}$$

Symmetric

$$[K_2] = \frac{16}{15ab}\begin{bmatrix}
0 & & & & & & & & & & & \\
0 & 0 & & & & & & & & & & \\
0 & 0 & 0 & & & & & & & & & \\
0 & 0 & 0 & 0 & & & & & & & & \\
0 & 0 & 0 & 0 & 0 & & & & & & & \\
0 & 0 & 0 & 15 & 0 & 0 & & & & & & \\
0 & 0 & 0 & 0 & 0 & 0 & 0 & & & & & \\
0 & 0 & 0 & 0 & 0 & 0 & 0 & 0 & & & & \\
0 & 0 & 0 & 0 & 0 & 0 & 15 & 0 & 0 & & & \\
0 & 0 & 0 & 0 & 0 & 0 & 0 & 15 & 0 & 0 & & \\
0 & 0 & 0 & 0 & 0 & 0 & 0 & 0 & 0 & 0 & 0 & \\
0 & 0 & 0 & 0 & 0 & 0 & 0 & 0 & 0 & 0 & 15 & 0
\end{bmatrix}$$

Symmetric

$$[K_3] = \frac{16}{15a^2}$$

$$\begin{bmatrix}
0 & & & & & & & & & & & \\
0 & 0 & & & & & & & & & & \\
0 & 0 & 0 & & & & & & & & & \\
0 & 0 & 0 & 0 & & & & \text{Symmetric} & & & & \\
0 & 0 & 0 & -15 & 0 & & & & & & & \\
0 & 0 & 0 & 0 & 0 & 0 & & & & & & \\
0 & 0 & 0 & 0 & 0 & 0 & 0 & & & & & \\
0 & 0 & 0 & 0 & 0 & 0 & -30 & 0 & & & & \\
0 & 0 & 0 & 0 & 0 & 0 & 0 & -10 & 0 & & & \\
0 & 0 & 0 & 0 & 0 & 0 & 0 & 0 & 0 & 0 & & \\
0 & 0 & 0 & -15 & 0 & 0 & 0 & 0 & 0 & 0 & 0 & \\
0 & 0 & 0 & -15 & 0 & 0 & 0 & 0 & 0 & 0 & 0 & 0
\end{bmatrix}$$

$$[K_4] = \frac{16a}{15b^3}$$

$$\begin{bmatrix}
0 & & & & & & & & & & & \\
0 & 0 & & & & & & & & & & \\
0 & 0 & 0 & & & & & & & & & \\
0 & 0 & 0 & 0 & & & & \text{Symmetric} & & & & \\
0 & 0 & 0 & 0 & 0 & & & & & & & \\
0 & 0 & 0 & 0 & 0 & 15 & & & & & & \\
0 & 0 & 0 & 0 & 0 & 0 & 0 & & & & & \\
0 & 0 & 0 & 0 & 0 & 0 & 0 & 0 & & & & \\
0 & 0 & 0 & 0 & 0 & 0 & 0 & 0 & 5 & & & \\
0 & 0 & 0 & 0 & 0 & 0 & 0 & 0 & 0 & 45 & & \\
0 & 0 & 0 & 0 & 0 & 0 & 0 & 0 & 0 & 0 & 0 & \\
0 & 0 & 0 & 0 & 0 & 0 & 0 & 0 & 0 & 0 & 0 & 15
\end{bmatrix}$$

$$[K_5] = \frac{16}{15b^2}$$

0											
0	0										
0	0	0									
0	0	0	0								
0	0	0	0	0							
0	0	0	0	-15	0						
0	0	0	0	0	0	0					
0	0	0	0	0	0	0	0				
0	0	0	0	0	0	0	-10	0			
0	0	0	0	0	0	0	0	-30	0		
0	0	0	0	0	-15	0	0	0	0	0	
0	0	0	0	0	-15	0	0	0	0	0	0

Symmetric

$$[K_6] = \frac{16}{15ab}$$

0											
0	0										
0	0	0									
0	0	0	0								
0	0	0	0	15							
0	0	0	0	0	0						
0	0	0	0	0	0	0					
0	0	0	0	0	0	0	20				
0	0	0	0	0	0	0	0	20			
0	0	0	0	0	0	0	0	0	0		
0	0	0	0	15	0	0	0	0	0	27	
0	0	0	0	15	0	0	0	0	0	15	27

Symmetric

APPENDIX IV

5.4 Derivation of In-Plane Stiffness Matrix

The displacement field representing in-plane behavior of the plate element was discussed in Section 3.3.2 and is given by Eq. 3.2 and Eq. 3.3. The nodal displacement vector is defined as:

$$\{\delta_i\}^T = < u_i \quad v_i > \tag{A4.1}$$

and the corresponding element displacement vector as:

$$\{\delta^e\}^T = < u_i \quad v_i \quad u_j \quad v_j \quad u_k \quad v_k \quad u_\ell \quad v_\ell > \tag{A4.2}$$

The vector of generalized coordinates is found by enforcing compatibility of displacements at the four nodal points:

$$\{\alpha\} = [C]^{-1} \{\delta^e\} \tag{A4.3}$$

The connection matrix [C] can be inverted with ease in the present case. The vectors of strains and stresses are defined as:

$$\{\epsilon\} = \begin{bmatrix} \epsilon_x \\ \epsilon_y \\ \gamma_{xy} \end{bmatrix} = \begin{bmatrix} \partial u/\partial x \\ \partial v/\partial y \\ \partial u/\partial y + \partial v/\partial x \end{bmatrix} \tag{A4.4}$$

and

$$\{\sigma\}^T = < \sigma_x \quad \sigma_y \quad \tau_{xy} > \tag{A4.5}$$

The relationship between stresses and strains is given by

$$\{\sigma\} = [D]\ \{\epsilon\} \tag{A4.6}$$

where for an isotropic material:

$$[D] = \frac{E}{1-\nu^2}\begin{bmatrix} 1 & \nu & 0 \\ \nu & 1 & 0 \\ 0 & 0 & \frac{1-\nu}{2} \end{bmatrix} \tag{A4.7}$$

and for an anisotropic material, the stress matrix is of the form:

$$[D] = \begin{bmatrix} D_{11} & D_{12} & D_{13} \\ D_{21} & D_{22} & D_{23} \\ D_{31} & D_{32} & D_{33} \end{bmatrix} \tag{A4.8}$$

$$\text{with } D_{ij} = D_{ji} \text{ for } i \neq j$$

Strains can be expressed in terms of element displacements as:

$$\{\epsilon\} = [Q]\ \{\alpha\} = [Q]\ [C]^{-1}\ \{\delta^e\} = [B]\ \{\delta^e\} \tag{A4.9}$$

The force-deformation relationship governing the in-plane behavior of the plate element is derived from a minimization of the total potential energy:

$$\{F^e\} = \left[\iint [B]^T\ [D]\ [B]\ dxdy\right]\ \{\delta^e\} \tag{A4.10}$$

Hence, the stiffness matrix is given by:

$$[K^e]_{8x8} = \iint_A [B]^T [D] [B] \, dxdy \qquad (A4.11)$$

The integration can be performed with ease, and the final result, given for the case of anisotropic material, and hence, suitable for the elastic-plastic analysis, is listed below.

$$
\begin{array}{cccccccc}
16\beta D_{11} & -12D_{12} & 8\beta D_{11} & 12D_{12} & -16\beta D_{11} & -12D_{12} & -8\beta D_{11} & 12D_{12} \\
+16\alpha D_{33} & +16\alpha D_{23} & -16\alpha D_{33} & -16\alpha D_{23} & +8\alpha D_{33} & +8\alpha D_{23} & -8\alpha D_{33} & -8\alpha D_{23} \\
 & -12D_{33} & & -12D_{33} & & +12D_{33} & & +12D_{33} \\
 & 16\alpha D_{22} & -12D_{12} & -16\alpha D_{22} & 12D_{12} & 8\alpha D_{22} & 12D_{12} & -8\alpha D_{22} \\
 & -24D_{23} & -16\alpha D_{23} & +8\beta D_{33} & +8\alpha D_{23} & -16\beta D_{33} & -8\alpha D_{23} & +24D_{23} \\
 & +16\beta D_{33} & +12D_{33} & & -12D_{33} & & +12D_{33} & -8\beta D_{33} \\
 & & 16\beta D_{11} & 12D_{12} & -8\beta D_{11} & -12D_{12} & -16\beta D_{11} & 12D_{12} \\
 & & +16\alpha D_{33} & +16\alpha D_{23} & -8\alpha D_{33} & -8\alpha D_{23} & +8\alpha D_{33} & +8\alpha D_{23} \\
 & & & +12D_{33} & & -12D_{33} & & -12D_{33} \\
 & & & 16\alpha D_{22} & -12D_{12} & -8\alpha D_{22} & -12D_{12} & 8\alpha D_{22} \\
 & & & +24D_{23} & -8\alpha D_{23} & -24D_{23} & +8\alpha D_{23} & -16\beta D_{33} \\
 & & & +16\beta D_{33} & -12D_{33} & -8\beta D_{33} & +12D_{33} & \\
 & & & & 16\beta D_{11} & 12D_{12} & 8\beta D_{11} & -12D_{12} \\
 & \text{Symmetric} & & & +16\alpha D_{33} & +16\alpha D_{23} & -16\alpha D_{33} & -16\alpha D_{23} \\
 & & & & & +12D_{33} & & +12D_{33} \\
 & & & & & 16\alpha D_{22} & 12D_{12} & -16\alpha D_{22} \\
 & & & & & +24D_{23} & -16\alpha D_{23} & +8\beta D_{33} \\
 & & & & & +16\beta D_{33} & -12D_{33} & \\
 & & & & & & 16\beta D_{11} & -12D_{12} \\
 & & & & & & +16\alpha D_{33} & +16\alpha D_{23} \\
 & & & & & & & -12D_{33} \\
 & & & & & & & 16\alpha D_{22} \\
 & & & & & & & -24D_{23} \\
 & & & & & & & +16\beta D_{33}
\end{array}
$$

Matrix $[K^e]$

Multiplier $\frac{h}{48}$ $\qquad \alpha = \frac{a}{b} \qquad \beta = \frac{b}{a}$

APPENDIX V

5.5 Evaluation of St. Venant Torsion Constant K_T for an Arbitrarily Shaped Solid Cross Section

Closed form solutions for the St. Venant torsion problem exist only for a few geometrically simple cross sections. An approximate solution based on the finite element concept is presented in this appendix. As shown in Ref. 46, the fundamental partial differential equation governing the behavior of a transversely loaded plate, given by Eq. 2.14, can be split into the two partial differential equations of the second order:

$$M = \frac{M_x + M_y}{1 + \nu} = -\left[\frac{\partial^2 w}{\partial x^2} + \frac{\partial^2 w}{\partial y^2}\right] \qquad \text{(A5.1)}$$

and

$$q = -\nabla^2 M = -\left[\frac{\partial^2 M}{\partial x^2} + \frac{\partial^2 M}{\partial y^2}\right] \qquad \text{(A5.2)}$$

when the plate rigidity is taken as unity. On the other hand, the stress function $\psi(x,y)$ introduced often to solve the problem of St. Venant torsion of a solid cross section, must satisfy the following differential equation:

$$\frac{\partial^2 \psi}{\partial x^2} + \frac{\partial^2 \psi}{\partial y^2} = -2G\emptyset' \qquad \text{(A5.3)}$$

where: $\psi(x,y)$ = Stress function introduced

$\emptyset'$ = Rate of twist

G = Shear modulus

The determination of the stress distribution over the cross section of a twisted bar consists in finding the function $\psi(x,y)$ which satisfies Eq. A5.3 and the given boundary conditions. Shear stresses are expressed as:

$$\tau_{xz} = \frac{\partial \psi}{\partial y} \tag{A5.4}$$

$$\tau_{yz} = -\frac{\partial \psi}{\partial x} \tag{A5.5}$$

and the twisting moment is given as:

$$T_{St.V.} = 2 \iint_A \psi dxdy = K_T G \emptyset' \tag{A5.6}$$

where: K_T = St. Venant torsion constant

The integration is to be taken over the area of the cross section. Recognizing that Eq. A5.2 is formally identical with Eq. A5.3, it can be concluded that the problems of solving the first equation for M or the second equation for ψ are analogous. Hence, instead of solving the torsion problem for a given cross section, one can solve the corresponding plate bending problem. Accordingly, a plate which is of the same shape as the cross section to be analyzed for torsion, is analyzed for a uniformly distributed transverse load

of unit intensity. Any conventional finite element program capable of analyzing plate bending problems can be used to find the moment field. The moment sum M defined by Eq. A5.1 can then be computed at each mesh point.

Pursuing this analogy, the St. Venant torsion moment is found to be:

$$T_{St.V.} = 2 \iint_A M \, dxdy = K_T G \frac{q}{2G} = K_T \frac{q}{2} \qquad (A5.7)$$

from which the St. Venant torsion constant is derived as:

$$K_T = 4 \iint_A M \, dxdy = 4V \qquad (A5.8)$$

where V is the volume under the surface created by plotting the moment sum values M at each mesh point. Having found the moment field, the integral in Eq. A5.8 can be evaluated using any conventional numerical integration procedure.

The shearing stresses in the twisted cross section correspond to the shear forces in the analogous plate bending problem.

$$\tau_{xz} = \frac{\partial M}{\partial y} = -\frac{\partial}{\partial y}\left[\frac{\partial^2 w}{\partial x^2} + \frac{\partial^2 w}{\partial y^2}\right] = Q_y \qquad (A5.9)$$

$$\tau_{yz} = -\frac{\partial M}{\partial x} = \frac{\partial}{\partial x}\left[\frac{\partial^2 w}{\partial x^2} + \frac{\partial^2 w}{\partial y^2}\right] = -Q_x$$

and can be evaluated once the displacement field is known.

A solid square cross section of unit width was analyzed to verify the proposed method for determining the St. Venant torsion constant K_T. According to this analogy, a square plate with four simple supports is to be analyzed for a uniformly distributed transverse load of unit intensity. The described refined plate element discussed in Chapter 2 was used to find the displacement field and the associated moment field. Simpson's rule was used for the numerical integration. Two meshes were processed and the following results were obtained:

Mesh	K_T (in.^{4})	Error in (%)
4 x 4	0.1382	-1.74%
8 x 8	0.1398	-0.57%
Exact Value	0.1406	Ref. 48

Due to the great versatility of the finite element method, this procedure can be applied to any arbitrary shape. Cross sections built-up of regions having varying material properties can be treated. This approach was taken in the evaluation of K_T for the AASHO Type III beam used in the investigation on lateral distribution of load, discussed in Chapter 3.

6. NOMENCLATURE

a.) Scalars

A_s = Cross-sectional area of stiffener

a = Half length of plate element

a_i = Coefficients of polynomial expansion

b = Half width of plate element

b_i = Coefficients of polynomial expansion

c = Length of correction vector

D = Plate stiffness

D_x, D_y, D_{xy}, D_1 = Coefficients of stress matrix for orthotropic material

D_{ij} = Coefficients of stress matrix for anisotropic material

E = Modulus of elasticity of plate

E_s = Modulus of elasticity of stiffener

G = Shear modulus

h = Plate thickness

I_s = Moment of inertia of the stiffener area with respect to plane of reference

I_w = Warping constant

K_T = St. Venant torsional constant

L = Length of stiffener element; or span length

M_x, M_y, M_{xy} = Plate bending moments per unit width

M_s = Bending moment in stiffener with respect to plane of reference

N_s = Axial force in stiffener

p = Distributed load per unit area of finite element

Q_x, Q_y = Plate shearing forces per unit width

q = Distributed load per unit area of plate

S_s = First moment of the stiffener area with respect to plane of reference

T = Total twisting moment in stiffener

$T_{St.V.}$ = St. Venant torsional moment

T_w = Warping torsional moment

U = In-plane displacement in x-direction of a point lying outside the middle plane of the plate

U^* = Complementary strain energy

u = In-plane displacement in x-direction of a point lying in the middle plane of the plate

V = In-plane displacement in y-direction of a point lying outside the middle plane of the plate

v = In-plane displacement in y-direction of a point lying in the middle plane of the plate

w = Lateral deflection in z-direction

Z = Shear force in stiffener in z-direction

α_i = Coefficients of polynomial expansion

γ_{xy} = Shearing strain

δ = Variation of functional

ϵ_x, ϵ_y = Strain in x-direction and y-direction, respectively

ϵ_{ij} = Components of strain tensor

η = Non-dimensionalized coordinate

θ_x, θ_y = Slope about x-axis and y-axis, respectively

λ = Positive scalar

ν = Poisson's Ratio

ξ = Non-dimensionalized coordinate

π = Total potential energy functional

π^* = Total complementary energy functional

σ_x, σ_y = Normal stresses in x-direction and y-direction, respectively

σ_s = Axial stress in stiffener

τ_{xy} = Shearing stress

$\phi_x, \phi_y, \phi_{xy}$ = Curvatures of plate surface

ϕ' = Rate of change of angle of twist

ψ = Stress function

∇^2 = Laplace operator

b.) Vectors and Matrices

$[B]$ = Matrix relating element displacements to generalized strains

$[C]$ = Matrix relating element displacements to generalized coordinates

$[\bar{C}]$ = Matrix relating modified element displacements to generalized coordinates

$[D]$ = Stress matrix relating generalized strains to generalized stresses

$\{F\}$ = Overall force vector of system

$\{F^e\}$ = Vector of generalized element forces

$\{F_i\}$ = Vector of generalized nodal forces

$[K]$ = Overall structural stiffness matrix

$[K^e]$ = Element stiffness matrix

$[K_i]$ = Component stiffness matrix

$[L]$ = Lower triangular matrix

$\{M\}$ = Vector of plate bending moments

$\{M_s\}$ = Vector of generalized forces acting on stiffener element

$< P >$ = Row vector listing polynomial terms

$[Q]$ = Matrix relating generalized coordinates to generalized strains

$\{R\}^e$ = Vector of external forces

$[T_l]$ = Transformation matrix relating element displacements to modified element displacements

$\{Y\}$ = Auxiliary vector used in Choleski decomposition

$\{\alpha\}$ = Vector of generalized coordinates

$\{\delta\}$ = Overall displacement vector of system

$\{\delta^e\}$ = Vector of generalized element displacements

$\{\delta_i\}$ = Vector of generalized nodal displacements

$\{\epsilon_s\}$ = Vector of generalized strains for beam element

$\{\phi\}$ = Vector of curvatures of plate surface

7. TABLES

TABLE 1: CLAMPED SQUARE PLATE - PROBLEM P1

a.) Center Deflection Under Uniformly Distributed Unit Load

Source	Mesh 2 x 2	Mesh 4 x 4	Mesh 8 x 8	Mesh 16 x 16	Multiplier
New Element	0.001594	0.001325	0.001284	0.001266	$\frac{qL^4}{D}$
ACM (Ref. 6)	0.001480	0.001403	0.001304	0.001275	
Exact Value	0.00126				

b.) Center Deflection Under Single Concentrated Load

Source	Mesh 2 x 2	Mesh 4 x 4	Mesh 8 x 8	Mesh 16 x 16	Multiplier
New Element	0.005912	0.005634	0.005611	0.005607	$\frac{PL^2}{D}$
ACM (Ref. 6)	0.005919	0.006134	0.005803	0.005672	
Exact Value	0.00560				

TABLE 2: SIMPLY SUPPORTED SQUARE PLATE - PROBLEM P2

a.) Center Deflection Under Uniformly Distributed Unit Load

Source	Mesh 2 x 2	Mesh 4 x 4	Mesh 8 x 8	Mesh 16 x 16	Multiplier
New Element	0.004187	0.004076	0.004064	0.004063	$\frac{qL^4}{D}$
ACM (Ref. 6)	0.003446	0.003939	0.004033	0.004056	
Exact Value	0.004062				

b.) Center Deflection Under Single Concentrated Load

Source	Mesh 2 x 2	Mesh 4 x 4	Mesh 8 x 8	Mesh 16 x 16	Multiplier
New Element	0.011265	0.011497	0.011572	0.011593	$\frac{PL^2}{D}$
ACM (Ref. 6)	0.013784	0.012327	0.011829	0.011671	
Exact Value	0.01160				

TABLE 3: CENTER DEFLECTION - PROBLEMS P3 AND P4

Problem P3: Center Deflection Under Uniformly Distributed Unit Load

Source	Mesh 2 x 2	Mesh 4 x 4	Mesh 8 x 8	Mesh 16 x 16	Multiplier
New Element	0.005208	0.005671	0.005769	0.005793	$\frac{qL^4}{D}$
ACM (Ref. 6)	0.005208	0.005779	0.005843	0.005821	
Exact Value	0.00581				

Problem P4: Center Deflection Under Uniformly Distributed Unit Load

Source	Mesh 2 x 2	Mesh 4 x 4	Mesh 8 x 8	Mesh 16 x 16	Multiplier
New Element	0.025770	0.025544	0.025512	0.025507	$\frac{qL^4}{D}$
ACM (Ref. 6)	0.021790	0.024296	0.025178	0.025422	
Ref. 82	0.0265				

TABLE 4: DEFLECTION PROFILES -

UNIFORMLY LOADED PLATE

Multiplier $\frac{qL^4}{D}$

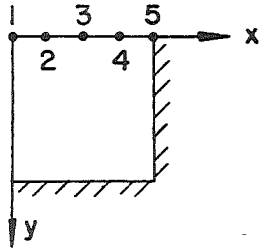

	Mesh	Point 1	Point 2	Point 3	Point 4	Point 5
Problem P1	4 x 4	0.001325		0.000805		0.
	8 x 8	0.001284	0.001145	0.000769	0.000283	0.
	16 x 16	0.001266	0.001131	0.000759	0.000279	0.
	Exact Value	0.001260				0.
Problem P2	4 x 4	0.004076		0.002948		0.
	8 x 8	0.004064	0.003778	0.002939	0.001624	0.
	16 x 16	0.004063	0.003776	0.002938	0.001623	0.
	Exact Value	0.004062	0.003776	0.002938	0.001623	0.
Problem P3	4 x 4	0.005671		0.004967		0.004228
	8 x 8	0.005769	0.005564	0.005058	0.004539	0.004319
	16 x 16	0.005793	0.005587	0.005081	0.004562	0.004343
	Exact Value	0.00581				
Problem P4	4 x 4	0.025544		0.023053		0.017791
	8 x 8	0.025512	0.024853	0.023018	0.020428	0.017754
	16 x 16	0.025507	0.024848	0.023013	0.020424	0.017750
	Ref. 82	0.0265				0.0170

TABLE 5: DEFLECTION PROFILES -

SINGLE CONCENTRATED LOAD

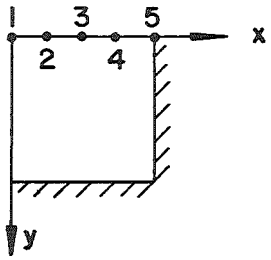

Multiplier $\frac{PL^2}{D}$

	Mesh	Point 1	Point 2	Point 3	Point 4	Point 5
Problem P1	4 x 4	0.005634		0.002573		0.
	8 x 8	0.005611	0.004417	0.002484	0.000781	0.
	16 x 16	0.005607	0.004404	0.002470	0.000771	0.
	Exact Value	0.00560				0.
Problem P2	4 x 4	0.011497		0.007144		0.
	8 x 8	0.011572	0.010066	0.007141	0.003670	0.
	16 x 16	0.011593	0.010068	0.007139	0.003669	0.
	Exact Value	0.01160	0.010066	0.007139	0.003668	0.
Problem P3	4 x 4	0.011341		0.008044		0.005671
	8 x 8	0.011538	0.010259	0.008153	0.006427	0.005769
	16 x 16	0.011585	0.010286	0.008176	0.006451	0.005793
	Exact Value					
Problem P4	4 x 4	0.039055		0.032957		0.022964
	8 x 8	0.039117	0.037131	0.032934	0.027859	0.022920
	16 x 16	0.039159	0.037128	0.032925	0.027850	0.022911
	Exact Value					

TABLE 6: PLATE MOMENTS M_x -

UNIFORMLY LOADED PLATE

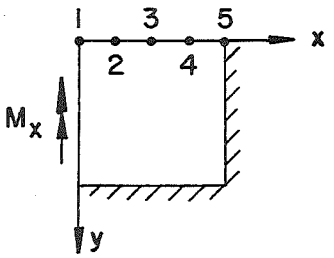

Multiplier qL^2

	Mesh	Point 1	Point 2	Point 3	Point 4	Point 5
Problem P1	4 x 4	0.0215		0.0109		-0.0574
	8 x 8	0.0230	0.0194	0.0104	-0.0102	-0.0515
	16 x 16	0.0229	0.0202	0.0108	-0.0102	-0.0515
	Exact Value	0.0231				-0.0513
Problem P2	4 x 4	0.0454		0.0383		0.
	8 x 8	0.0475	0.0454	0.0385	0.0248	0.
	16 x 16	0.0478	0.0457	0.0388	0.0248	0.
	Exact Value	0.0479	0.0458	0.0390	0.0250	0.
Problem P3	4 x 4	0.0254		0.0053		-0.0236
	8 x 8	0.0317	0.0250	0.0079	-0.0109	-0.0194
	16 x 16	0.0328	0.0261	0.0089	-0.0101	-0.0185
	Exact Value	0.0331				-0.0185
Problem P4	4 x 4	0.1069		0.0760		0.
	8 x 8	0.1101	0.1025	0.0803	0.0440	0.
	16 x 16	0.1112	0.1037	0.0814	0.0458	0.
	Ref. 82	0.109				0.

TABLE 7: PLATE MOMENTS M_x -

SINGLE CONCENTRATED LOAD

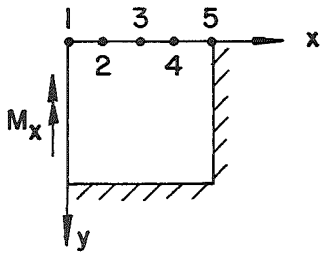

Multiplier P

	Mesh	Point 1	Point 2	Point 3	Point 4	Point 5
Problem P1	4 x 4			-0.0092		-0.1376
	8 x 8		0.0548	-0.0025	-0.0522	-0.1299
	16 x 16		0.0680	-0.0010	-0.0525	-0.1265
	Exact Value					-0.1257
Problem P2	4 x 4			0.0460		0.
	8 x 8		0.1093	0.0568	0.0242	0.
	16 x 16		0.1226	0.0586	0.0242	0.
	Exact Value		0.1231	0.0585	0.0251	0.
Problem P3	4 x 4			-0.0274		-0.0784
	8 x 8		0.0516	-0.0117	-0.0562	-0.0721
	16 x 16		0.0663	-0.0085	-0.0538	-0.0702
	Exact Value					
Problem P4	4 x 4			0.0926		0.
	8 x 8		0.1822	0.1094	0.0468	0.
	16 x 16		0.1974	0.1126	0.0500	0.
	Exact Value					0.

TABLE 8: PLATE MOMENTS M_y -
UNIFORMLY LOADED PLATE

Multiplier qL^2

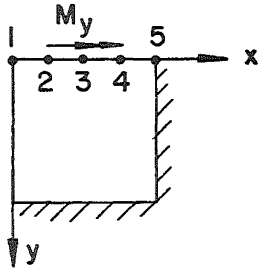

	Mesh	Point 1	Point 2	Point 3	Point 4	Point 5
Problem P1	4 x 4	0.0215		0.0098		-0.0214
	8 x 8	0.0230	0.0202	0.0121	-0.0015	-0.0176
	16 x 16	0.0229	0.0203	0.0125	-0.0001	-0.0158
	Exact Value	0.0231				-0.0154
Problem P2	4 x 4	0.0454		0.0350		0.
	8 x 8	0.0475	0.0444	0.0348	0.0205	0.
	16 x 16	0.0478	0.0447	0.0355	0.0203	0.
	Exact Value	0.0479	0.0448	0.0356	0.0204	0.
Problem P3	4 x 4	0.0254		0.0411		0.0548
	8 x 8	0.0317	0.0341	0.0406	0.0488	0.0527
	16 x 16	0.0328	0.0349	0.0410	0.0483	0.0517
	Exact Value	0.0331				0.0512
Problem P4	4 x 4	0.1069		0.1119		0.1706
	8 x 8	0.1101	0.1126	0.1208	0.1307	0.1617
	16 x 16	0.1112	0.1137	0.1214	0.1341	0.1570
	Ref. 82	0.109				0.140

TABLE 9: PLATE MOMENTS M_y -

SINGLE CONCENTRATED LOAD

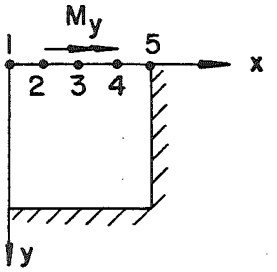

Multiplier P

	Mesh	Point 1	Point 2	Point 3	Point 4	Point 5
Problem P1	4 x 4			0.0489		-0.0532
	8 x 8		0.1232	0.0488	-0.0021	-0.0429
	16 x 16		0.1253	0.0478	-0.0016	-0.0379
	Exact Value					-0.0377
Problem P2	4 x 4			0.1040		0.
	8 x 8		0.1764	0.0999	0.0489	0.
	16 x 16		0.1784	0.0990	0.0456	0.
	Exact Value		0.1776	0.0982	0.0456	0.
Problem P3	4 x 4			0.0942		0.0784
	8 x 8		0.1433	0.0930	0.0755	0.0721
	16 x 16		0.1447	0.0917	0.0740	0.0702
	Exact Value					
Problem P4	4 x 4			0.2033		0.2272
	8 x 8		0.2645	0.2122	0.1941	0.2142
	16 x 16		0.3316	0.2292	0.1992	0.1962
	Exact Value					

TABLE 10: PLATE MOMENTS M_{xy} -
UNIFORMLY LOADED PLATE

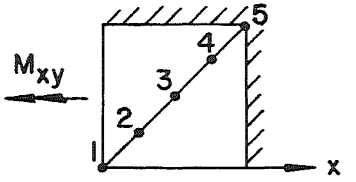

Multiplier qL^2

	Mesh	Point 1	Point 2	Point 3	Point 4	Point 5
Problem P1	4 x 4	0.		0.0105		0.
	8 x 8	0.	0.0036	0.0082	0.0097	0.
	16 x 16	0.	0.0027	0.0075	0.0076	0.
	Exact Value	0.				0.
Problem P2	4 x 4	0.		0.0133		0.0319
	8 x 8	0.	0.0037	0.0134	0.0252	0.0288
	16 x 16	0.	0.0038	0.0134	0.0252	0.0324
	Exact Value	0.	0.0037	0.0134	0.0252	0.0324
Problem P3	4 x 4	0.		0.0196		0.
	8 x 8	0.	0.0056	0.0176	0.0300	0.
	16 x 16	0.	0.0055	0.0174	0.0280	0.
	Exact Value	0.				0.
Problem P4	4 x 4	0.		0.0291		
	8 x 8	0.	0.0074	0.0290	0.0642	
	16 x 16	0.	0.0075	0.0289	0.0642	
	Exact Value	0.				

TABLE 11: EFFECT OF BOUNDARY CONDITIONS ON CENTER DEFLECTION - PROBLEM P1

a.) Center Deflection Under Uniformly Distributed Load

Bondary Conditions	Mesh 2 x 2	Mesh 4 x 4	Mesh 8 x 8	Mesh 16 x 16	Multi-plier
Type I	0.001594	0.001325	0.001284	0.001266	$\frac{qL^4}{D}$
Type II	0.001571	0.001322	0.001284	0.001266	
Exact Value	0.001260				

b.) Center Deflection Under Concentrated Load

Boundary Conditions	Mesh 2 x 2	Mesh 4 x 4	Mesh 8 x 8	Mesh 16 x 16	Multi-plier
Type I	0.005912	0.005634	0.005611	0.005607	$\frac{PL^2}{D}$
Type II	0.005895	0.005627	0.005611	0.005607	
Exact Value	0.00560				

TABLE 12: EFFECT OF BOUNDARY CONDITIONS ON CENTER DEFLECTION - PROBLEM P2

a.) Center Deflection Under Uniformly Distributed Load

Boundary Conditions	Mesh 2 x 2	Mesh 4 x 4	Mesh 8 x 8	Mesh 16 x 16	Multiplier
Type I	0.004187	0.004076	0.004064	0.004063	$\frac{qL^4}{D}$
Type II	0.004066	0.004063	0.004062	0.004062	
Type III	0.004065	0.004063	0.004062	0.004062	
Exact Value	0.004062				

b.) Center Deflection Under Concentrated Load

Boundary Conditions	Mesh 2 x 2	Mesh 4 x 4	Mesh 8 x 8	Mesh 16 x 16	Multiplier
Type I	0.011265	0.011497	0.011572	0.011593	$\frac{PL^2}{D}$
Type II	0.011184	0.011478	0.011570	0.011593	
Type III	0.011180	0.011478	0.011570	0.011593	
Exact Value	0.01160				

TABLE 13: EFFECT OF BOUNDARY CONDITIONS

ON PLATE MOMENTS M_x - PROBLEM P1

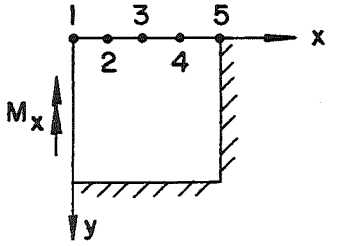

a.) Uniformly Distributed Load: Mesh 16 x 16

Boundary Conditions	Point 1	Point 2	Point 3	Point 4	Point 5	Multi-plier
Type I	0.0229	0.0201	0.0108	-0.0102	-0.0509	qL^2
Type II	0.0229	0.0201	0.0108	-0.0102	-0.0515	
Exact Value	0.0231				-0.0513	

b.) Single Concentrated Load: Mesh 16 x 16

Boundary Conditions	Point 1	Point 2	Point 3	Point 4	Point 5	Multi-plier
Type I		0.0684	-0.0008	-0.0525	-0.1247	P
Type II		0.0684	-0.0008	-0.0525	-0.1265	
Exact Value					-0.1257	

TABLE 14: EFFECT OF BOUNDARY CONDITIONS

ON PLATE MOMENTS M_x - PROBLEM P2

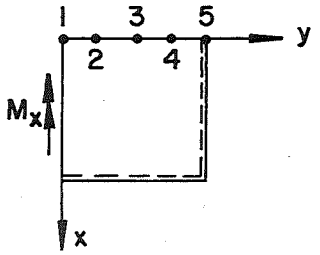

a.) Uniformly Distributed Load: Mesh 16 x 16

Boundary Conditions	Point 1	Point 2	Point 3	Point 4	Point 5	Multi-plier
Type I	0.0478	0.0457	0.0388	0.0248	-0.0010	
Type II	0.0478	0.0457	0.0387	0.0248	-0.0002	qL^2
Type III	0.0478	0.0457	0.0388	0.0248	0.	
Exact Value	0.0479	0.0458	0.0390	0.0250	0.	

b.) Single Concentrated Load: Mesh 16 x 16

Boundary Conditions	Point 1	Point 2	Point 3	Point 4	Point 5	Multi-plier
Type I		0.1230	0.0588	0.0244	-0.0025	
Type II		0.1230	0.0588	0.0245	-0.0004	P
Type III		0.1226	0.0586	0.0242	0.	
Exact Value		0.1231	0.0585	0.0251	0.	

TABLE 15: EFFECT OF ORTHOTROPY OF BRIDGE DECK ON DEFLECTION AND STRESS RESULTANTS IN BEAMS

Mesh 10 x 8 - Truck in Lane 4

Bartonsville Bridge - Cross-Section M

$\frac{D_y}{D_x}$	Deflection at Midspan			Bending Moment Section M			Axial-Force Section M		
	Beam A	Beam B	Beam C	Beam A	Beam B	Beam C	Beam A	Beam B	Beam C
1.0	0.03056	0.09168	0.13260	332.039	2679.252	4466.444	2.041	64.172	107.902
0.9	0.02933	0.09191	0.13491	292.709	2680.437	4537.636	1.067	64.156	109.758
0.8	0.02800	0.09210	0.13749	251.609	2678.925	4616.972	0.066	64.062	111.819
Units	in.			K. in.			K.		

TABLE 16: EFFECT OF MESH SIZE ON DEFLECTION AND STRESS RESULTANTS IN BEAMS

Truck in Lane 4

Bartonsville Bridge - Cross-Section M

Mesh	Deflection at Midspan			Bending Moment Section M			Axial-Force Section M		
	Beam A	Beam B	Beam C	Beam A	Beam B	Beam C	Beam A	Beam B	Beam C
10 x 4	0.02920	0.09053	0.13221	310.519	2728.905	4459.719	1.574	65.179	107.968
10 x 8	0.03056	0.09168	0.13260	332.039	2679.252	4466.444	2.041	64.172	107.902
10 x 16	0.03089	0.09193	0.13268	337.776	2668.198	4472.175	2.187	63.923	107.944
Test	0.035	0.086	0.129						
Units	in.			K. in.			K.		

TABLE 17: EFFECT OF MESH SIZE ON DEFLECTION AND STRESS RESULTANTS IN BEAMS

Truck in Lane 3

Bartonsville Bridge - Cross-Section M

Mesh	Deflection at Midspan			Bending Moment Section M			Axial-Force Section M		
	Beam A	Beam B	Beam C	Beam A	Beam B	Beam C	Beam A	Beam B	Beam C
10 x 4	0.05784	0.12160	0.11975	1236.754	3965.505	3955.342	23.877	94.797	95.166
10 x 8	0.06036	0.12253	0.12041	1235.371	3961.652	3950.800	23.880	94.362	94.798
10 x 16	0.06107	0.12278	0.12054	1233.704	3959.843	3948.402	23.853	94.250	94.704
Test	0.066	0.112	0.116						
Units	in.			K. in.			K.		

TABLE 18: EFFECT OF MESH SIZE ON DEFLECTION AND STRESS RESULTANTS IN BEAMS

Truck in Lane 2

Bartonsville Bridge - Cross-Section M

Mesh	Deflection at Midspan			Bending Moment Section M			Axial-Force Section M		
	Beam A	Beam B	Beam C	Beam A	Beam B	Beam C	Beam A	Beam B	Beam C
10 x 4	0.10492	0.13670	0.08981	2902.377	4492.236	2696.199	65.286	107.433	64.308
10 x 8	0.10832	0.13778	0.09097	2871.726	4506.656	2648.289	64.680	107.335	63.297
10 x 16	0.10934	0.13814	0.09122	2864.479	4515.217	2637.752	64.471	107.373	63.054
Test	0.110	0.123	0.089						
Units	in.			K. in.			K.		

TABLE 19: EFFECT OF MESH SIZE ON DEFLECTION AND STRESS RESULTANTS IN BEAMS

Truck in Lane 1

Bartonsville Bridge - Cross-Section M

Mesh	Deflection of Midspan			Bending Moment Section M			Axial Force Section M		
	Beam A	Beam B	Beam C	Beam A	Beam B	Beam C	Beam A	Beam B	Beam C
10 x 4	0.16964	0.12713	0.05654	5339.568	4000.892	1386.085	125.198	93.948	30.090
10 x 8	0.17356	0.12915	0.05796	5311.649	4018.698	1362.395	124.362	93.806	29.625
10 x 16	0.17481	0.12978	0.05828	5299.971	4023.451	1354.966	124.002	93.786	29.502
Test	0.156	0.113	0.065						
Units	in.			K. in.			K.		

TABLE 20: AVAILABLE SOLUTIONS FOR LIMIT LOAD - SIMPLY SUPPORTED SQUARE PLATE

Method	Author	Ref.	Yield Criterion			
			Johansen	Tresca	Von Mises	
Lower Bound	Wolfensberger	65	0.945			Multiplier 24 M_p/L^2
	Ranaweera and Leckie	79		0.920	0.995	
	Shull and Hu	63		0.826		
	Koopman and Lance	64		0.964		
	Hodge and Belytscho	78			1.036	
	Prager	80	1.000			
Upper Bound	Ranaweera and Leckie	79		0.961	1.044	
	Shull and Hu	63		1.000		
	Koopman and Lance	64		1.000		
	Hodge	56			1.106	
	Prager	80	1.000			
Finite Difference	Lopez and Ang	44			1.031	
	Bhaumik and Hanley	66	1.041	0.922	1.000	
Finite Element	Armen et al	67			1.137	
	Present Analysis Mesh: 8 x 8				0.982	

TABLE 21: AVAILABLE SOLUTIONS FOR LIMIT LOAD - CLAMPED SQUARE PLATE

Method	Author	Ref.	Yield Criterion			Multiplier 24 M_p/L^2
			Johansen	Tresca	Von Mises	
Lower Bound	Wolfensberger	65	1.560			
	Ranaweera and Leckie	79		1.553	1.710	
	Koopman and Lance	64		1.596		
	Hodge and Belytscho	78			1.786	
Upper Bound	Ranaweera and Leckie	79		1.682	1.844	
	Koopman and Lance	64		1.712		
	Hodge	56			2.052	
Finite Difference	Lopez and Ang	44			1.901	
	Bhaumik and Hanley	66	1.746	1.560	1.740	
Finite Element	Armen et al.	67			2.590	
	Present Analysis Mesh: 8 x 8 Mesh: 12 x 12				 2.220 1.865	

8. FIGURES

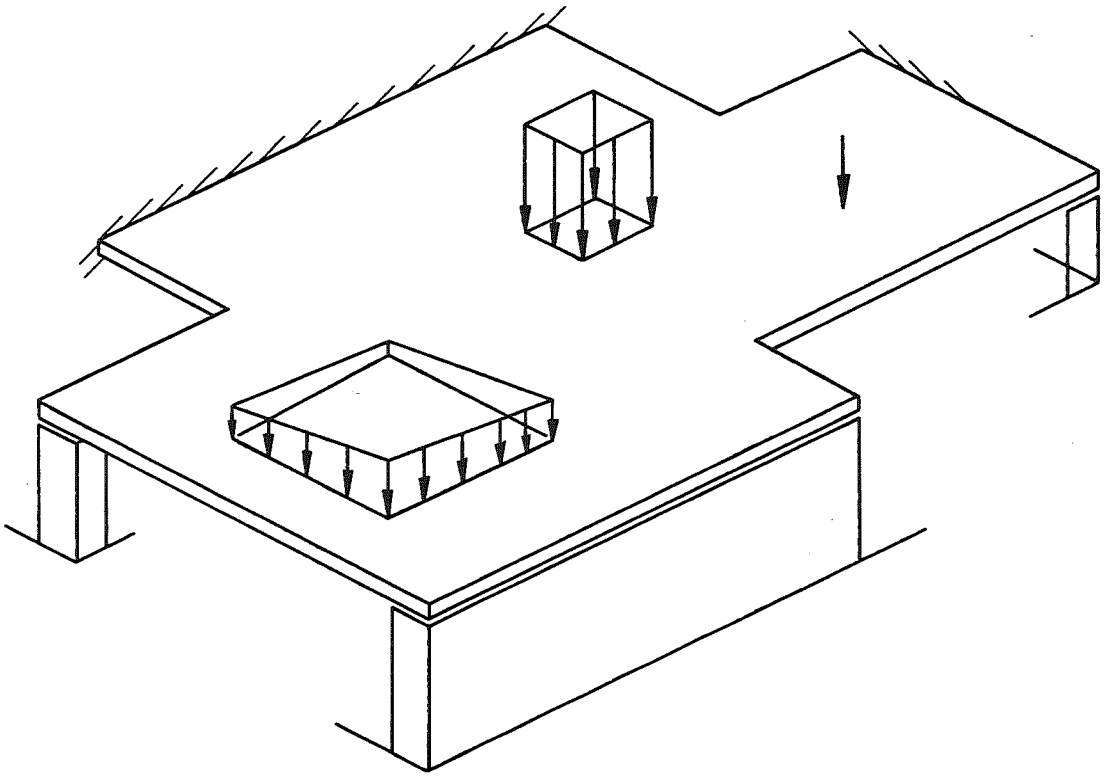

Fig. 1 Plate of Arbitrary Loading and Geometry

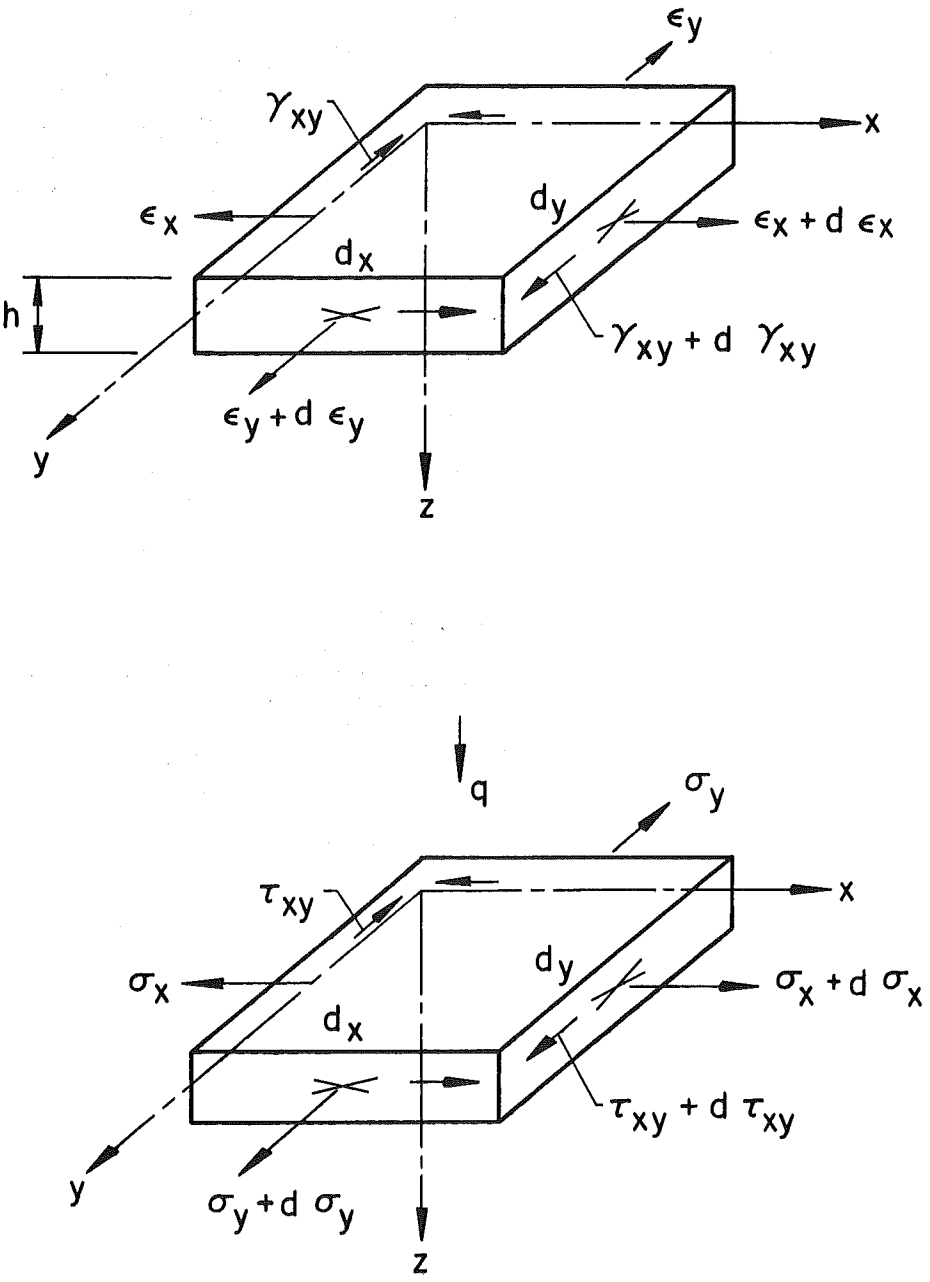

Fig. 2 Sign Convention for Stresses and Strains Acting on a Plate Element

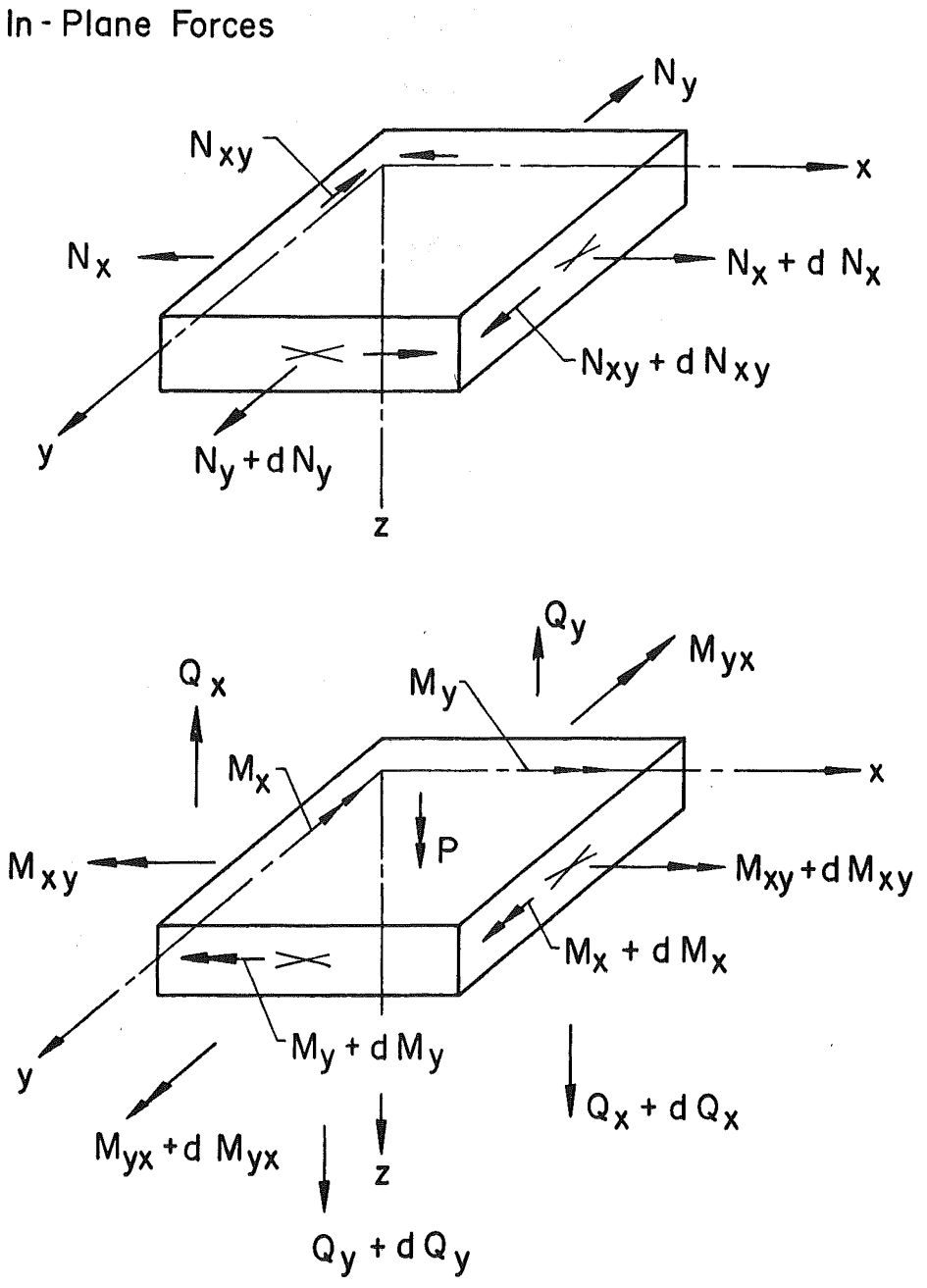

Fig. 3 Sign Convention for Stress Resultants Acting on a Plate Element

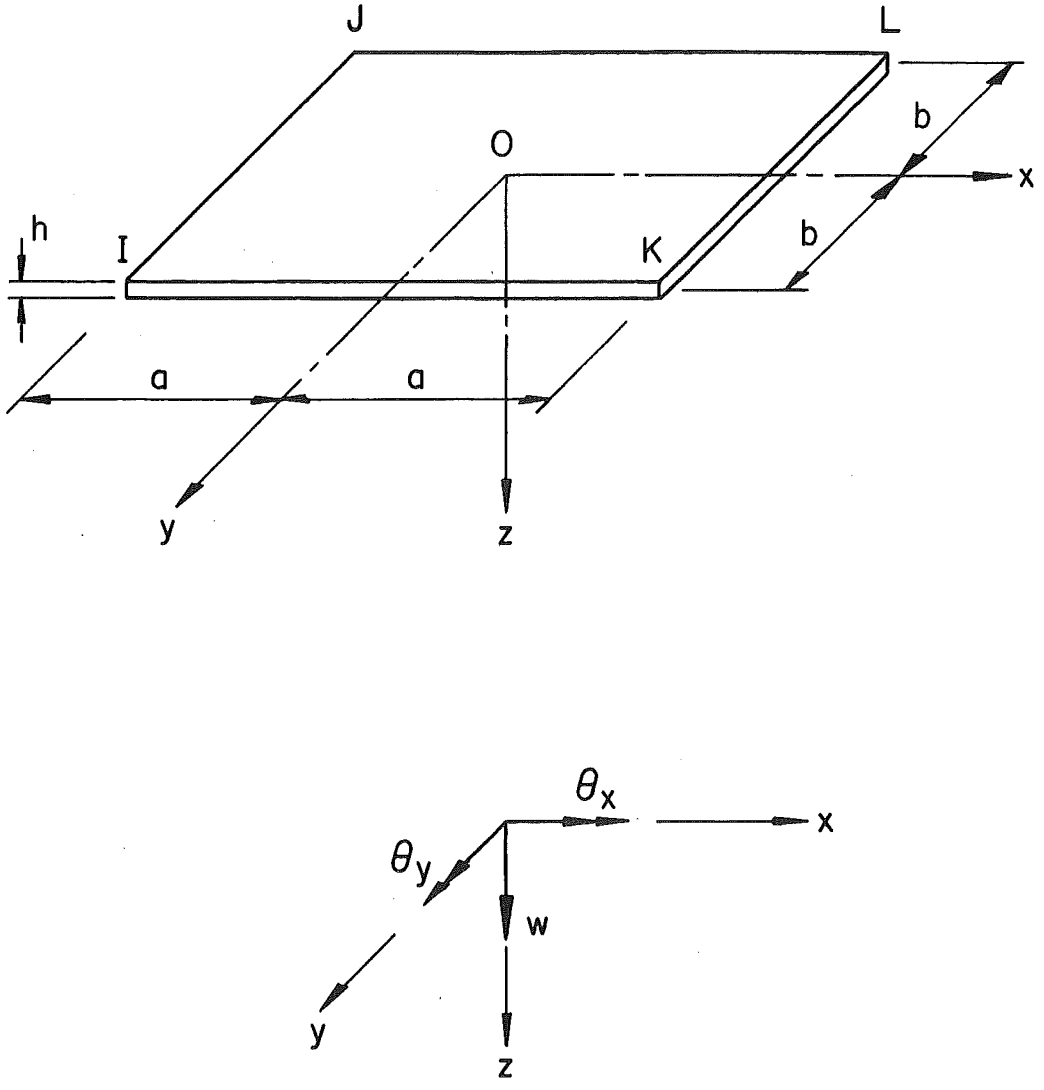

Fig. 4 Rectangular Plate Element and Basic Displacement Components

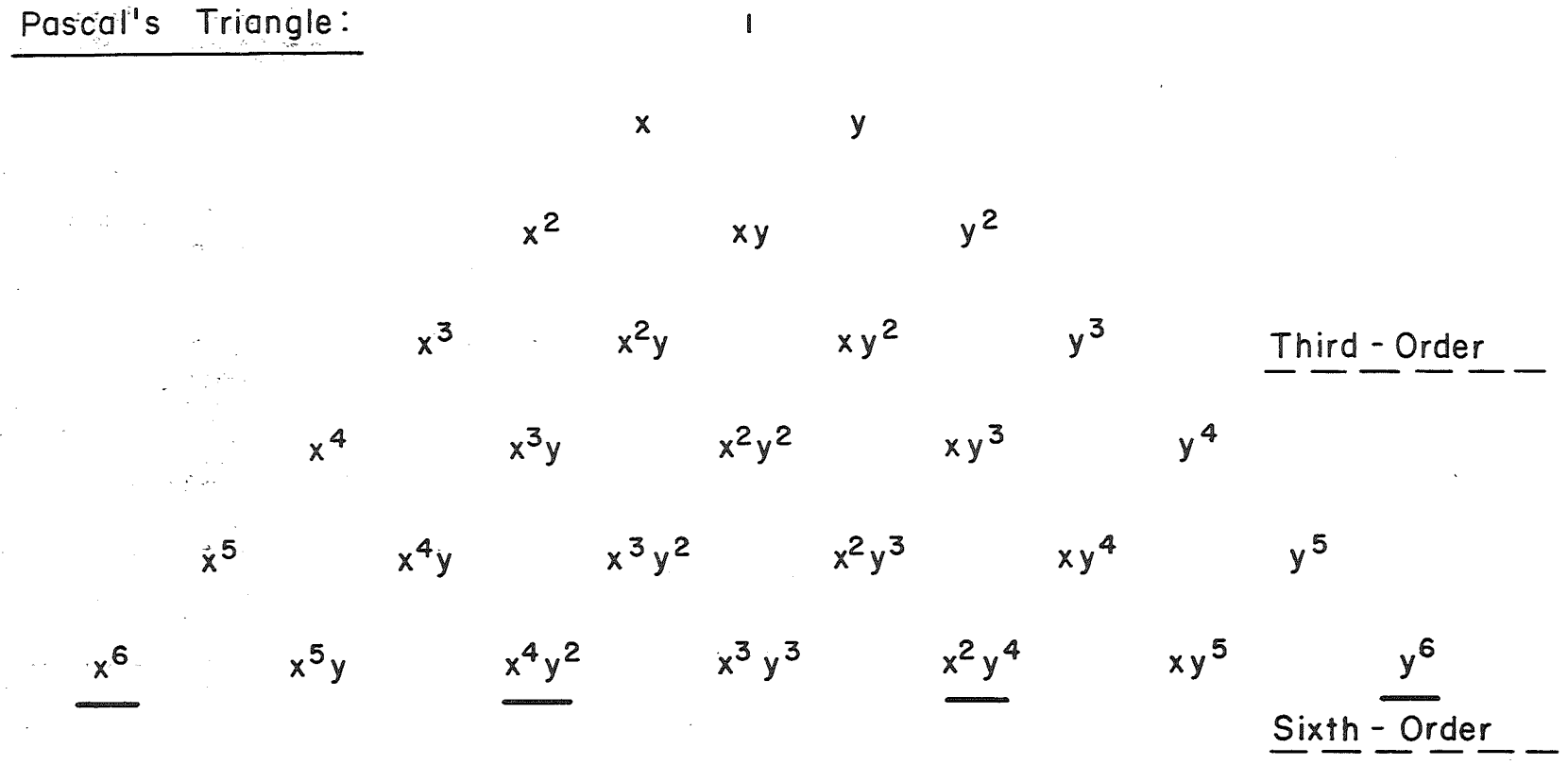

Fig. 5 Polynomial Expansion Represented by Pascal's Triangle

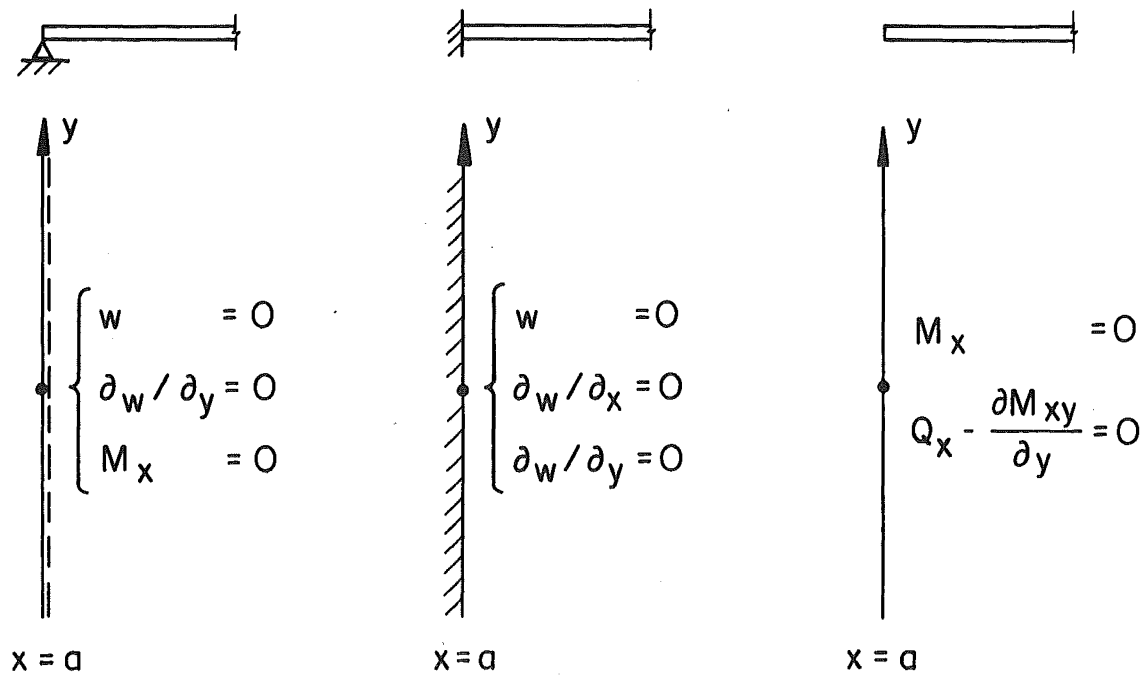

Fig. 6 Typical Plate Boundary Conditions

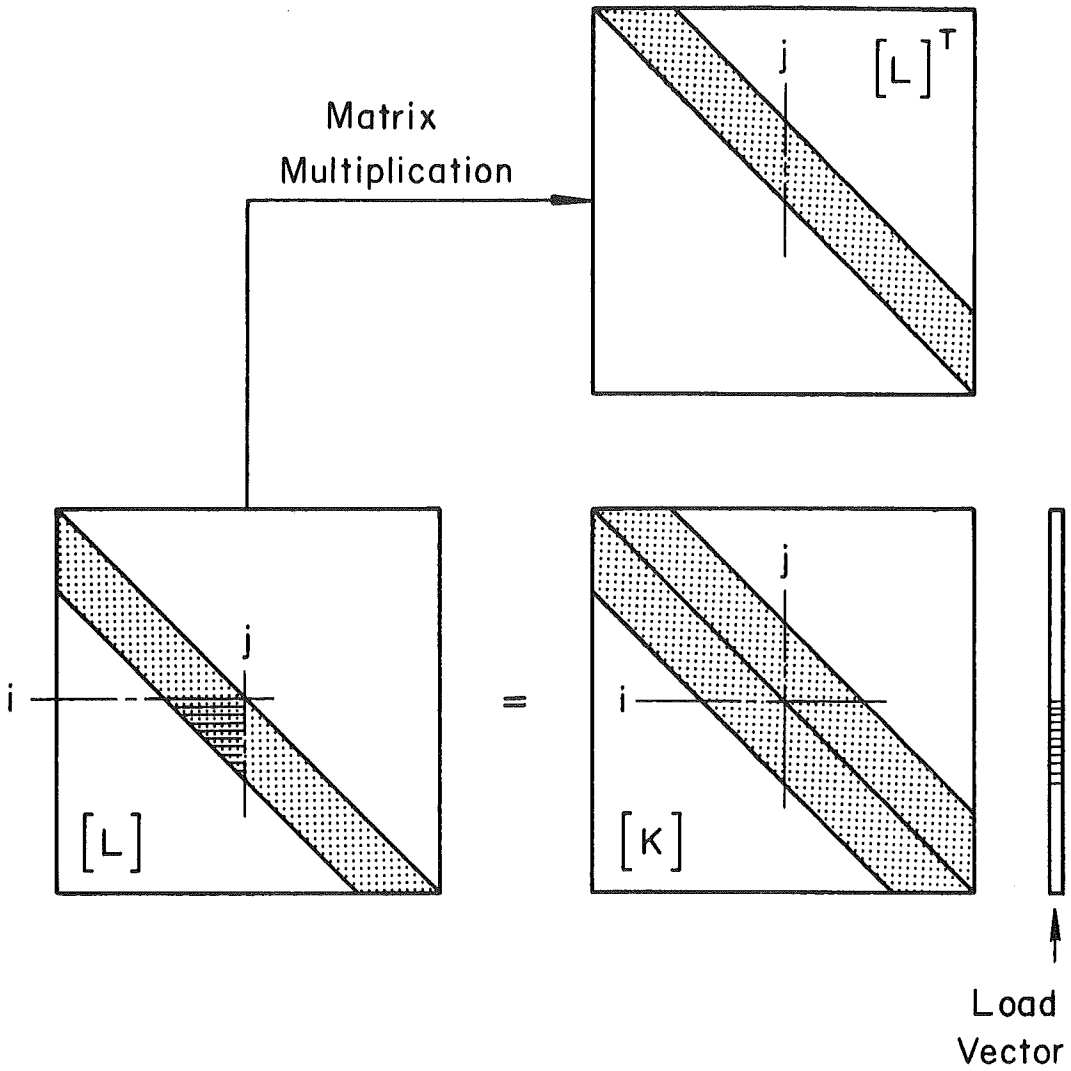

$$[K] = [L]\,[L]^T$$

Fig. 7 Banded Stiffness Matrix and its Choleski Decomposition

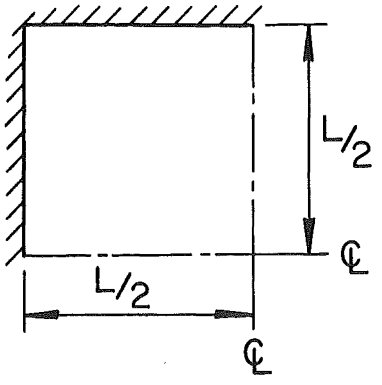

Problem P1:

Square Isotropic Plate
with Four Fixed Supports

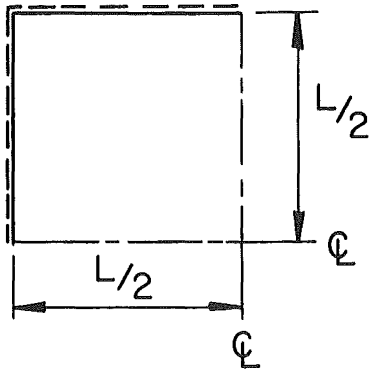

Problem P2:

Square Isotropic Plate
with Four Simple Supports

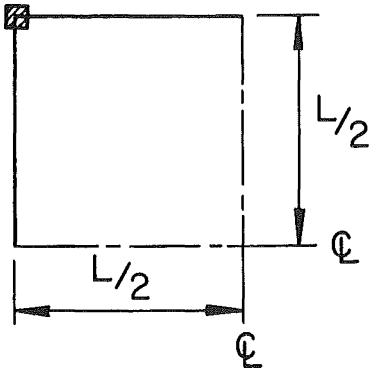

Problem P3:

Plate Supported by Rows
of Equidistant Columns
(Flat Plate)

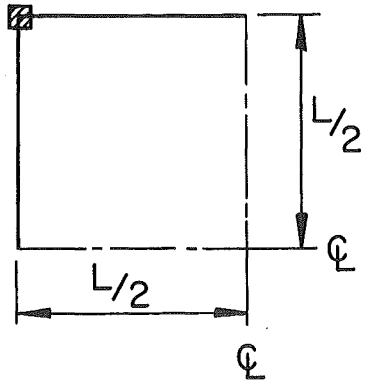

Problem P4:

Square Isotropic Plate
Supported at Corners

Fig. 8 Selected Example Structures for Testing the Refined Plate Element

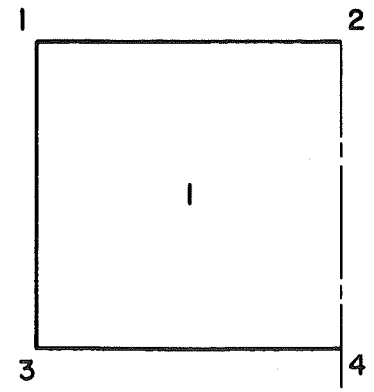

Mesh 2 x 2

1 Element

4 Nodal Points

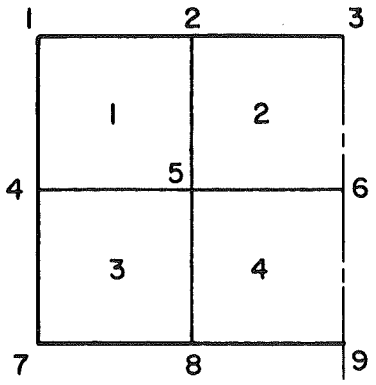

Mesh 4 x 4

4 Elements

9 Nodal Points

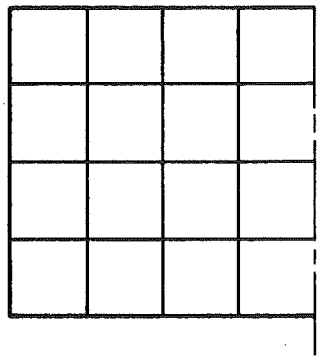

Mesh 8 x 8

16 Elements

25 Nodal Points

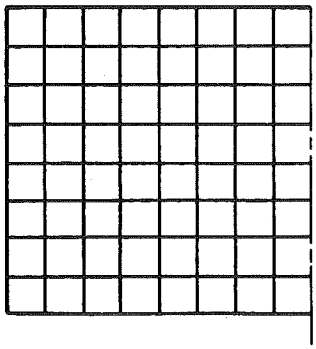

Mesh 16 x 16

64 Elements

81 Nodal Points

Fig. 9 Discretization of a Plate Quadrant

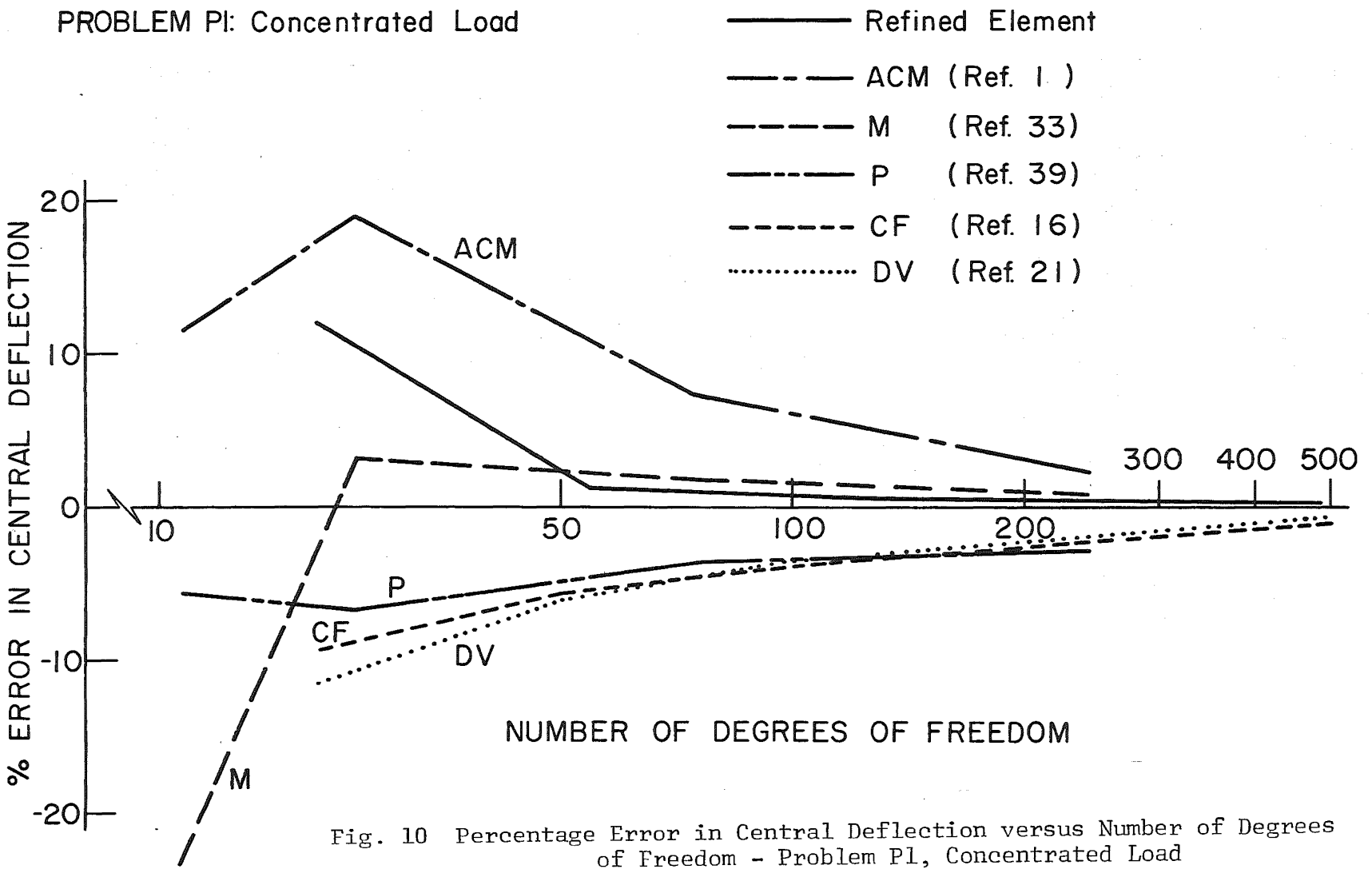

Fig. 10 Percentage Error in Central Deflection versus Number of Degrees of Freedom - Problem P1, Concentrated Load

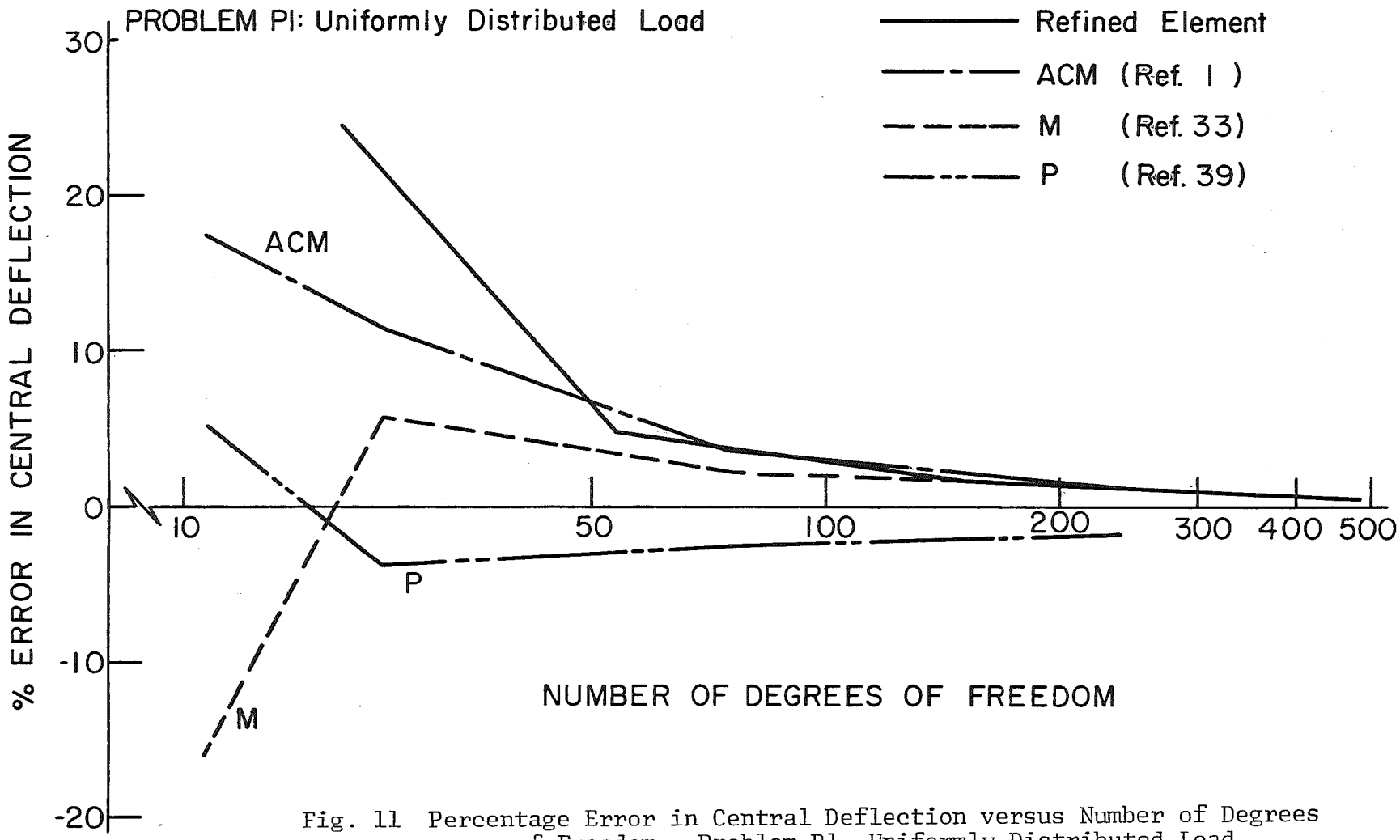

Fig. 11 Percentage Error in Central Deflection versus Number of Degrees of Freedom - Problem P1, Uniformly Distributed Load

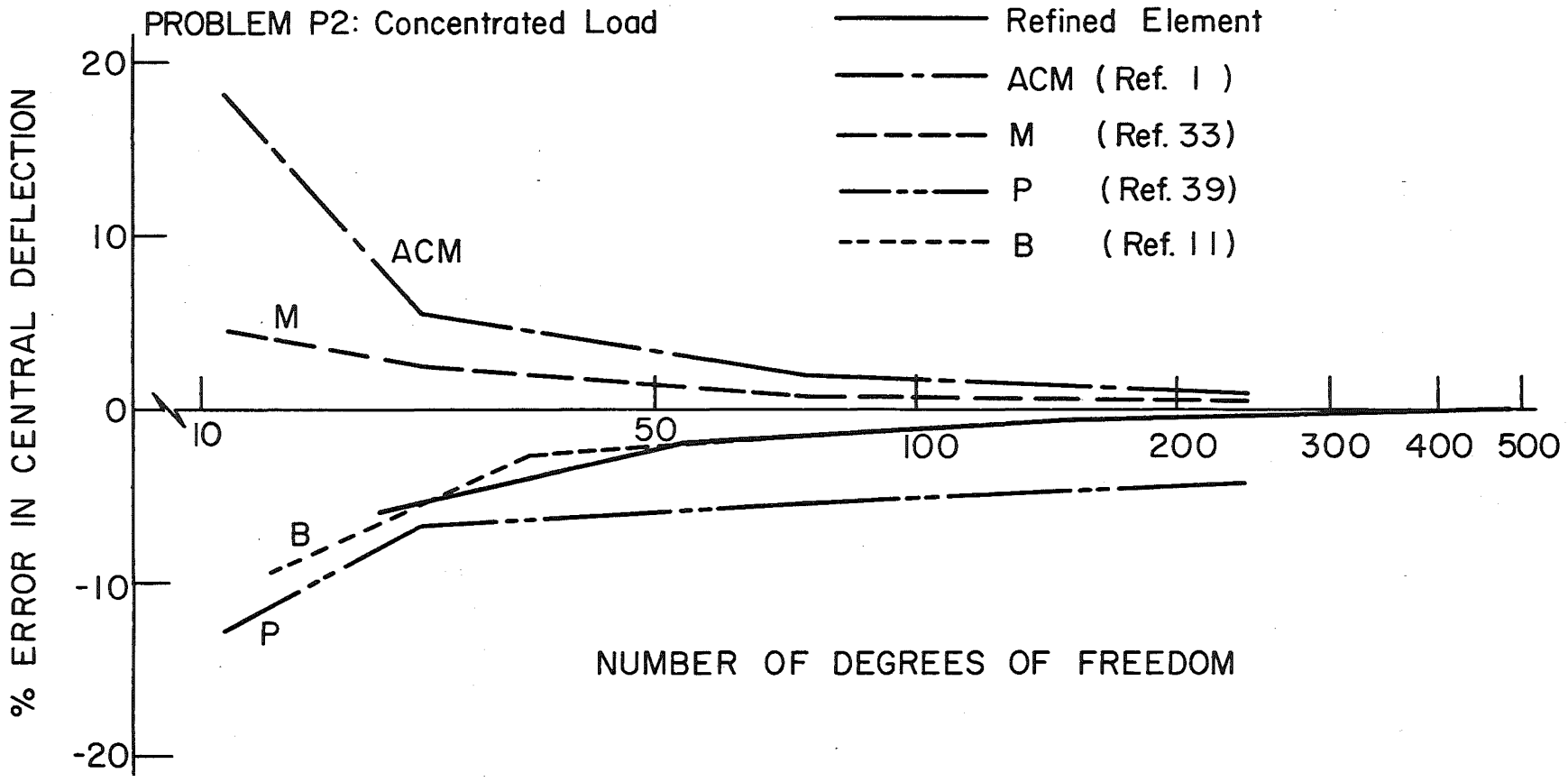

Fig. 12 Percentage Error in Central Deflection versus Number of Degrees of Freedom - Problem P2, Concentrated Load

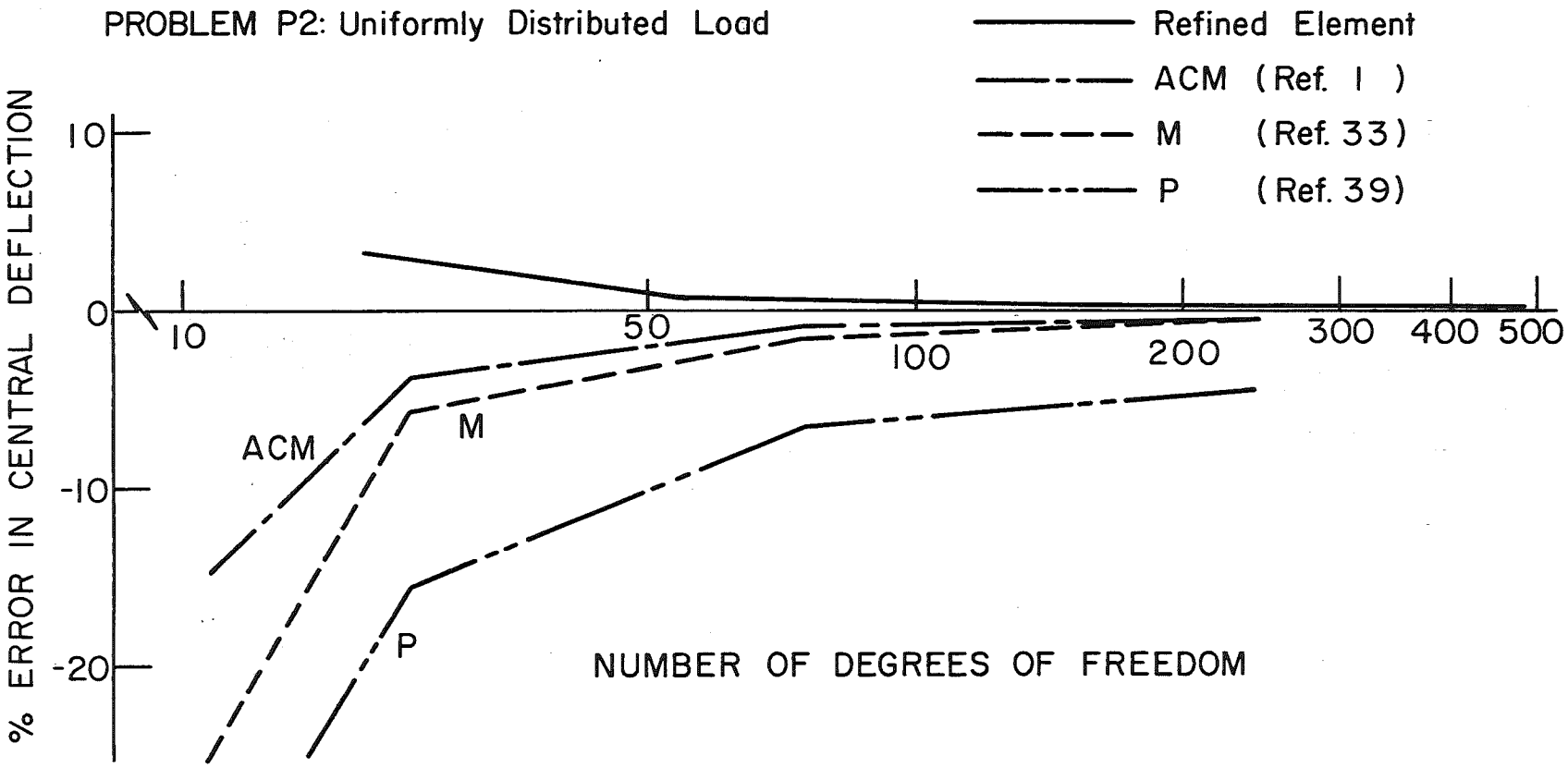

Fig. 13 Percentage Error in Central Deflection versus Number of Degrees of Freedom - Problem P2, Uniformly Distributed Load

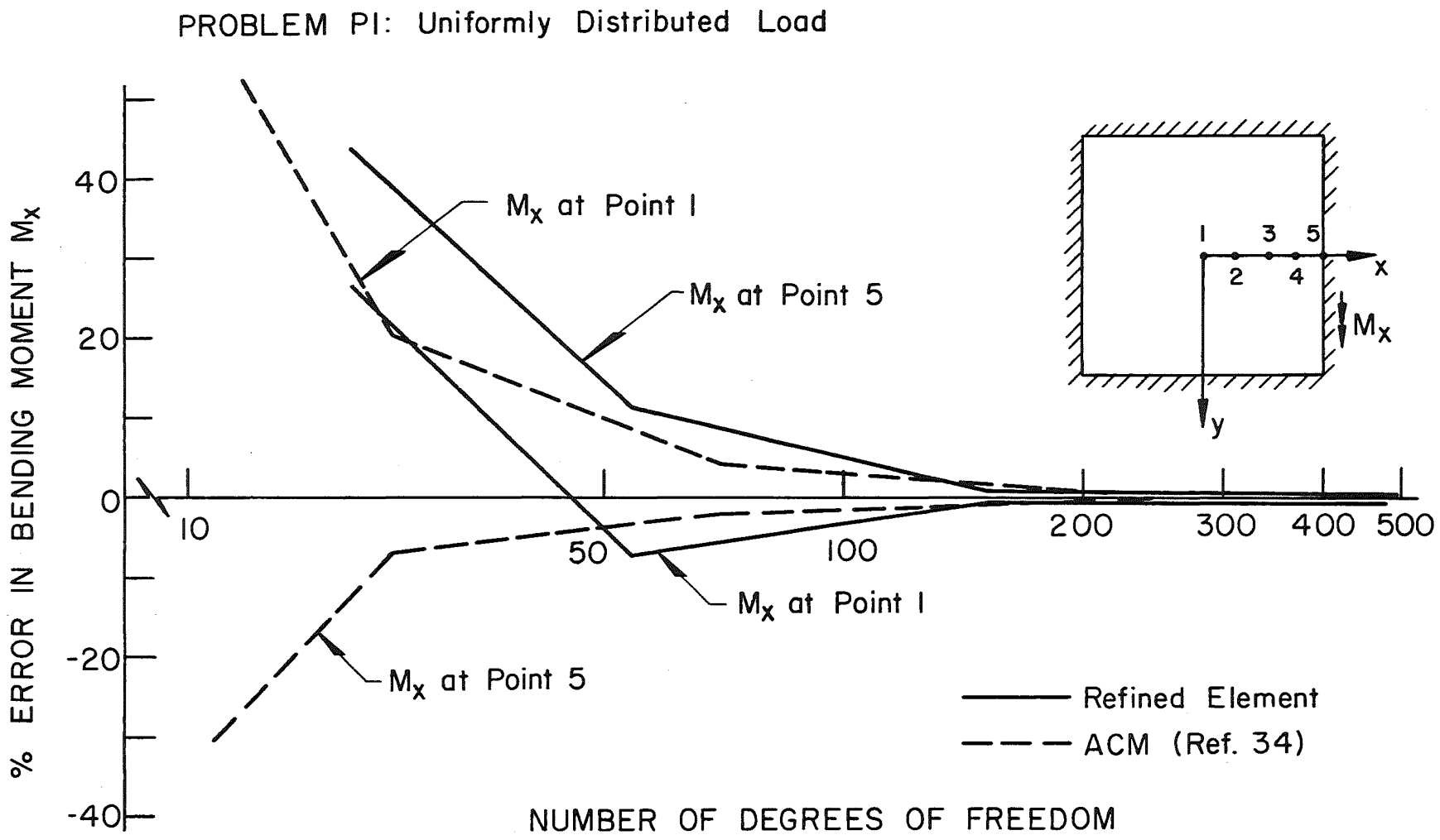

Fig. 14 Percentage Error in Plate Bending Moment M_x versus Number of Degrees of Freedom - Problem P1

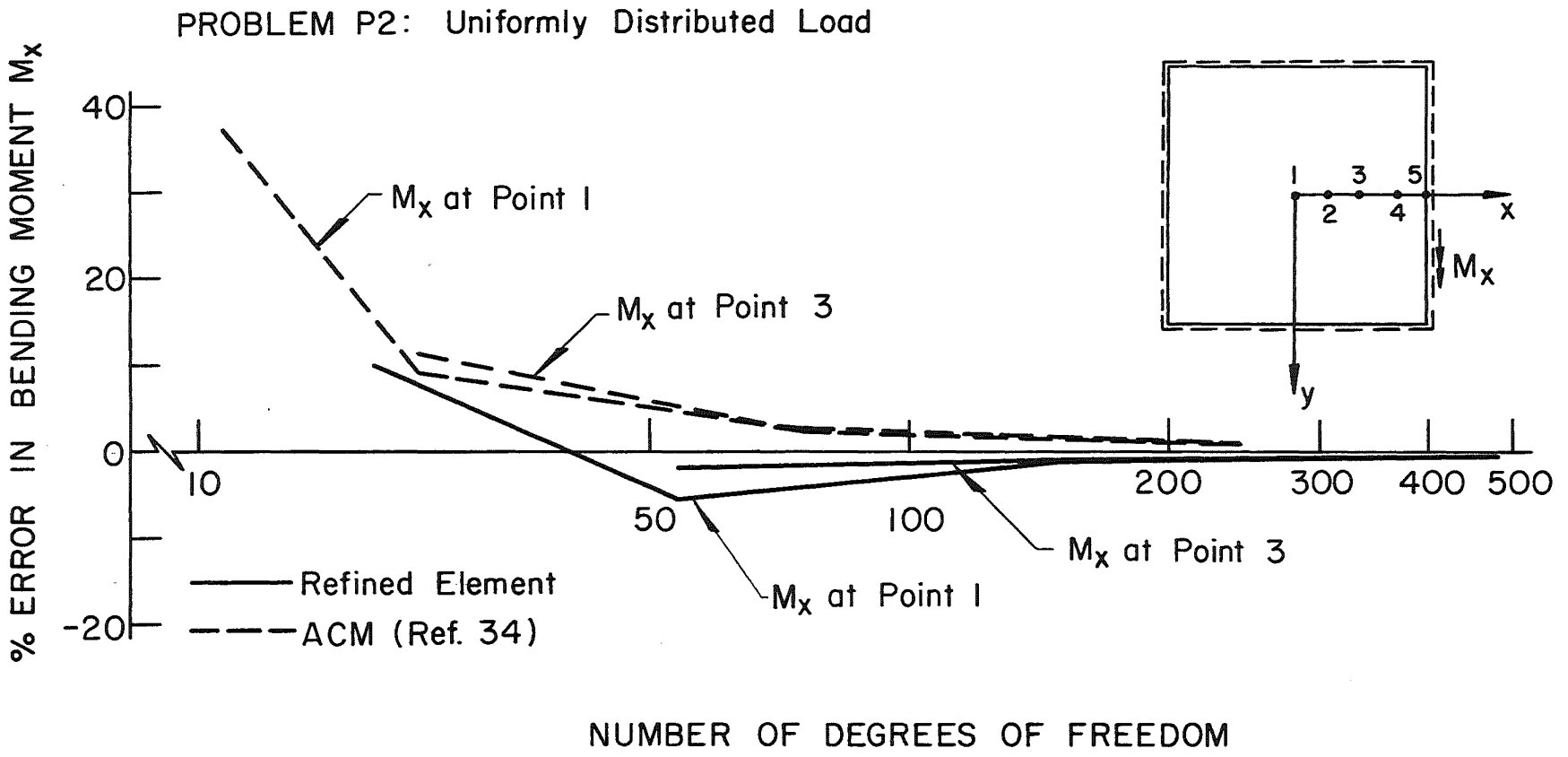

Fig. 15 Percentage Error in Plate Bending Moment M_x versus Number of Degrees of Freedom - Problem P2

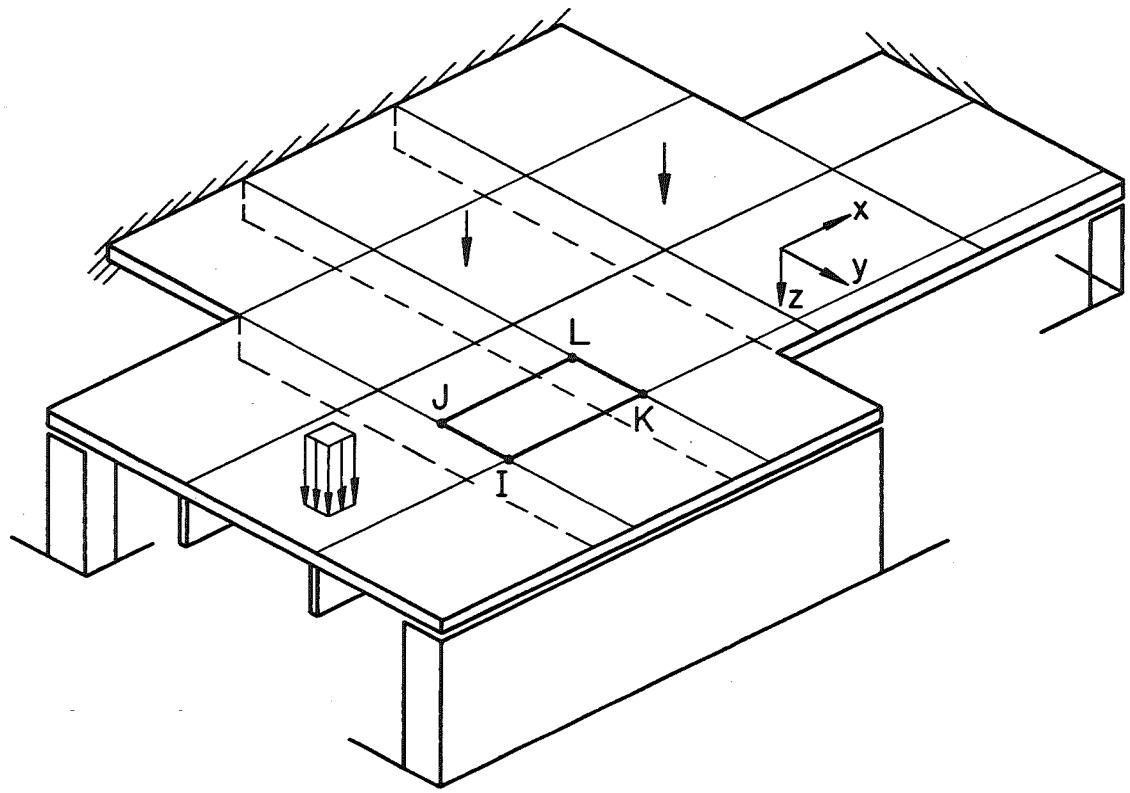

Fig. 16 Stiffened Plate of Arbitrary Loading and Geometry

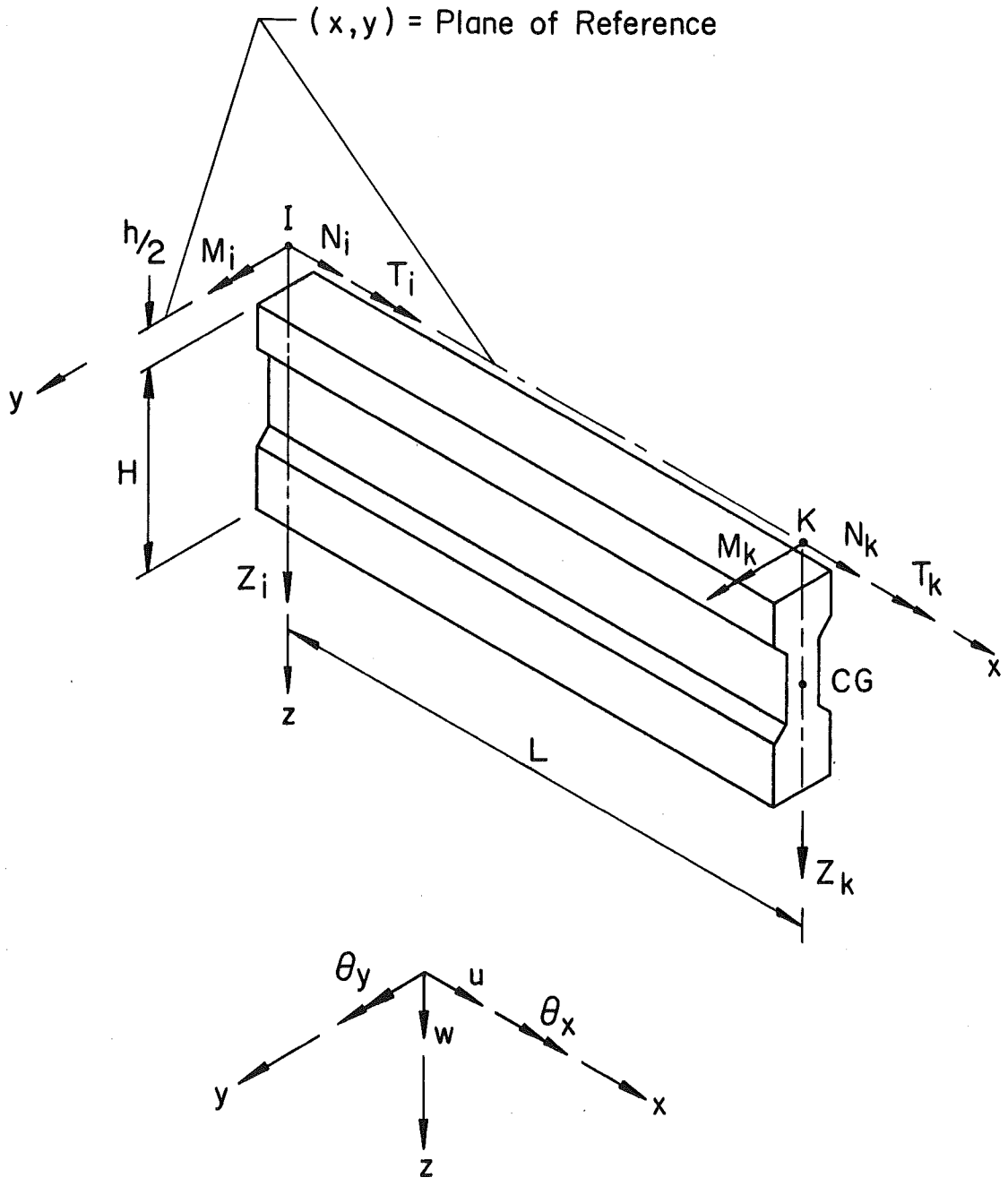

Fig. 17 Eccentrically Attached Stiffener Element

DESIGN DIMENSIONS

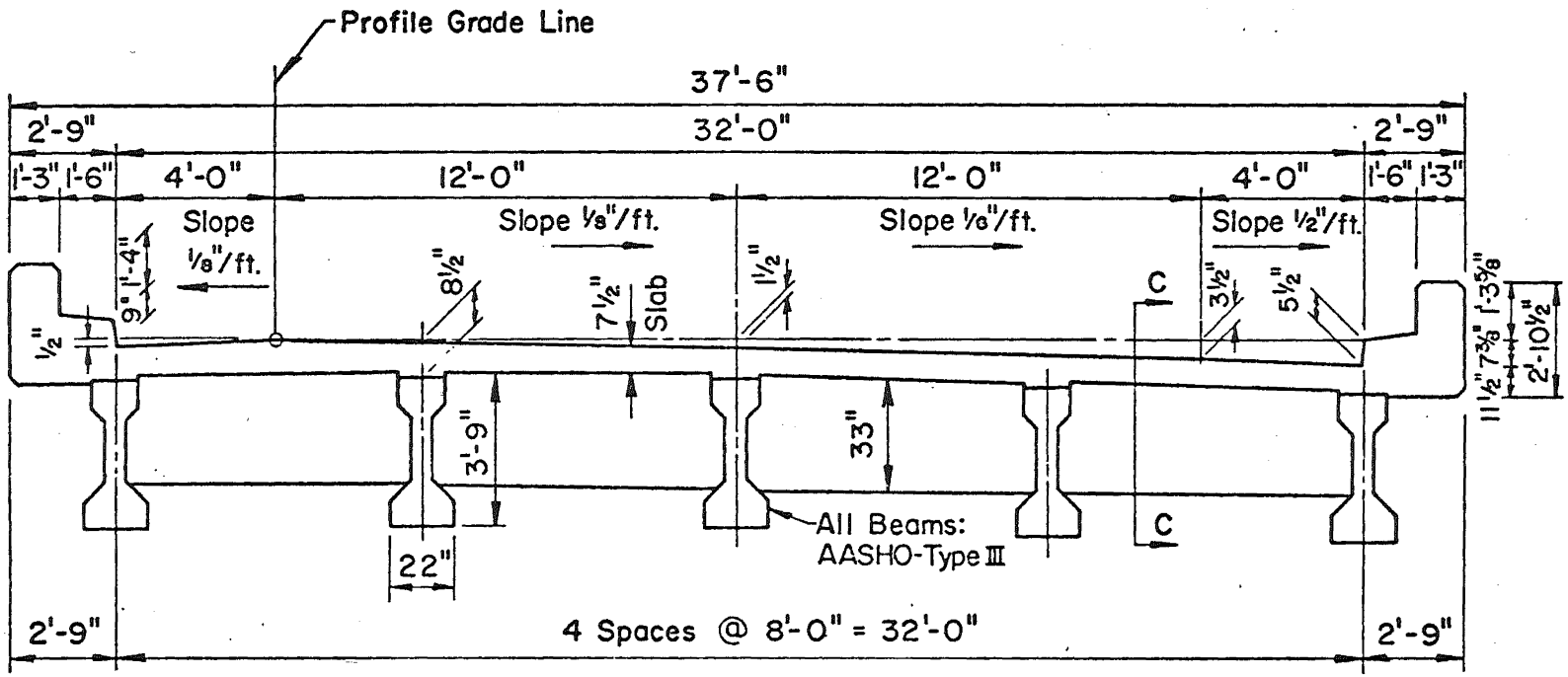

Fig. 18 Cross Section of Test Bridge

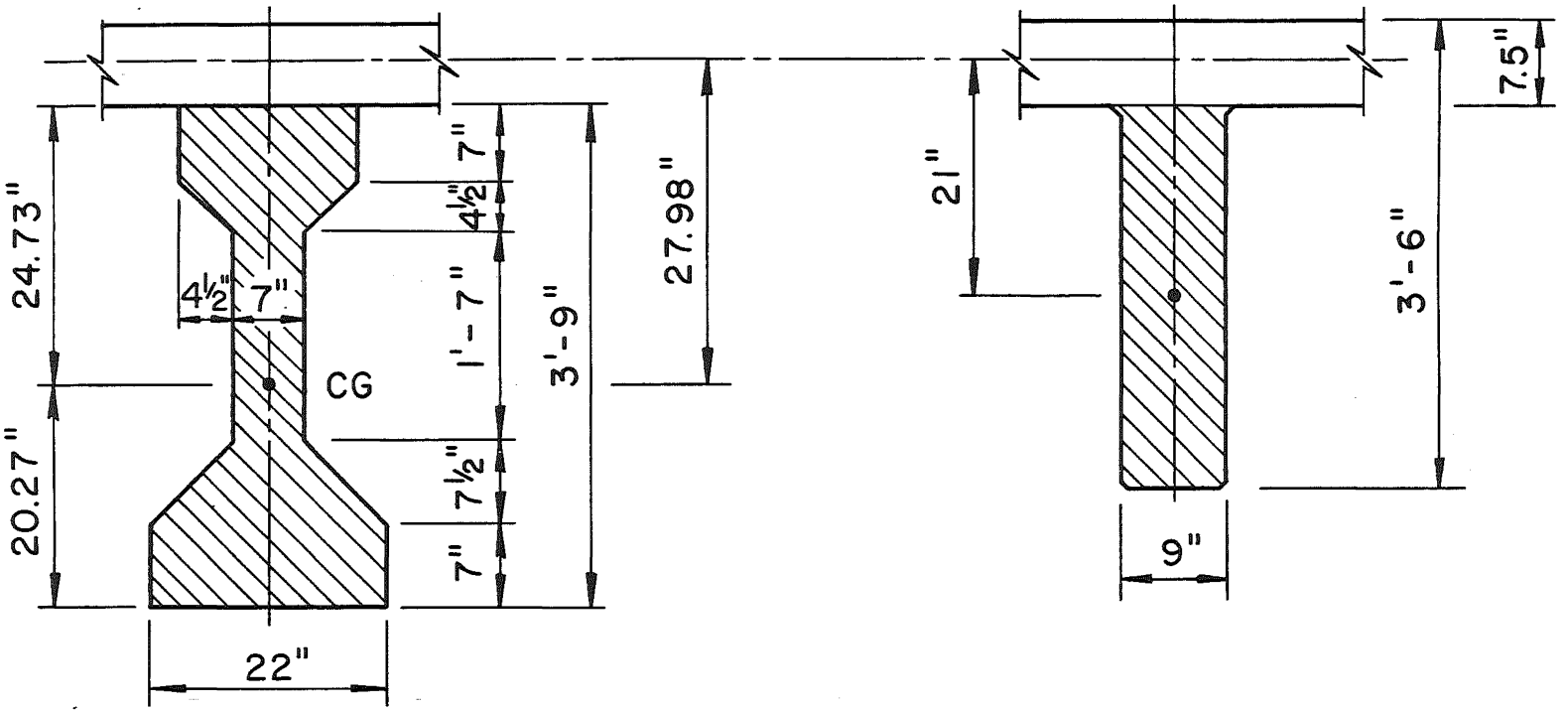

Fig. 19 Cross-Sectional Dimensions of Beams and Midspan Diaphragm

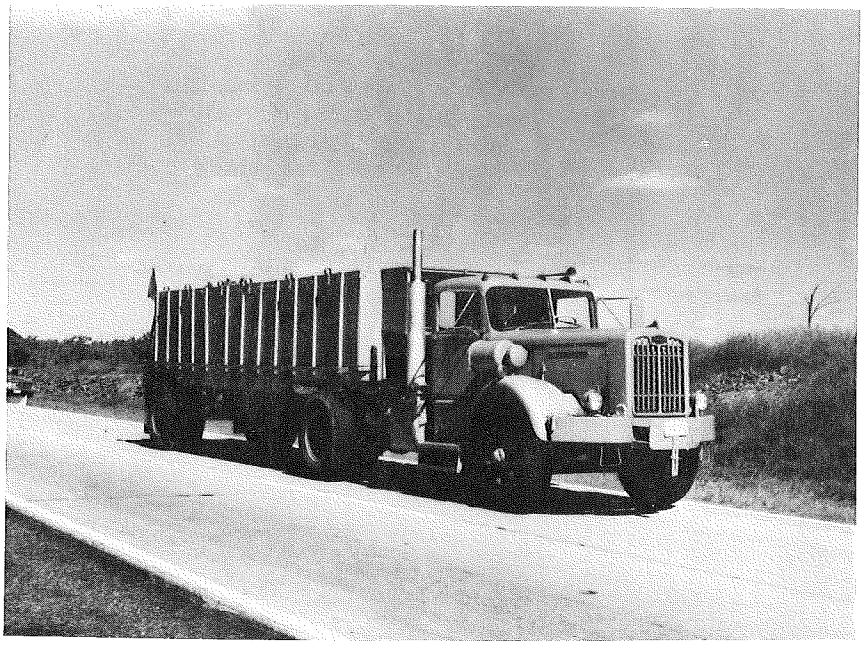

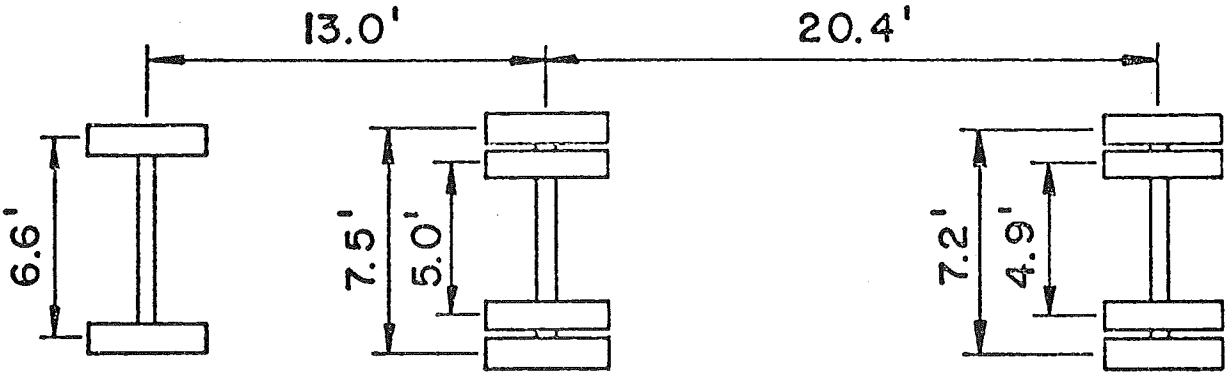

AXLE AND WHEEL SPACING

FRONT	DRIVE	REAR
10.36k	32.20k	32.20k

AXLE LOADS

Fig. 20 Test Vehicle

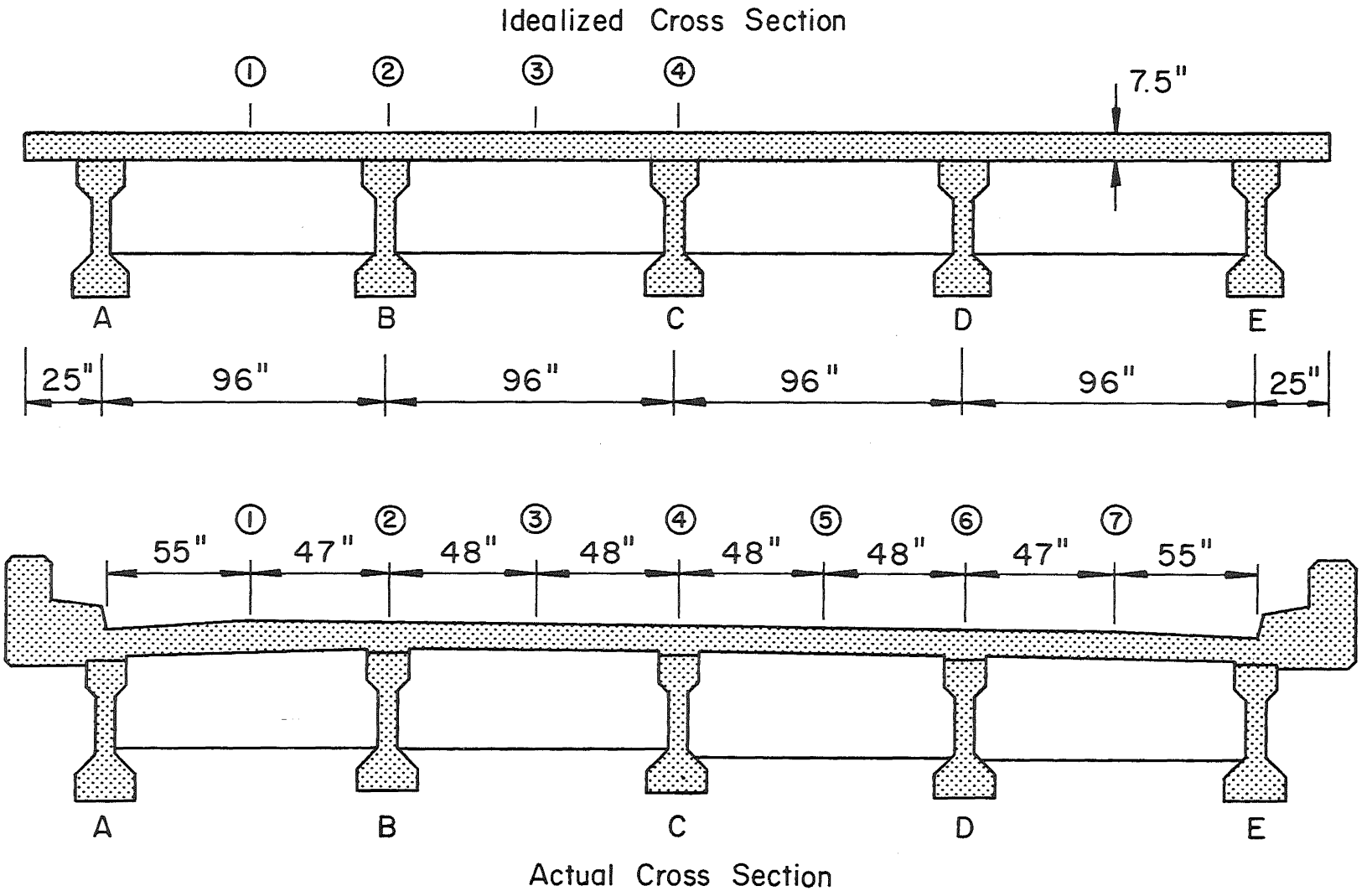

Fig. 21 Idealized and Actual Bridge Cross Section and Loading Lanes

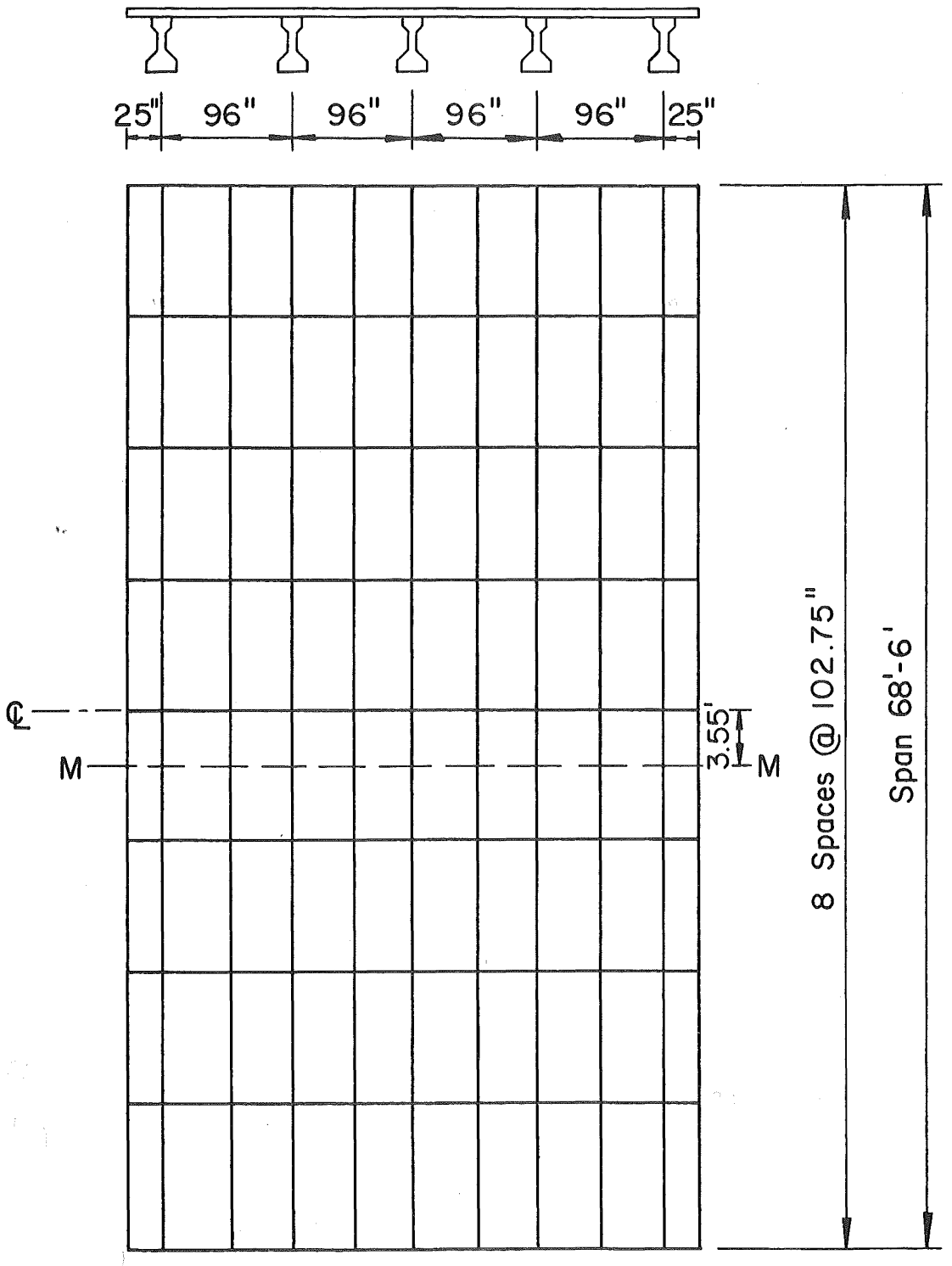

Fig. 22 Discretization of I-Beam Bridge: Mesh 10*8

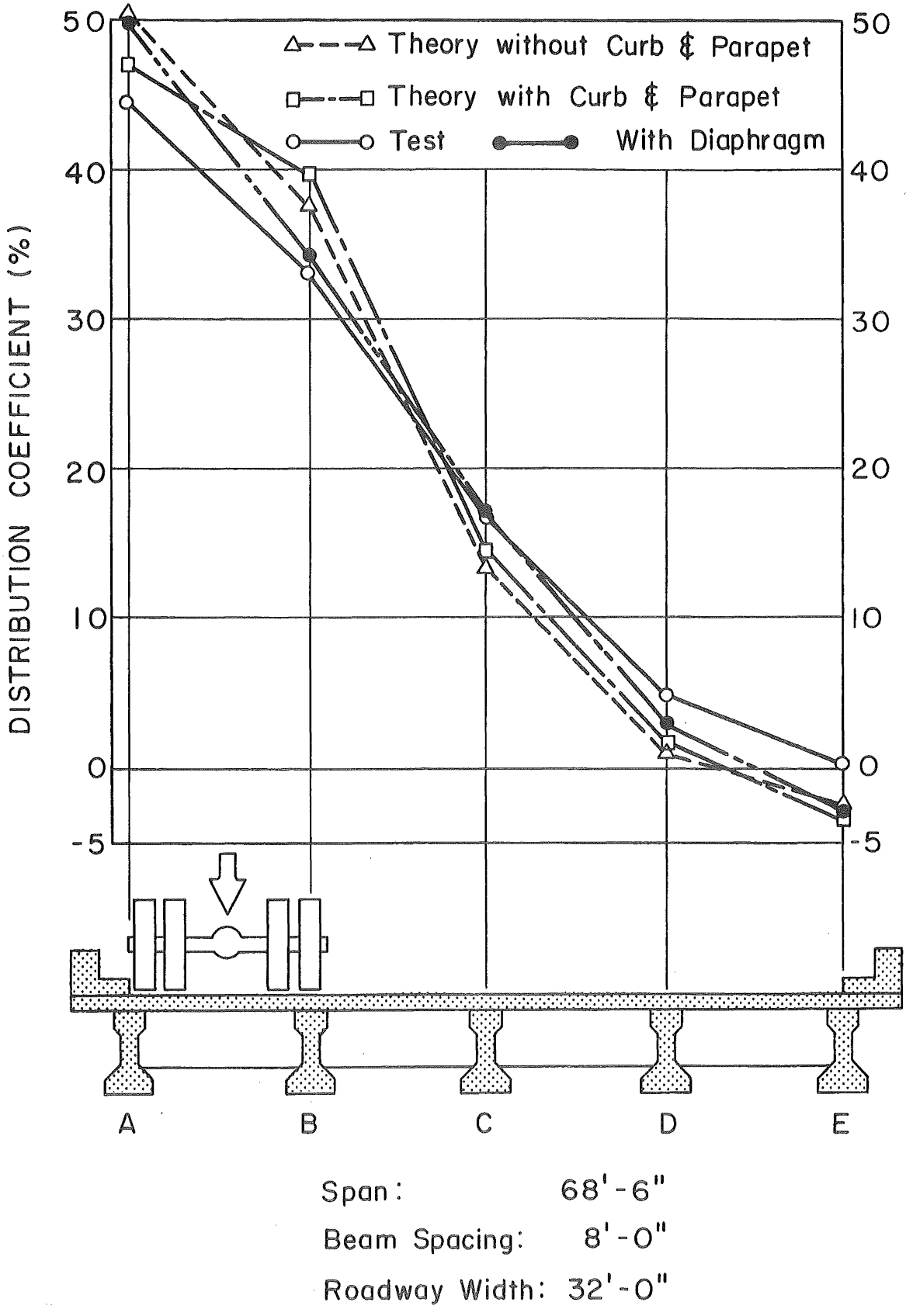

Fig. 23 Distribution Coefficients - Load in Lane 1

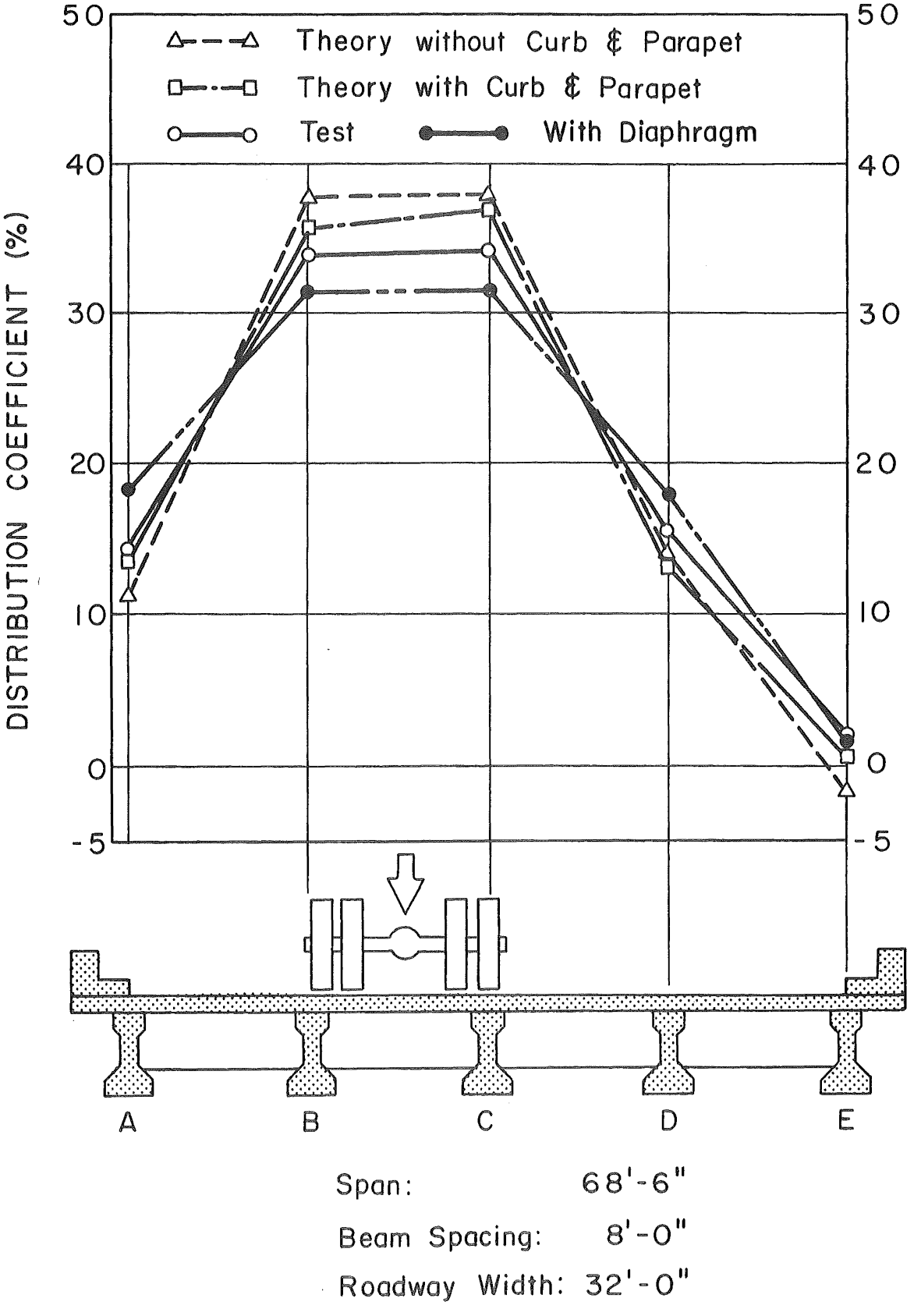

Fig. 24 Distribution Coefficients - Load in Lane 3

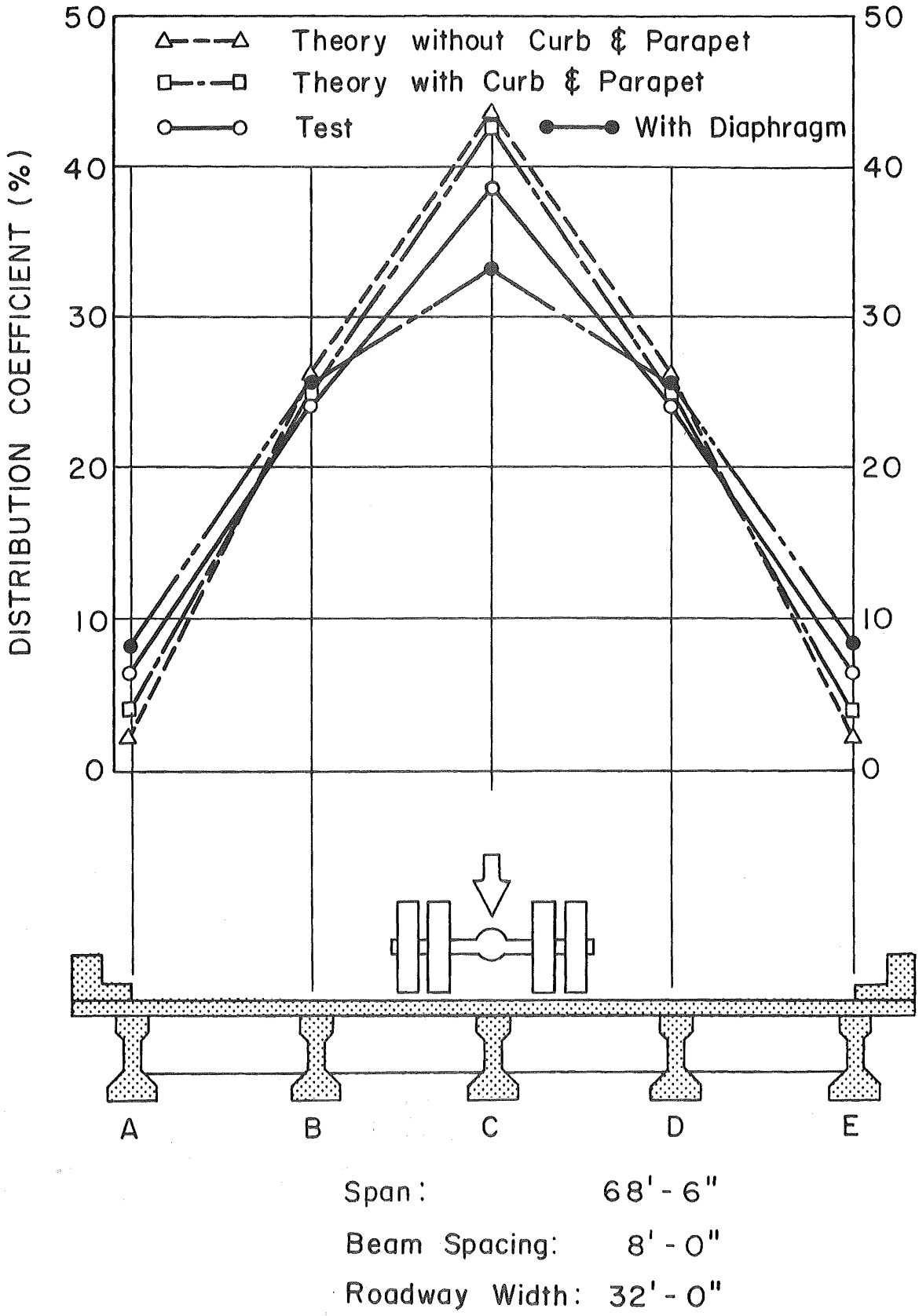

Fig. 25 Distribution Coefficients - Load in Lane 4

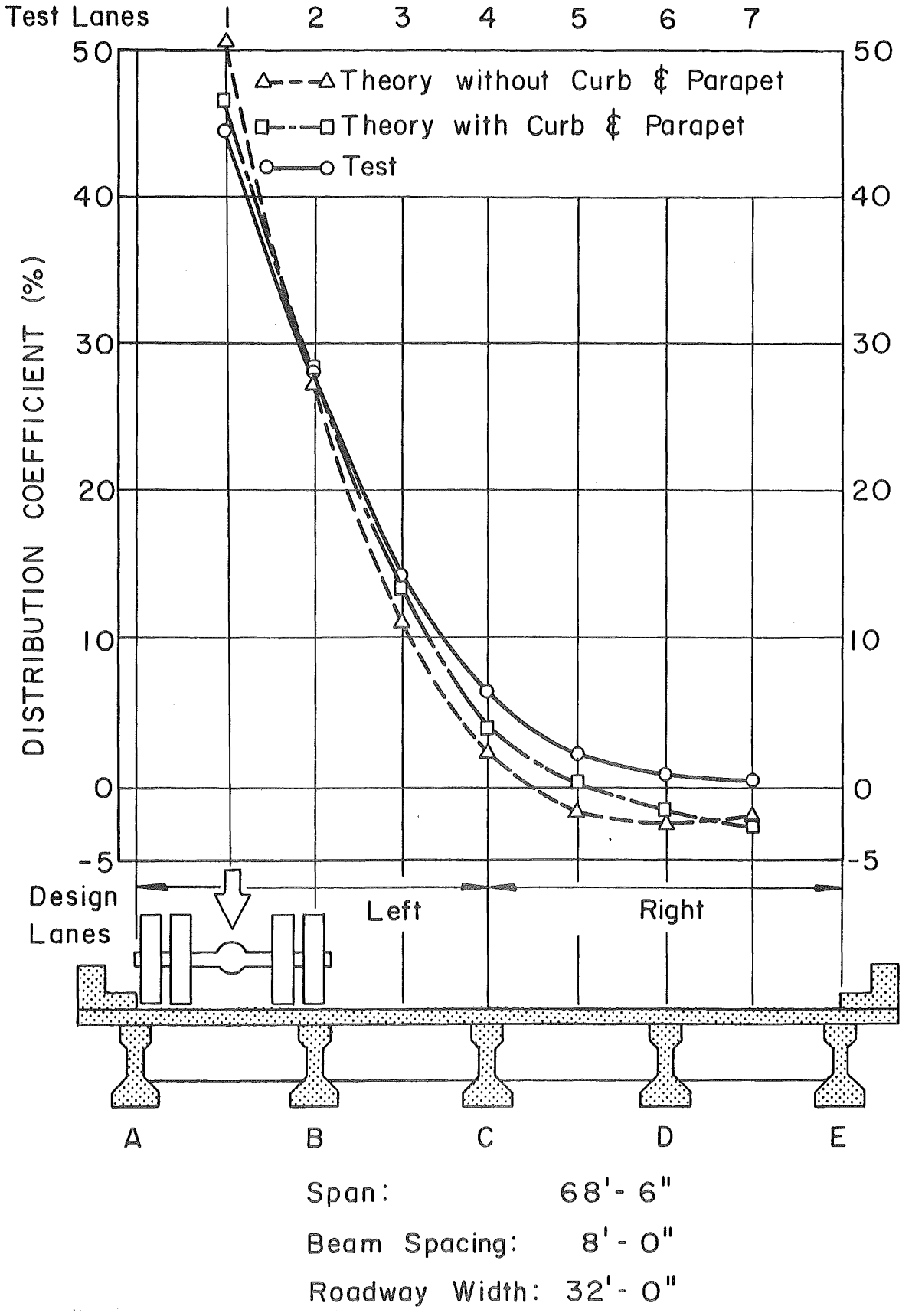

Fig. 26 Influence Line for Bending Moment - Beam A

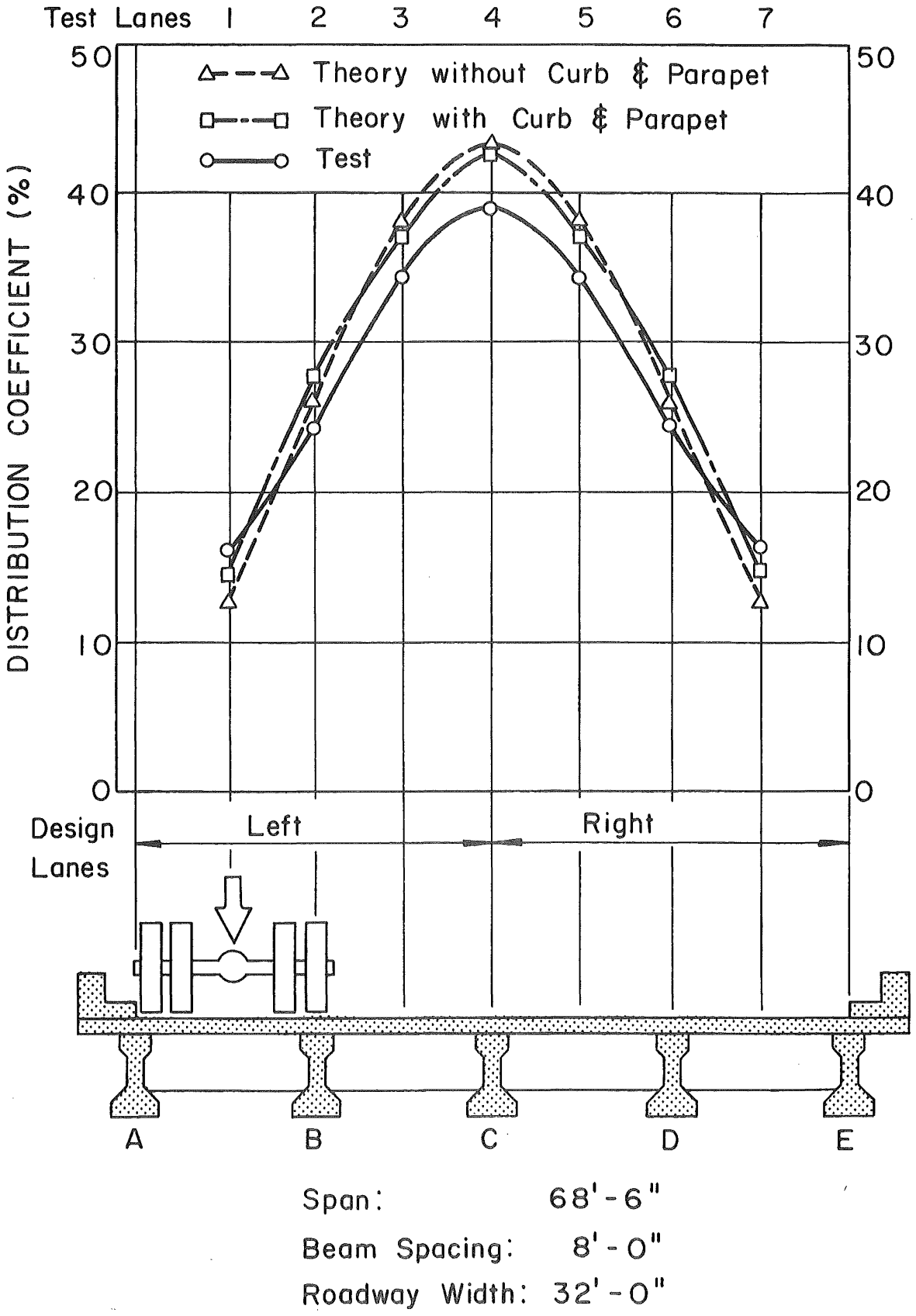

Fig. 27 Influence Line for Bending Moment - Beam C

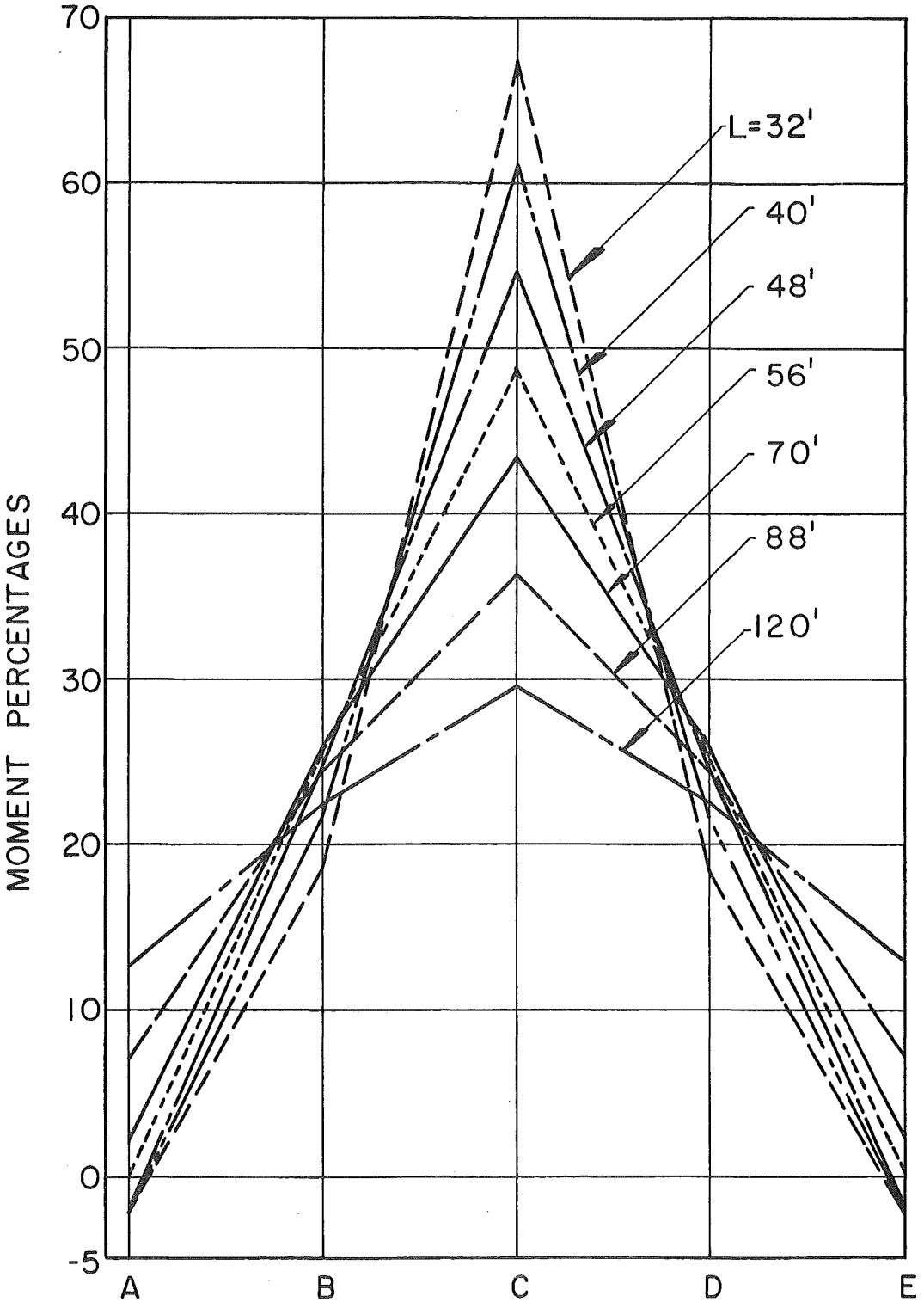

Fig. 28 Effect of Span Length on Load Distribution

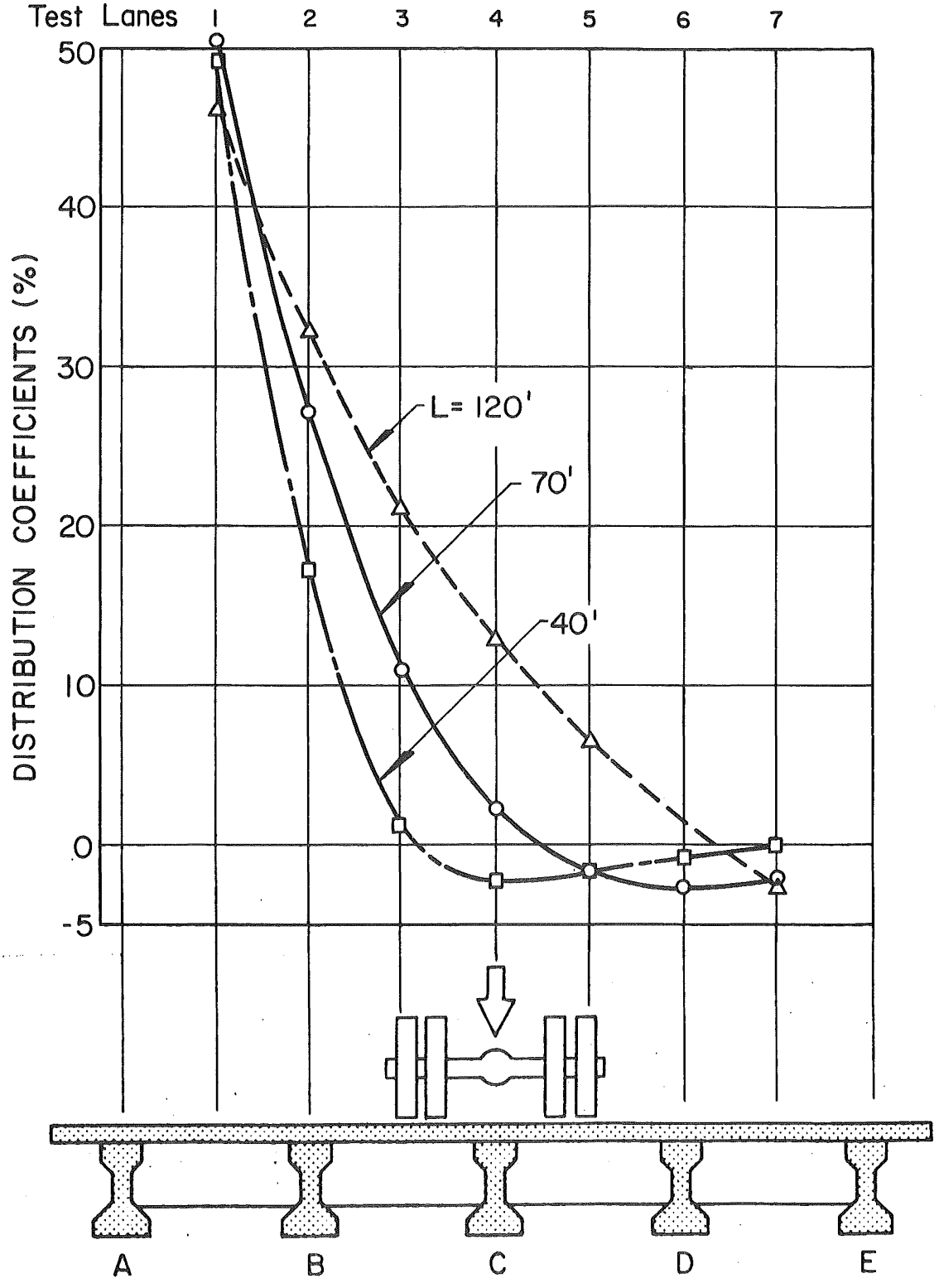

Fig. 29 Influence Lines for Bending Moment - Beam A
Effect of Span Length

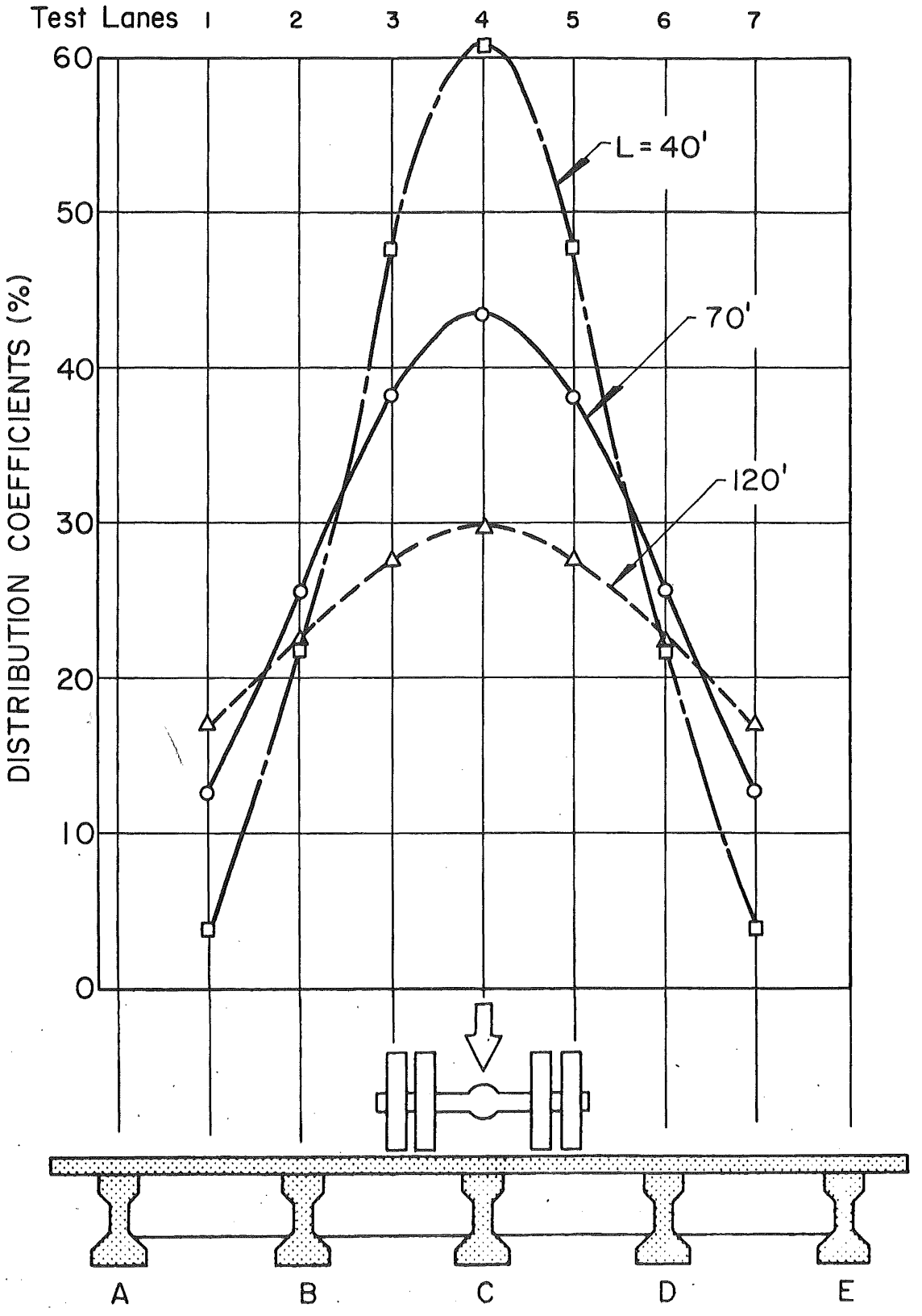

Fig. 30 Influence Lines for Bending Moment - Beam C
Effect of Span Length

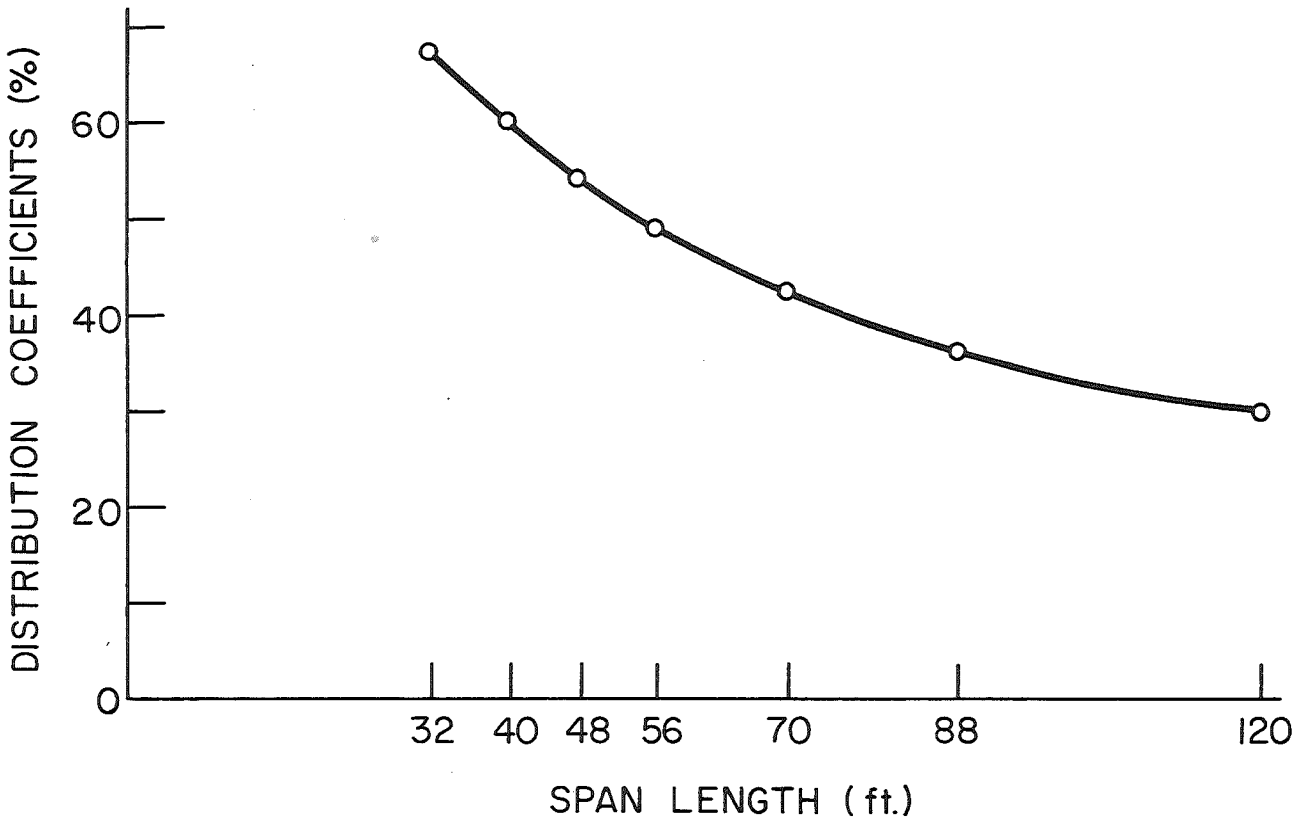

Fig. 31 Effect of Span Length on Center Beam Moment - Beam C

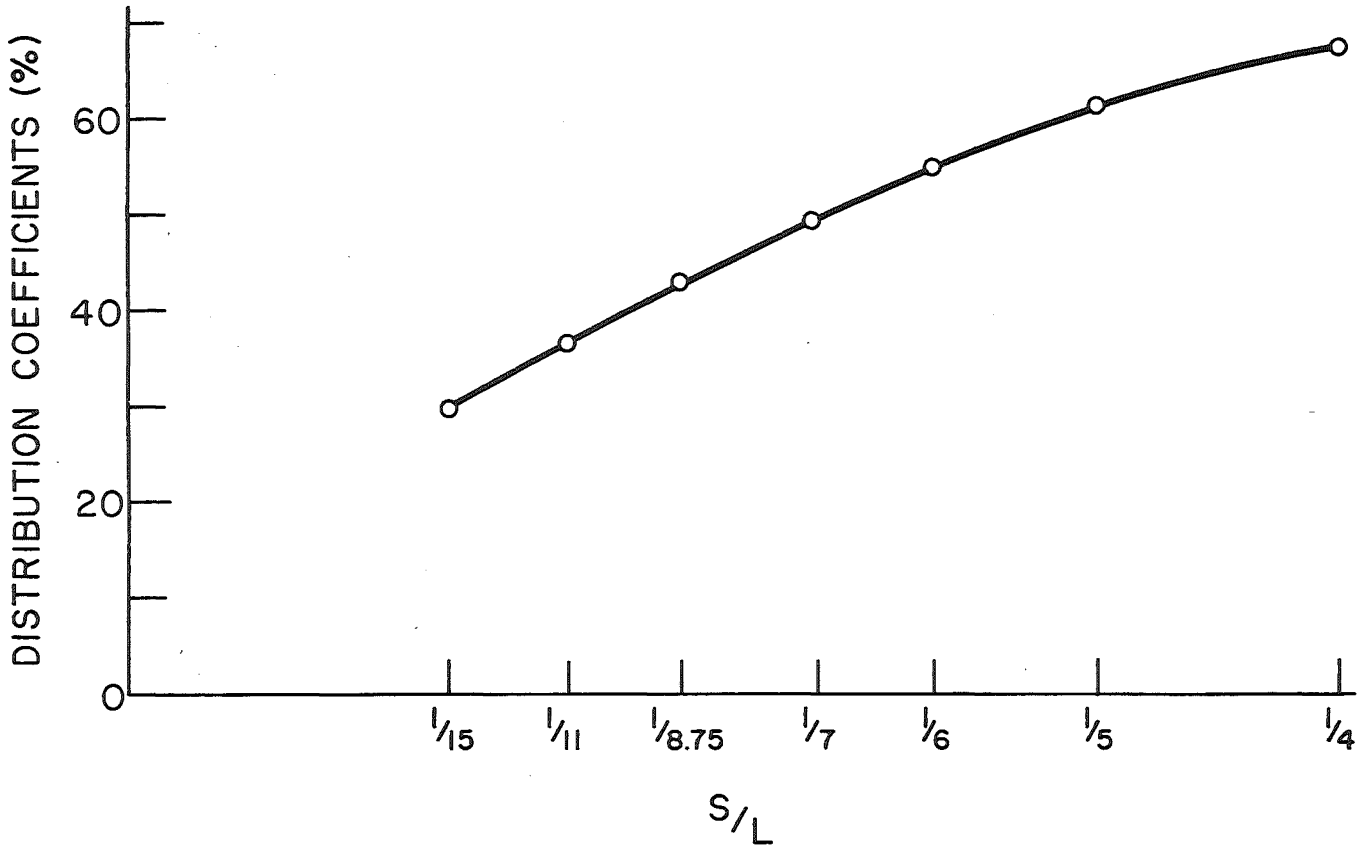

Fig. 32 Distribution Factor for Beam C versus s/L

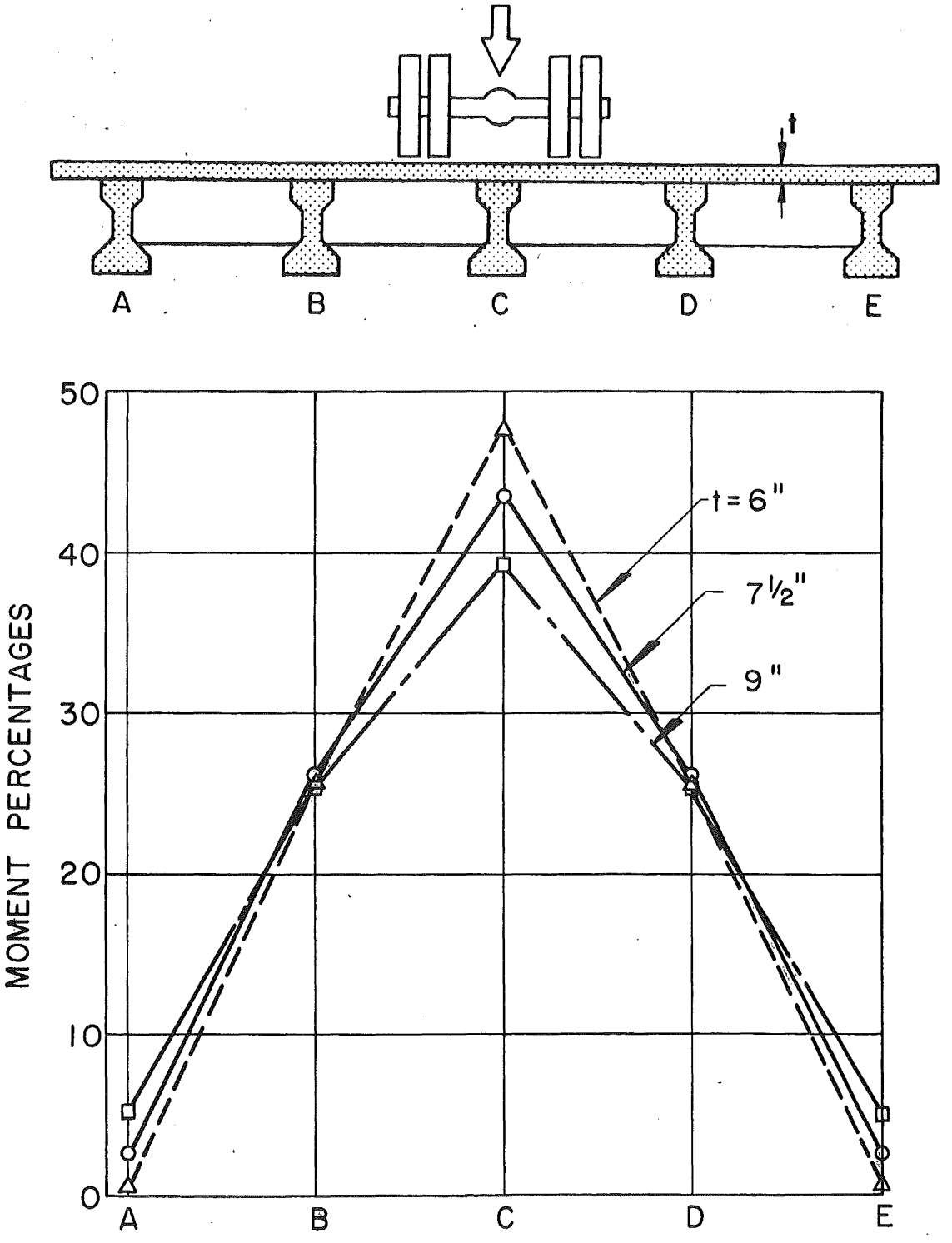

Fig. 33 Effect of Slab Thickness on Load Distribution

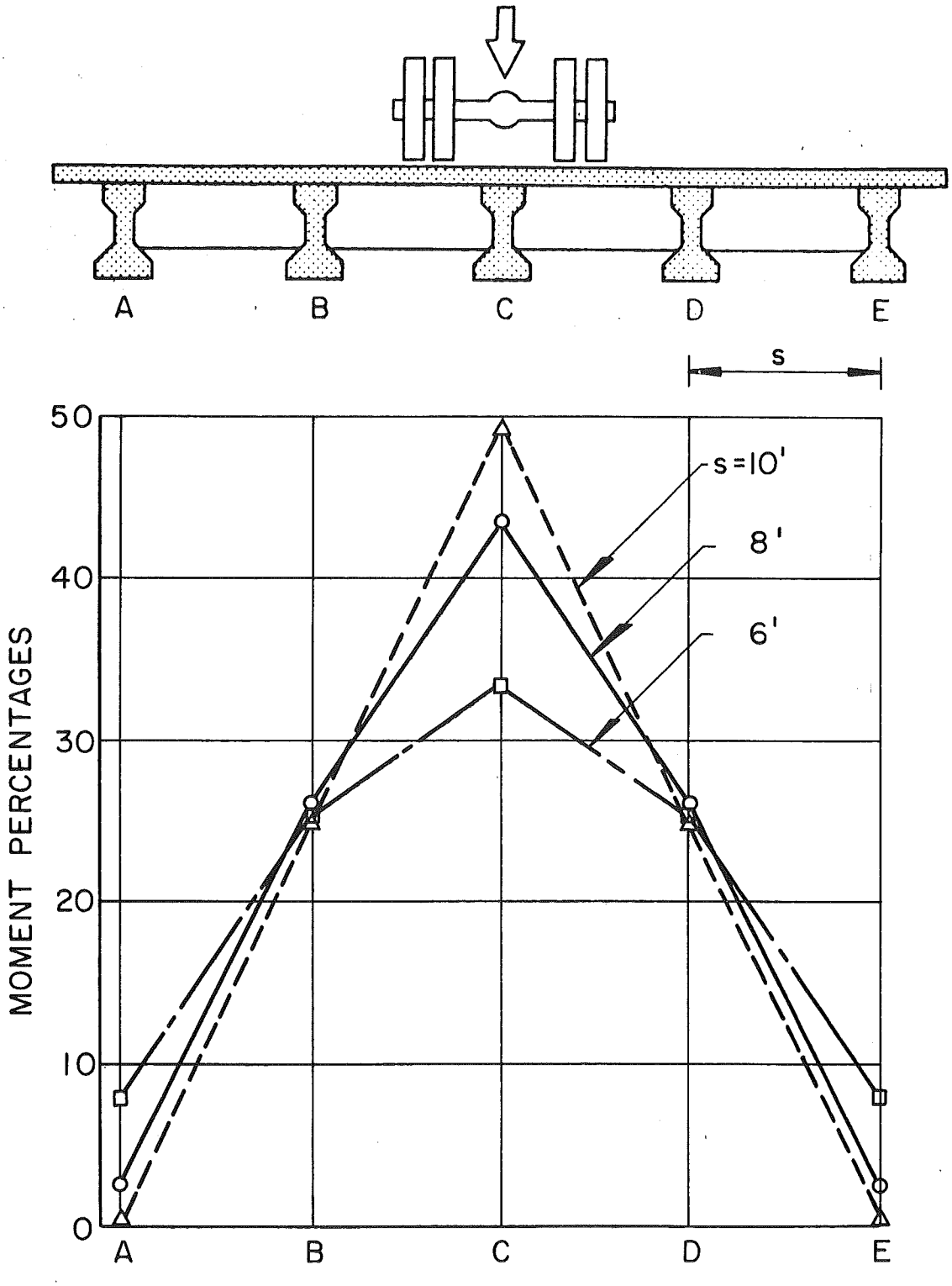

Fig. 34 Effect of Beam Spacing on Load Distribution

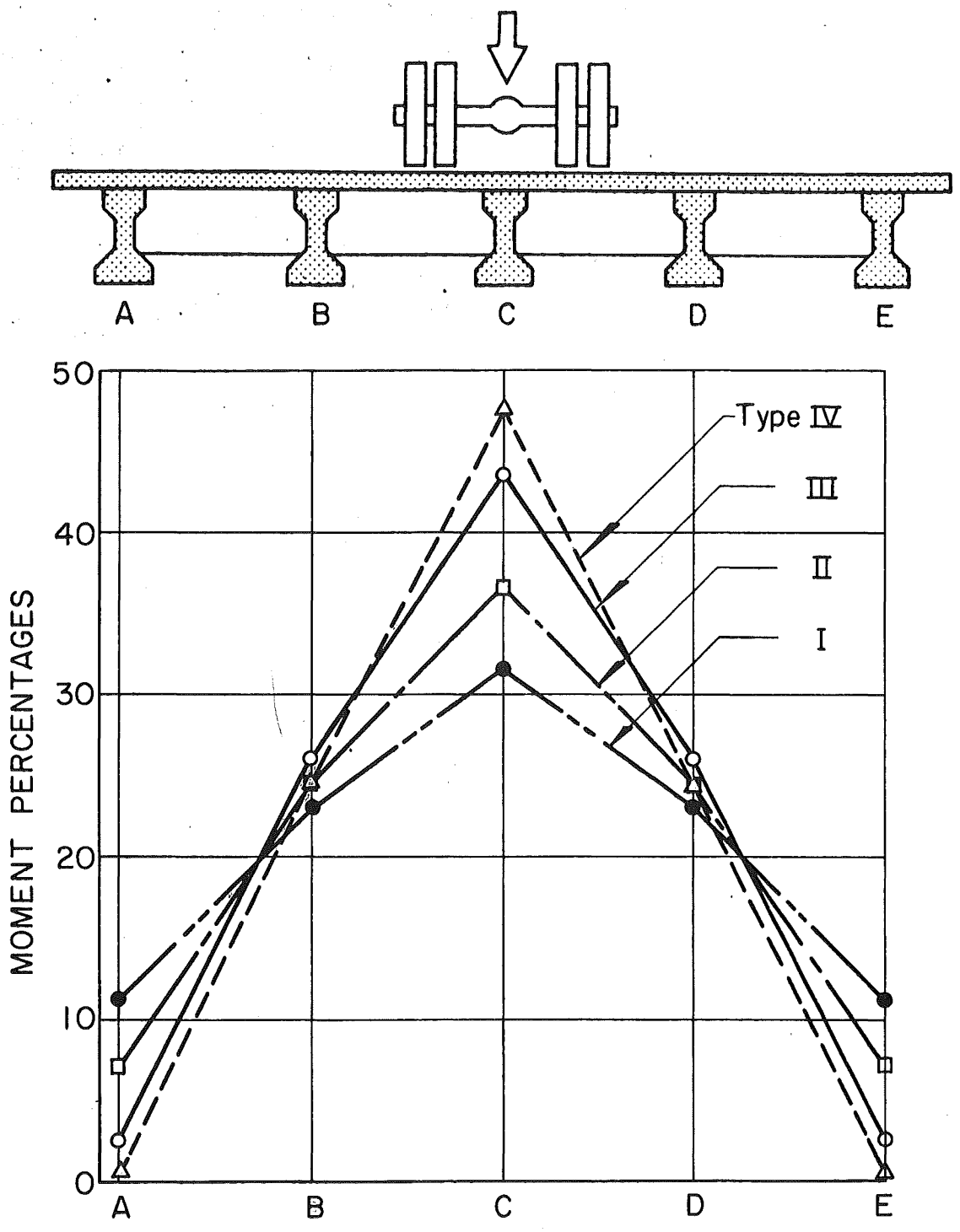

Fig. 35 Effect of Beam Size on Load Distribution

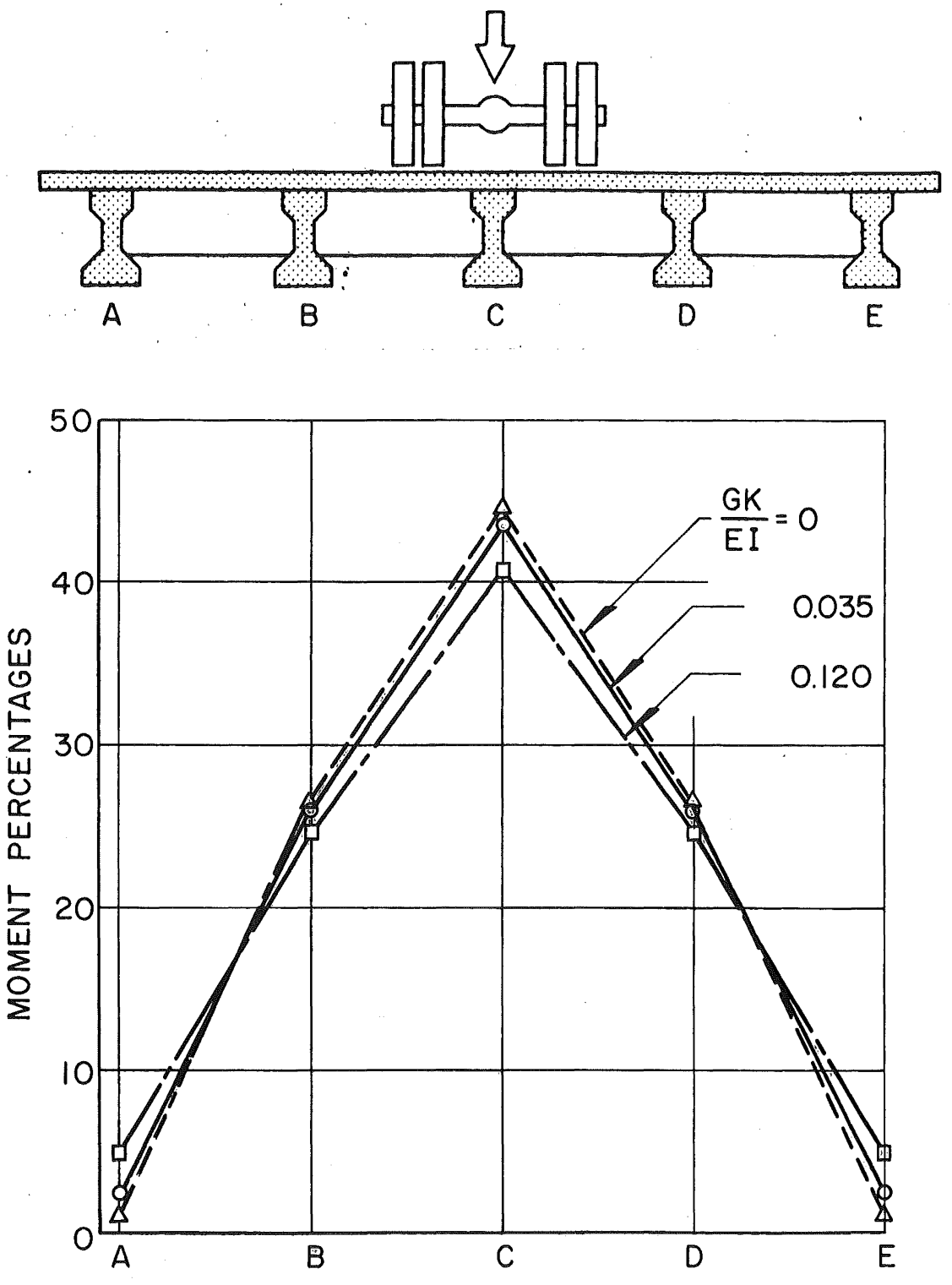

Fig. 36 Effect of Torsional Stiffness of Beams on Lateral Load Distribution

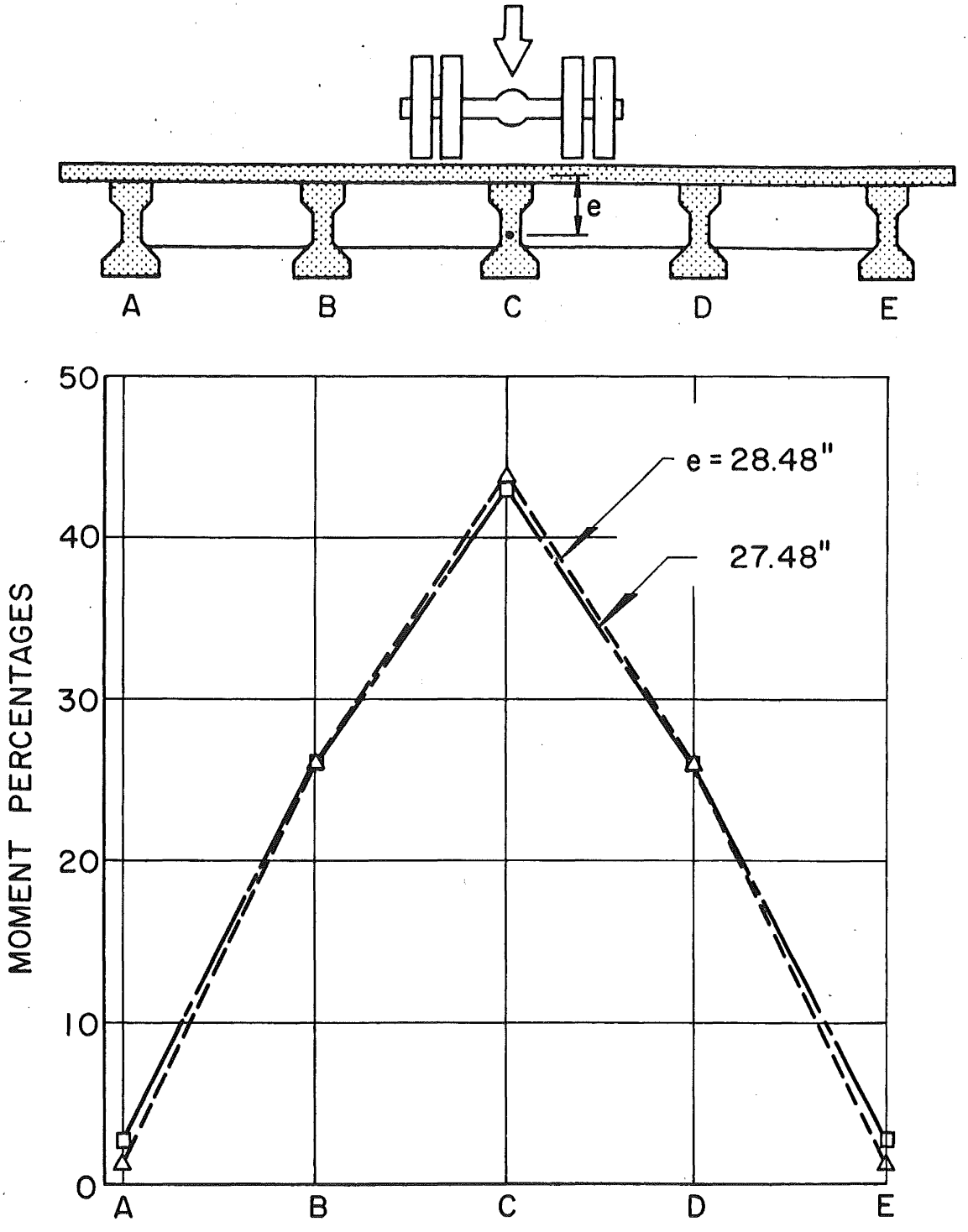

Fig. 37 Effect of Eccentricity of Beams on Lateral Load Distribution

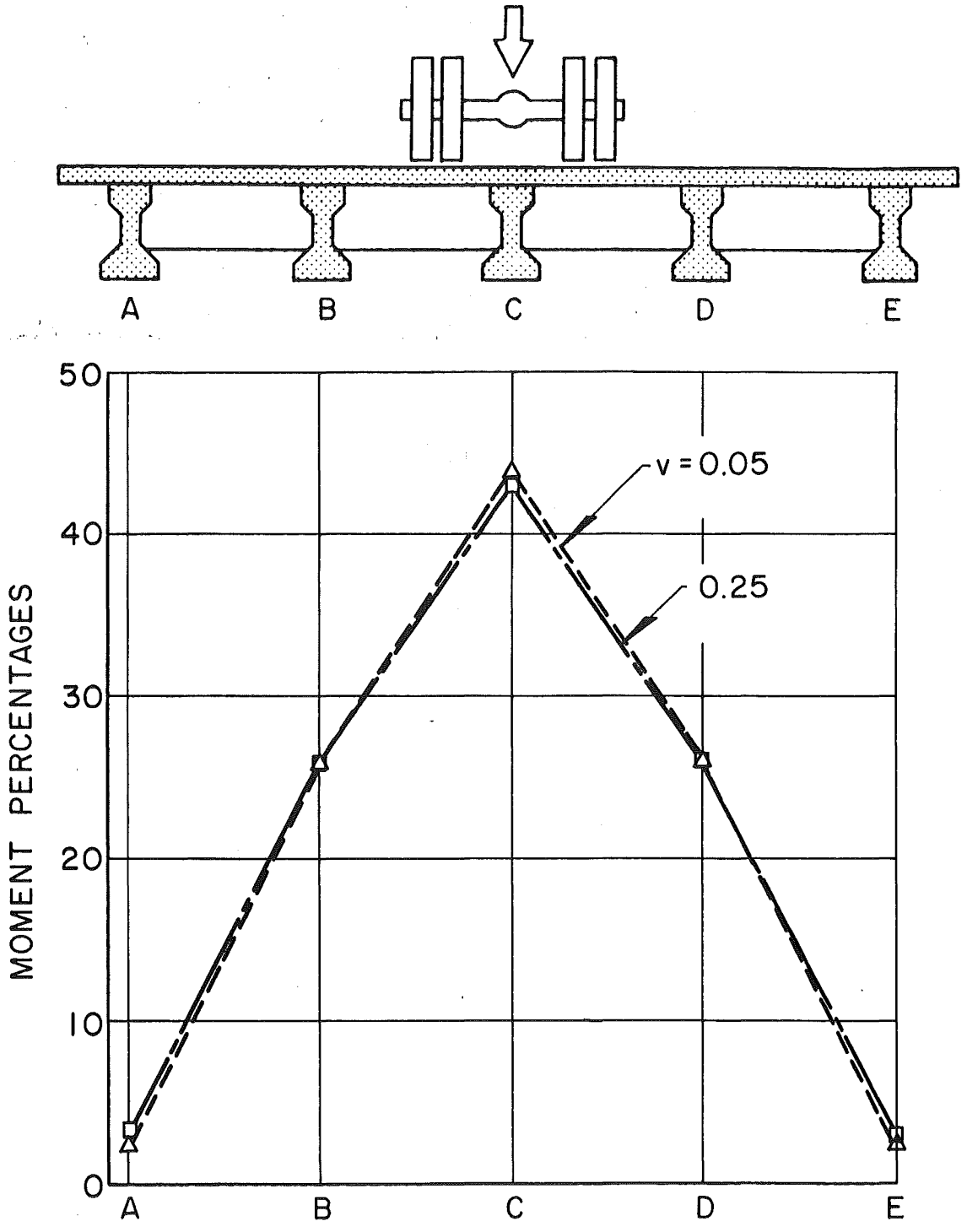

Fig. 38 Effect of Poisson's Ratio on Lateral Load Distribution

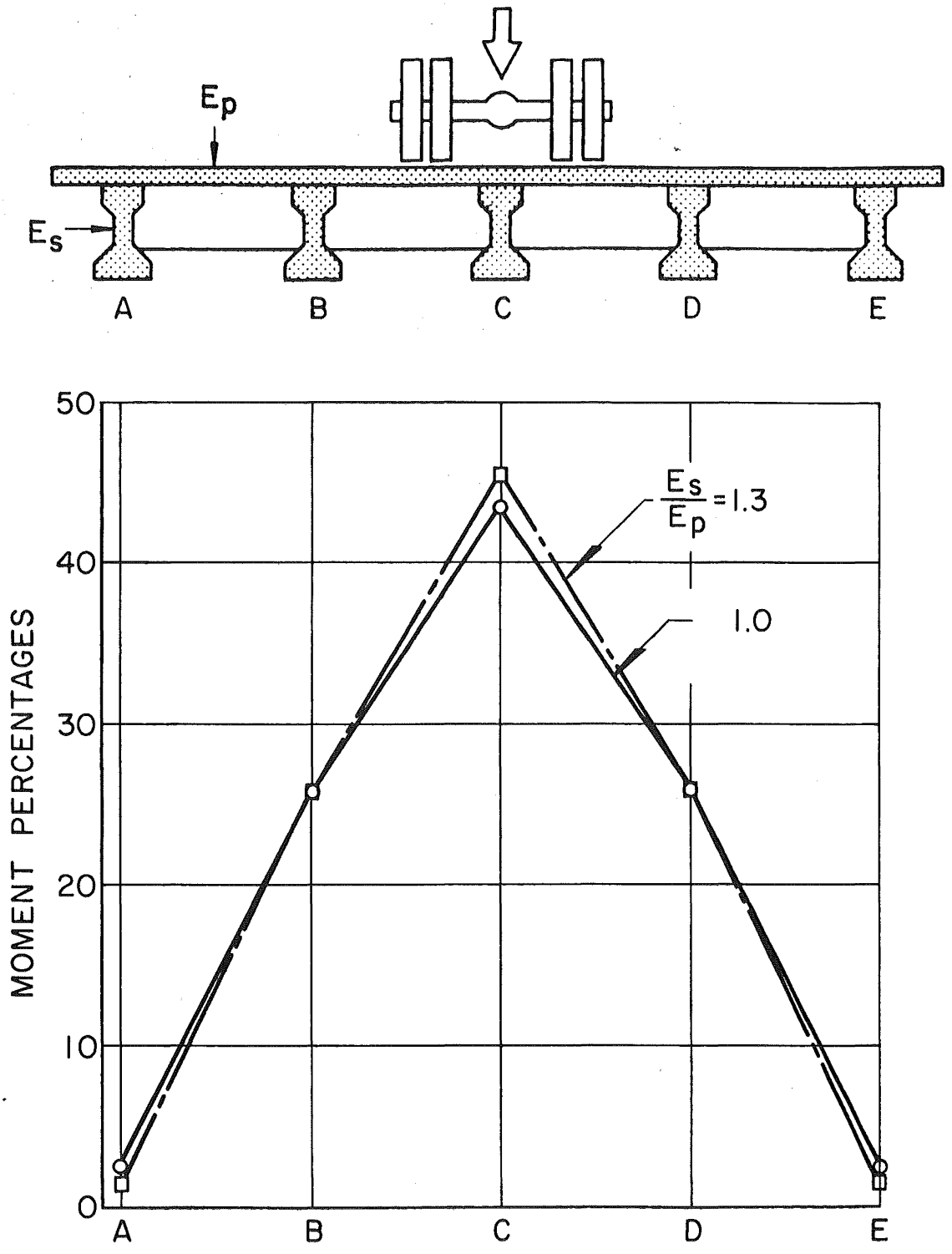

Fig. 39 Effect of Ratio of Moduli of Elasticity on Lateral Load Distribution

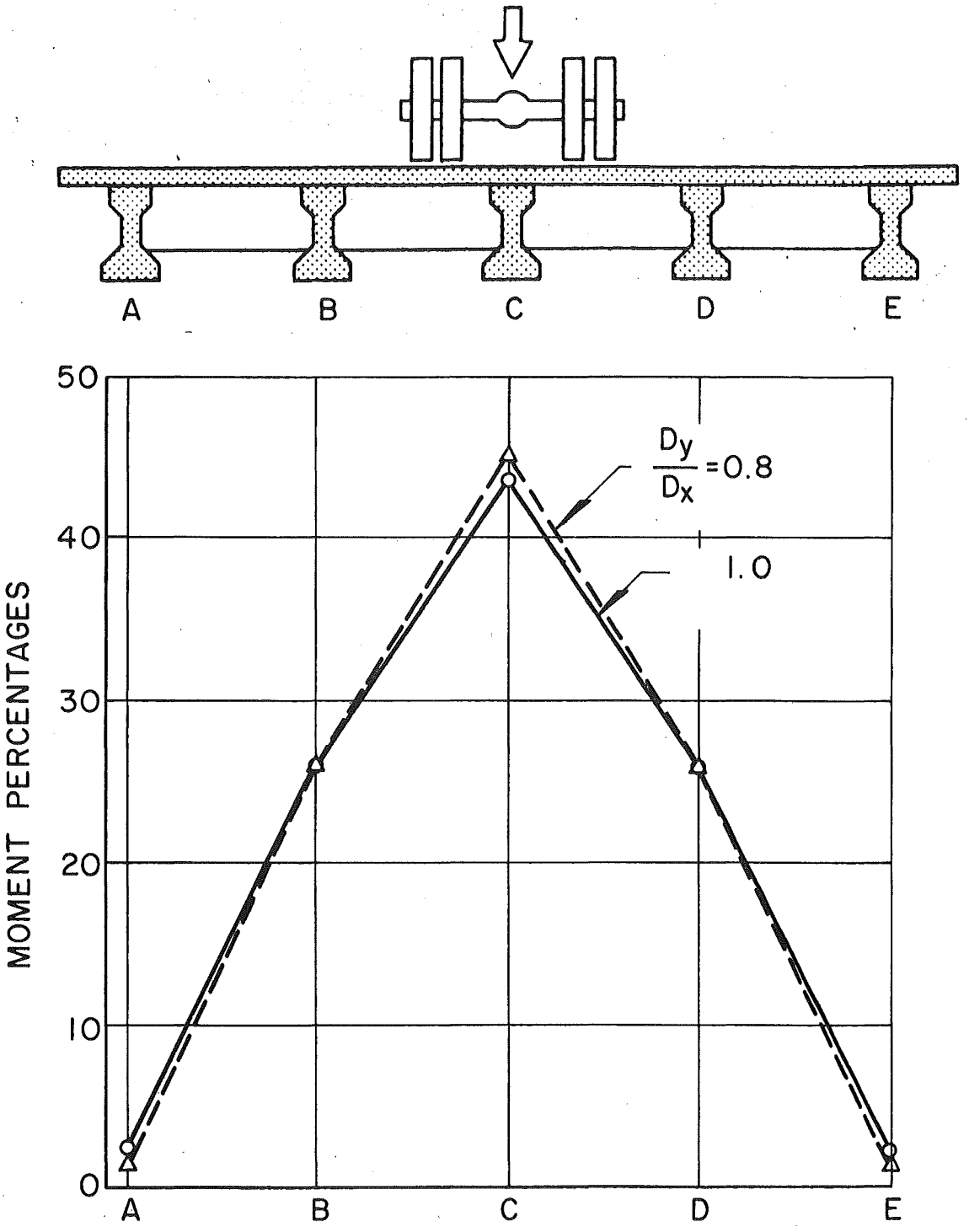

Fig. 40 Effect of Orthotropy of Deck on Lateral Load Distribution

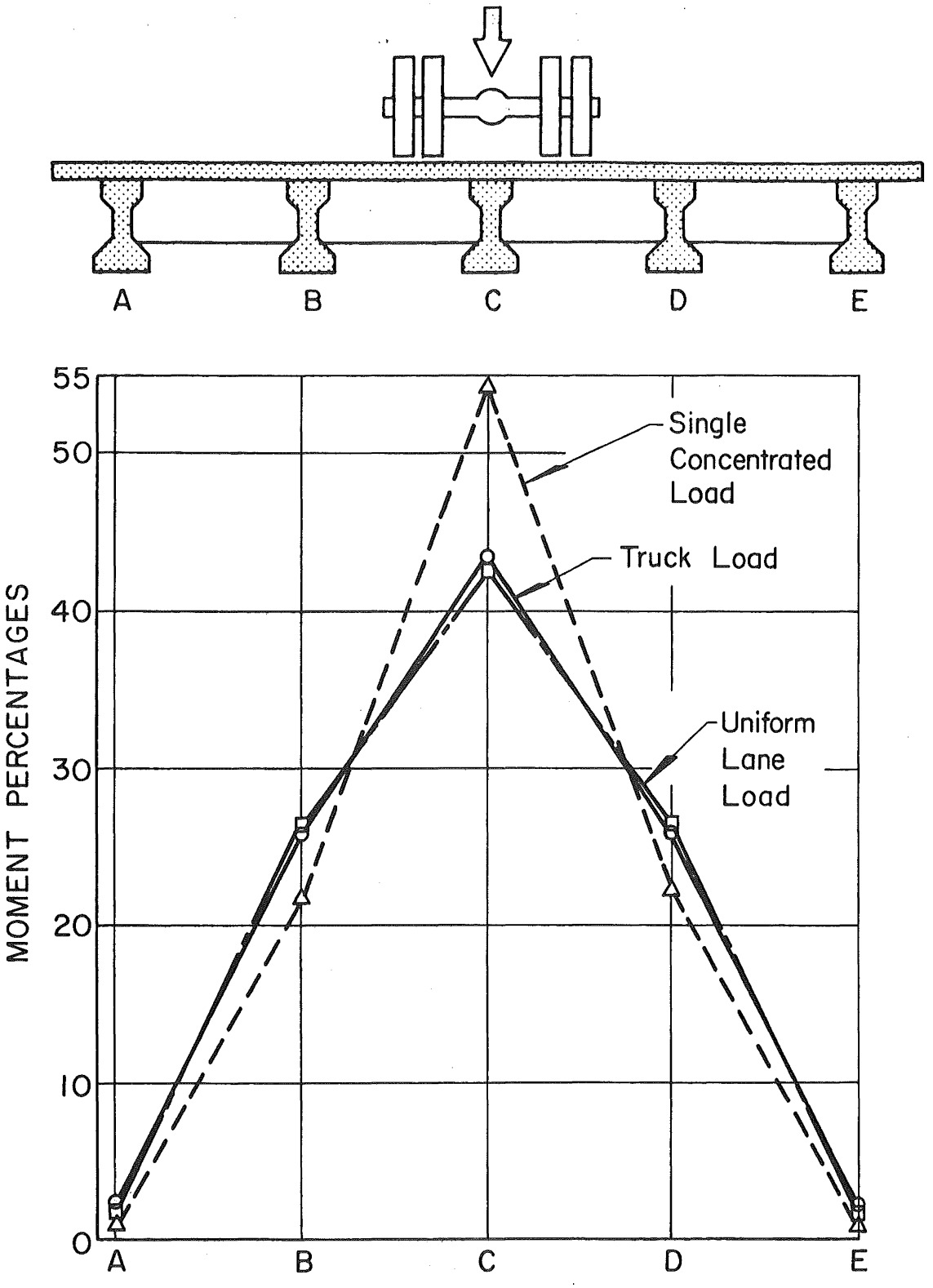

Fig. 41 Effect of Type of Load on Lateral Load Distribution

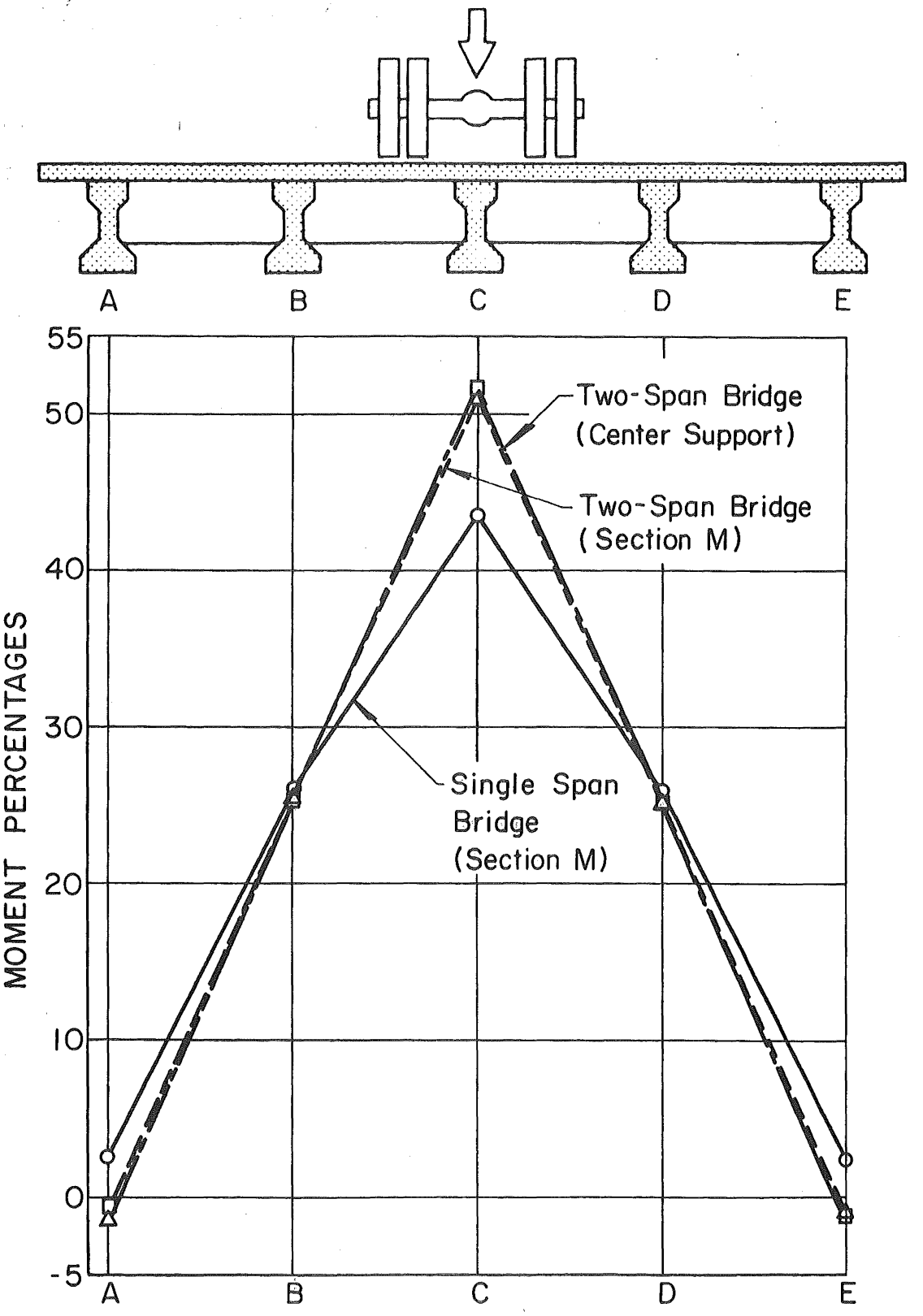

Fig. 42 Effect of Boundary Conditions on Lateral Load Distribution

9. REFERENCES

1. Adini, A. and Clough, R. W.
   ANALYSIS OF PLATE BENDING BY THE FINITE ELEMENT METHOD, Report submitted to the National Science Foundation, 1960.

2. Allwood, R. and Cornes, G.
   A POLYGONAL FINITE ELEMENT FOR PLATE BENDING PROBLEMS USING ASSUMED STRESS APPROACH, International Journal for Numerical Methods in Engineering, Vol. 1, No. 2, 1969.

3. American Association of State Highway Officials
   STANDARD SPECIFICATIONS FOR HIGHWAY BRIDGES, Ninth Edition, AASHO, Washington, D.C., 1965.

4. American Association of State Highway Officials
   STANDARD SPECIFICATIONS FOR HIGHWAY BRIDGES, Tenth Edition, Washington, D.C., 1969.

5. Argyris, J. H.
   THE MATRIX ANALYSIS OF STRUCTURES WITH CUT-OUTS AND MODIFICATIONS, Proceedings Ninth International Congress on Applied Mechanics, Section II, Mechanics Solids, September 1956.

6. Argyris, J. H.
   ON THE ANALYSIS OF COMPLEX ELASTIC STRUCTURES, Applied Mechanics Rev., 11, 1958.

7. Bares, R. and Massonnet, C.
   LE CALCUL DES GRILLAGES DE POUTRES ET DALLES ORTHOTROPES Selon La Methode Guyon - Massonnet - Bares, Dunod, Paris, 1966.

8. Becker, M.
   THE PRINCIPLES AND APPLICATIONS OF VARIATIONAL METHODS, Research Monograph No. 27, the M.I.T. Press, Cambridge, Massachusetts, 1964.

9. Bell, K.
A REFINED TRIANGULAR PLATE BENDING FINITE ELEMENT, International Journal of Numerical Methods in Engineering, Vol. 1, No. 1, January 1969.

10. Birkhoff, G. and Garabedian, H.
SMOOTH SURFACE INTERPOLATION, Journal of Mathematics and Physics, Vol. 39, pp. 258-268, 1960.

11. Bogner, F. K., Fox, R. L. and Schmit, L. A.
THE GENERATION OF INTERELEMENT, COMPATIBLE STIFFNESS AND MASS MATRICES BY THE USE OF INTERPOLATION FORMULAS, Proceedings First Conference on Matrix Methods in Structural Mechanics, Wright-Patterson Air Force Base, Ohio, November 1965.

12. Chen, C. and VanHorn, D. A.
STATIC AND DYNAMIC FLEXURAL BEHAVIOR OF A PRESTRESSED CONCRETE I-BEAM BRIDGE - BARTONSVILLE BRIDGE, Fritz Engineering Laboratory Report No. 349.2, January 1971.

13. Clarkson, J.
THE ELASTIC ANALYSIS OF FLAT GRILLAGES, Cambridge University Press, 1965.

14. Clough, R. W.
THE FINITE ELEMENT METHOD IN STRUCTURAL MECHANICS, Chapter 7 of Stress Analysis, edited by O. C. Zienkiewicz and G. S. Hollister, John Wiley and Sons, 1965.

15. Clough, R. and Tocher, J.
FINITE ELEMENT STIFFNESS MATRICES FOR THE ANALYSIS OF PLATE BENDING, First Conference on Matrix Methods in Structural Mechanics, Wright-Patterson Air Force Base, Ohio, November 1965.

16. Clough, R. and Felippa, C.
A REFINED QUADRILATERAL ELEMENT FOR ANALYSIS OF PLATE BENDING, Proceedings Second Conference on Matrix Methods in Structural Mechanics, Wright-Patterson Air Force Base, Ohio, October 1968.

17. Deak, A. and Pian, T.
APPLICATION OF SMOOTH-SURFACE INTERPOLATION TO THE FINITE ELEMENT ANALYSIS, AIAA Journal, Vol. 5, No. 1, January 1969.

18. Ergatoudis, J. G.
ISO-PARAMETRIC FINITE ELEMENTS IN TWO- AND THREE-DIMENSIONAL ANALYSIS, Ph.D. Dissertation, University of Wales, Swansea, 1968.

19. Fraijs de Veubeke, B.
UPPER AND LOWER BOUNDS IN MATRIX STRUCTURAL ANALYSIS, Pergamon Press, Oxford, 1964.

20. Fraijs de Veubeke, B.
DISPLACEMENT AND EQUILIBRIUM MODELS IN THE FINITE ELEMENT METHOD, Stress Analysis (Zienkiewicz and Hollister, Ed.), J. Wiley Book Co. Ltd., London, 1965.

21. Fraijs de Veubeke, B.
A CONFORMING FINITE ELEMENT FOR PLATE BENDING, International Journal of Solids and Structures, Vol. 4, No. 1, 1968.

22. Galambos, T. V.
STRUCTURAL MEMBERS AND FRAMES, Prentice-Hall, Inc., New Jersey, 1968.

23. Gallagher, R. H.
ANALYSIS OF PLATE AND SHELL STRUCTURES, Proceedings on Application of Finite Element Methods in Civil Engineering, Vanderbilt University, November 1969.

24. Girkmann, K.
FLAECHENTRAGWERKE, Sixth Edition, Springer, Vienna, 1963.

25. Gustafson, W. C. and Wright, R. N.
ANALYSIS OF SKEWED COMPOSITE GIRDER BRIDGES, ASCE Proceedings, Vol. 94, No. ST4, April 1968.

26. Hendry, A. W. and Jaeger, L. G.
THE ANALYSIS OF GRID FRAMEWORKS AND RELATED STRUCTURES, Chatto and Windus, London, 1958.

27. Hrennikoff, A.
SOLUTIONS OF PROBLEMS OF ELASTICITY BY THE FRAMEWORK METHOD, Trans. ASME, Journal of Applied Mechanics, Vol. 8, No. 4, December 1941.

28. Irons, B. M. and Zienkiewicz, O. C.
THE ISO-PARAMETRIC ELEMENT SYSTEM - A NEW CONCEPT IN FINITE ELEMENT ANALYSIS, Conference - Recent Advances in Stress Analysis, Royal Aero Society, London, March, 1968.

29. Kerfoot, R. P. and Ostapenko, A.
GRILLAGES UNDER NORMAL AND AXIAL LOADS - PRESENT STATUS, Fritz Engineering Laboratory Report No. 323.1, June 1967.

30. Kollbrunner, C. F. and Basler, K.
TORSION IN STRUCTURES, Springer, New York, 1963.

31. Lightfoot, E. and Sawko, F.
GRID FRAMEWORKS RESOLVED BY GENERALIZED SLOPE-DEFLECTION, Engineering, London, Vol. 187, pp. 18-20, 1959.

32. Lopez, L. A. and Ang, A. H. S.
FLEXURAL ANALYSIS OF ELASTIC-PLASTIC RECTANGULAR PLATES, Civil Engineering Studies, Structural Research Series No. 305, University of Illinois, Urbana, Illinois, May 1966.

33. Melosh, R. J.
A STIFFNESS MATRIX FOR THE ANALYSIS OF THIN PLATES IN BENDING, Journal of Aeronautical Sciences, Vol. 28, 34, 1961.

34. Melosh, R. J.
BASIS FOR DERIVATION OF MATRICES FOR THE DIRECT STIFFNESS APPROACH, AIAA Journal, Vol. 1, pp. 1631-1637, July 1963.

35. Melosh, R. J. and Bamford, R. M.
EFFICIENT SOLUTION OF LOAD-DEFLECTION EQUATIONS, Journal of Structural Division, ASCE, Vol. 95, No. ST4, April 1969.

36. Motarjemi, D. and VanHorn, D. A.
THEORETICAL ANALYSIS OF LOAD DISTRIBUTION IN PRESTRESSED CONCRETE BOX-BEAM BRIDGES, Fritz Engineering Laboratory Report No. 315.9, October 1969.

37. Newmark, N. M.
NUMERICAL METHODS OF ANALYSIS OF BARS, PLATES AND ELASTIC BODIES, Edited by L. E. Grinter, MacMillan Co., New York, 1949.

38. Oliveira, E. R.
THEORETICAL FOUNDATIONS OF THE FINITE ELEMENT METHOD, International Journal of Solids and Structures, Vol. 4, No. 10, October 1968.

39. Pappenfuss, S. W.
LATERAL PLATE DEFLECTION BY STIFFNESS MATRIX METHODS WITH APPLICATION TO A MARQEE, M.S. Thesis, Department of Civil Engineering, University of Washington, Seattle, 1959.

40. Pian, T. H.
ELEMENT STIFFNESS MATRICES FOR BOUNDARY COMPATIBILITY AND FOR PRESCRIBED BOUNDARY STRESSES, First Conference on Matrix Methods in Structural Mechanics, Wright-Patterson Air Force Base, Ohio, October 1968.

41. Pian, T. H. and Tong, P.
BASIS OF FINITE ELEMENT METHODS FOR SOLID CONTINUA, International Journal for Numerical Methods in Engineering, Vol. 1, No. 1, January 1969.

42. Prandtl, L.
ZUR TORSION VON PREISMATISCHEN STAEBEN, Physik. Z., 4, 1903, pp. 758-759.

43. Przemieniecki, J. S.
THEORY OF MATRIX STRUCTURAL ANALYSIS, McGraw-Hill, New York, 1968.

44. Severn, R. and Taylor, P.
THE FINITE ELEMENT METHOD FOR FLEXURE OF SLABS WHEN STRESS DISTRIBUTIONS ARE ASSUMED, Proceedings Institute of Civil Engineers, 34, p. 153, 1966.

45. Sokolnikoff, I. S.
MATHEMATICAL THEORY OF ELASTICITY, McGraw-Hill, New York, 1956.

46. Timoshenko, S. P. and Woinosky-Krieger, S.
THEORY OF PLATES AND SHELLS, Second Edition, McGraw-Hill, New York, 1959.

47. Timoshenko, S. P. and Gere, J. M.
THEORY OF ELASTIC STABILITY, Second Edition, McGraw-Hill, New York, 1961.

48. Turner, M. J., Clough, R. W., Martin, H. C. and Topp, L. J.
STIFFNESS AND DEFLECTION ANALYSIS OF COMPLEX STRUCTURES, Journal of Aeronautical Sciences, 23, No. 9, 1956.

49. VanHorn, D. A.
STRUCTURAL BEHAVIOR CHARACTERISTICS OF PRESTRESSED CONCRETE BOX-BEAM BRIDGES, Fritz Engineering Laboratory Report No. 315.8, June, 1969.

50. Vitols, V., Clifton, R. and Au, T.
ANALYSIS OF COMPOSITE BEAM BRIDGES BY ORTHOTROPIC PLATE THEORY, ASCE Proceedings, Vol. 89, No. ST4, Pt. 1, Paper 3581, August 1963.

51. Washizu, K.
VARIATIONAL METHODS IN ELASTICITY AND PLACTICITY, Pergamon Press, Oxford, 1960.

52. Wegmuller, A. and VanHorn, D. A.
SLAB BEHAVIOR OF A PRESTRESSED CONCRETE I-BEAM BRIDGE - BARTONSVILLE BRIDGE, Fritz Engineering Laboratory Report No. 349.3, May 1971.

53. Wegmuller, A.
FINITE ELEMENT ANALYSES OF ELASTIC-PLASTIC PLATES AND ECCENTRICALLY STIFFENED PLATES, Ph.D. Dissertation, Civil Engineering Department, Lehigh University, 1971.

54. Wegmuller, A. and Kostem, C. N.
EFFECT OF IMPERFECTIONS ON THE STATIC RESPONSE OF BEAM-SLAB TYPE HIGHWAY BRIDGES, Proceedings of the Speciality Conference on Finite Element Method in Civil Engineering, Montreal, Canada, 1972.

55. Whetstone, W. D.
COMPUTER ANALYSIS OF LARGE LINEAR FRAMES, Journal of Structural Division, ASCE, Vol. 95, No. ST11, November 1969.

56. Zienkiewicz, O. C. and Cheung, Y. K.
THE FINITE ELEMENT METHOD IN STRUCTURAL AND CONTINUUM MECHANICS, Second Edition, McGraw-Hill, New York, 1970.

10. ACKNOWLEDGMENTS

The authors would like to express their appreciation to Dr. D. A. VanHorn for his comments on the application of the developed methodology to highway bridges and to Dr. Suresh Desai for his continuing interest and encouragement.

Acknowledgments are also due to Mrs. Ruth Grimes, who typed the manuscript, Mr. John Gera and Mrs. Sharon Balogh, who prepared the drawings included in this report, and to the Lehigh University Computing Center for providing its facilities for the extensive computer work.

Special thanks are due to the National Science Foundation for sponsoring the research project Overloading Behavior of Beam-Slab Highway Bridges (Grant No. GK-23589). The reported investigation was carried out within the framework of this project.